Published in "Stellar astrophysics for the local group" : VIII Canary Islands Winter School of Astrophysics. Edited by A. Aparicio, A. Herrero, and F. Sanchez. Cambridge ; New York : Cambridge University Press, 1998

Calibration of the Extragalactic Distance Scale

By BARRY F. MADORE[1], WENDY L. FREEDMAN[2]

[1]NASA/IPAC Extragalactic Database, Infrared Processing & Analysis Center, California Institute of Technology, Jet Propulsion Laboratory, Pasadena, CA 91125, USA

[2]Observatories, Carnegie Institution of Washington, 813 Santa Barbara St., Pasadena CA 91101, USA

The calibration and use of Cepheids as primary distance indicators is reviewed in the context of the extragalactic distance scale. Comparison is made with the independently calibrated Population II distance scale and found to be consistent at the 10% level. The combined use of ground-based facilities and the *Hubble Space Telescope* now allow for the application of the Cepheid Period-Luminosity relation out to distances in excess of 20 Mpc. Calibration of secondary distance indicators and the direct determination of distances to galaxies in the field as well as in the Virgo and Fornax clusters allows for multiple paths to the determination of the absolute rate of the expansion of the Universe parameterized by the Hubble constant. At this point in the reduction and analysis of Key Project galaxies H_0 = 72km/sec/Mpc ± 2 (random) ± 12 [systematic].

Table of Contents

1. INTRODUCTION TO THE LECTURES

Even some of the earliest tentative steps out of our Milky Way galaxy and into the local Universe were guided by Cepheid variables. Indeed, the very first convincing demonstration of the size of our Universe rested on the identification by Edwin Hubble (1929) of Cepheid variables in the nearest galaxies NGC 6822, M31 and M33. Armed with empirical knowledge of the relationship between luminosity and period, discovered for Cepheids by Henrietta Leavitt only a few years earlier, Hubble used the Cepheids to set the scale size for galaxies themselves, and for the Universe in which they are expanding away from each other.

This series of lectures will detail the role played by Cepheids in the calibration of the extragalactic distance scale. In preparation for that application, the physics of Cepheids will be outlined and their empirical calibration will be presented. The properties of individual Cepheids varying through their pulsational cycle will be detailed, and the structure of the instability strip for the time-averaged properties of Cepheids will be discussed. Concerns about the metallicity sensitivity of the Period-Luminosity relation will be dealt with in a number of ways, from theoretical considerations acting as a guide, to direct tests and finally intercomparisons of independent distance determinations to serve as external checks. Means of determining distances freed from the effects of interstellar reddening and extinction will also be outlined.

Secure with the foundations provided by Cepheid variables and an application of their period-luminosity relation, we move on to the recent use of the *Hubble Space Telescope* in the rapid determination of distances to ``nearby'' galaxies useful for calibrating so-called ``secondary distance indicators'' needed to extend the distance scale out past the perturbing effects of the Virgo cluster and well out to cosmologically significant distances unaffected by peculiar motions and large-scale flows.

We digress slightly en route to highlight a new distance indicator that is fundamentally different, from and yet absolutely complementary to, the Cepeids as a distance indicator, the tip of the red giant branch (TRGB) method. The TRGB is well understood to mark the onset of helium core burning in low-mass Population II stars, and is independently calibrated through the RR Lyrae distance scale.

2. CEPHEIDS

These lectures will first concentrate on our developing understanding of the very basic principles characterizing the variability seen in individual Cepheids, as well as the systematics and trends observed for Cepheids as an ensemble. The emphasis will be on Cepheids as accurate extragalactic distance indicators, and will only touch upon the debate concerning the exact value of the zero point later, when the recent results from the Hipparcos satellite are discussed. Previous work on the zero point of the

Cepheid period-luminosity relation is adequately covered in recent commentaries by Feast & Walker (1987), Walker (1988) and Schmidt (1991), all of which suggest that there is a convergence of opinion at the level of about ± 0.10 mag. As optimistic as these reports are, readers are still referred to the cautioning remarks by Turner (1990).

We begin by presenting a physical basis from which to view Cepheids as distance indicators. (However, for dissenting views on this whole process, interested readers are referred to Clube & Dawe 1980, and to Stift 1982, 1990). We then go on to discuss the difficulties and uncertainties caused by reddening and metallicity effects. Following sections put into perspective the explicit determination of reddening made possible by employing panoramic and long-wavelength detectors. We then review the status of the Cepheid-based distances to Local Group galaxies and then link it to those beyond the Local Group being observed by the *Hubble Space Telescope*. The impact of these distances on a determination of the Hubble constant concludes the lectures. Later sections look at the differences between the PLC and the PL relation, discuss an implicit method for dealing with reddening, and finally, examine the prospects for determining reddenings to individual Cepheids.

For historical notes on Cepheids as distance indicators the interested reader is referred to the monographs by Fernie (1969), Sandage (1972, 1988a), Stothers (1983), Walker (1988), Madore (1986) and Tanvir (1997) and references therein. Other, more recent reviews of Cepheids in the context of the extragalactic distance scale can be found in Madore (1985), Freedman (1988), Feast & Walker (1987), Madore & Freedman (1991), Jacoby *et al.* (1992), and Freedman & Madore (1996). A review by Hodge (1981) on the extragalactic distance scale is itself especially relevant in as much as many of the major topics of concern raised by him regarding the Cepheid PL relation have now largely been addressed at least by direct observations. The evolutionary status of Cepheids is most recently reviewed by Chiosi (1990), while Simon (1990) gives a detailed look at the convergence of techniques used to calibrate the Galactic PL relation, and the confrontation of these observations with pulsation theory. And finally, Chiosi et al. (1993) have published theoretical PL relations which they then map to both optical and near-infrared wavelengths in a modern attempt to illucidate the effects of metallicity on those zero points.

3. BRIEF SUMMARY OF THE OBSERVED PROPERTIES OF CEPHEID VARIABLES

At the time of this writing, Cepheids have now been surveyed for and discovered in over two dozen galaxies. Including surveys of the Magellanic Clouds, light curves for approximately 3,000 Cepheids have been obtained. Over 1,100 Cepheids are known in each of the Magellanic Clouds. These numbers are rapidly increasing as additional galaxies are being surveyed with the *HST*, and as the MACHO survey for microlensing in fields toward the Large Magellanic Cloud (Cook 1996) progresses.

Cepheids are high-luminosity, radially-pulsating, variable stars. Their spectral types range from early F to late K (see Code 1947; Kraft 1960); while their intrinsic brightnesses at visual wavelengths range

from -2 > M_V > -7 mag making them ideal candidates for distance indicators on Galactic and extragalactic scales. The periods of Population I classical Cepheids range from approximately 2 to over 100 days. Cepheids are characterized by their distinctive light curves having a rapid rise to maximum light, followed by a slower linear decline to minimum light. Due to their variability, they are easily isolated, identified and classified. Below a period of about 9 days (*e.g.*, Bohm-Vitense 1994) Cepheids are observed to pulsate in both the fundamental, in addition to the first harmonic (overtone) mode. But perhaps most importantly for the distance determinations, detailed stellar pulsation models of these objects indicate that we understand the basic physics underlying their luminosities, colors and periods. In this regard, Cepheids appear to stand alone in the extragalactic distance scale; however, we shall argue in this series of lectures that there is a second, fully complementary path using the brightest Population II red giant stars that has similar accuracy and precision to the Population I Cepheid route.

Although Cepheids exhibit strong correlations between their periods, luminosities and colors, the amplitudes of Cepheids do not appear to correlate with other observables. Rather, examples of Cepheids having amplitudes from 0.4 to about 1.5 mag in the V band can be found at almost all periods, with the greatest upper bound on the amplitudes occurring preferentially around 25-30 days (*e.g.*, see Schaltenbrand & Tammann 1970). On the other hand, for an individual Cepheid, the monochromatic amplitude is observed to decrease toward redder wavelengths (see Figures 1 and 2). As a practical matter, the large amplitudes at bluer wavelengths suggest that Cepheid searches should be carried out at shorter wavelengths (Freedman, Grieve &Madore 1985; Madore & Freedman 1991).

Finally, in searching for Cepheid variables, it is useful to know their frequency relative to other types of variables of comparable luminosity. Averaging over the discovery statistics for complete surveys in fields published before the launch of HST, for the SMC, LMC, M31 and NGC 300, Madore & Freedman (1985) found that more than 70% of all variables reported are classical Cepheids, 16% are irregular variables, 5% are Mira-type long-period variables, 7% are eclipsing variables, and the remaining 2% are W Virginis stars.

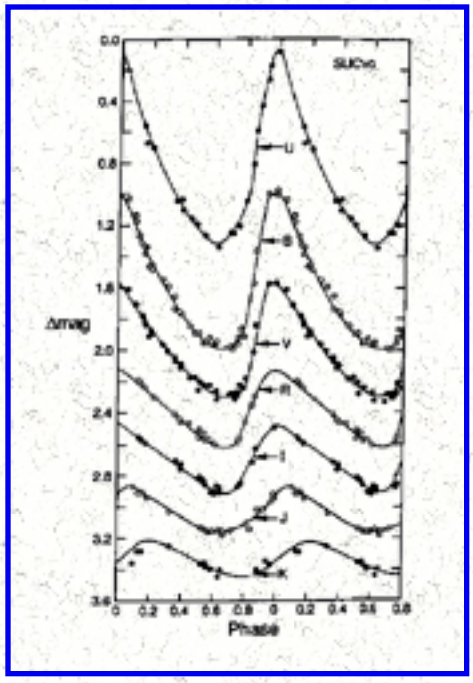

Figure 1. Variations of amplitude and phase for a typical Galactic Cepheid as a function of increasing wavelength. Note the monotonic drop in amplitude, the progression toward more symmetric light variation, and the phase shift of maximum toward later phases, all with increasing wavelength.

4. SIMPLE PHYSICAL CONSIDERATIONS

$$L = 4 \pi R^2 \sigma T_e^4$$

the bolometric luminosities *L of all stars*, (including Cepheids), can be derived. The radius R is a geometric term, parameterizing the total emitting surface area $4 \pi R^2$, and the effective temperature T_e is a thermal term, used to parameterize the areal surface brightness, given by σT_e^4. Expressed in magnitudes, Stephan's Law becomes

$$M_{BOL} = -5 \log R - 10 \log T_e + C$$

and it is schematically shown in Figure 2. It should be noted that *the entire* M_{BOL} - *log* T_e *plane is mapped by* Equation (2), and that within the context of this relation alone, for any value of *log* T_e, an unbounded range of radius R is independently possible. However, once R *and* T_e are each specified, M_{BOL} is uniquely defined. Additional constraints, outside of Stephan's Law itself, must be involved if bounds on permitted values of the independent geometric and thermal variables are to be considered. An important constraint is provided by stellar evolution. In terms of timescales and allowed equilibrium configurations, the core-hydrogen-burning main sequence is one of the most striking and well known examples of such a ``constraint'' on populating the *HR* diagram. Hydrostatic equilibrium can be achieved for long periods of time along the hydrogen-burning main sequence, and as a result we are constrained to observe most of the stars there most of the time. There are, of course, other constraints.

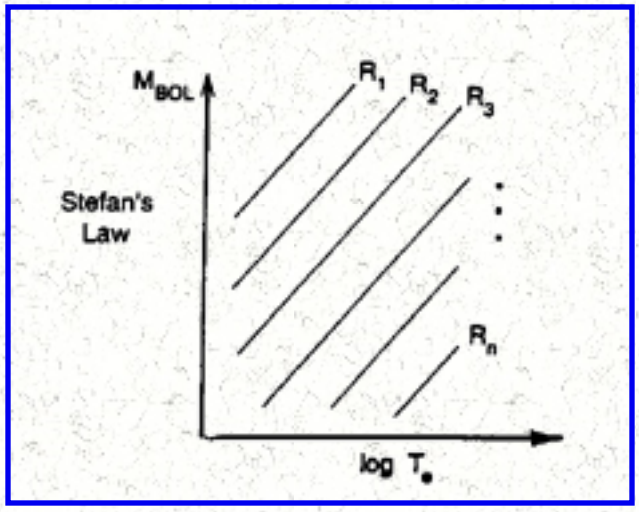

Figure 2. Stefan's Law expressed in graphical form projected onto the theoretical M_{BOL} - $logT_e$ plane where loci of constant radius are indicated by upward sloping lines.

For mechanical systems it is well known that $P \rho^{1/2} = Q$, where Q is a structural constant, and P is the natural free pulsation period, determined by gravity through ρ, the mean density of the system, in turn defined by $M = 4/3\ \pi\ R^3\ \rho$, where M is the total mass of the system. If it is assumed that mass is predominantly a function of R and T_{eff}, then the pulsation period can be used as the second observable parameter instead of requiring the radius to be observed directly.

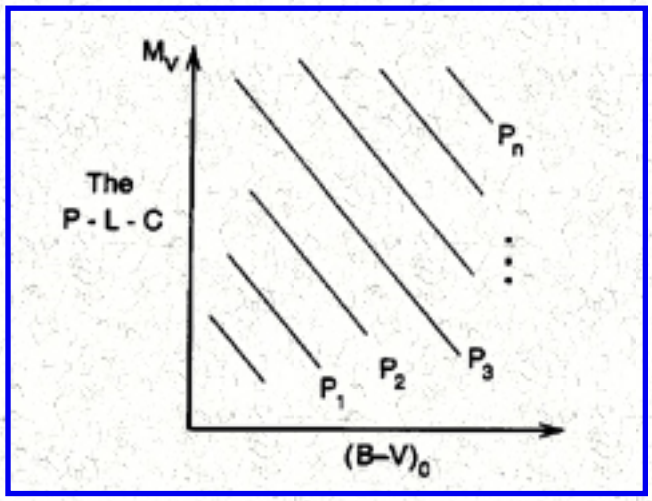

Figure 3. The PLC relation expressed in graphical form as projected onto the observational M_V - (B-V) plane, where loci of constant period are downward sloping lines.

If we then linearly map log (T_e) into an observable intrinsic color (*i.e.*, B-V), and map radius into an observable period, we thereby predict a new two-parameter description of the luminosity of (pulsating) stars. This is precisely the physical basis for the period-luminosity-color (PLC) relation for Cepheids, as was so elegantly introduced and explained over a quarter of a century ago (Sandage 1958, Sandage & Gratton 1963, Sandage & Tammann 1968). In its linearized form for pulsating variables, Stefan's law takes on the following form of the PLC: $M_V = \alpha\ logP + \beta\ (B\text{-}V)_0 + \gamma$. In analogy to plotting Stephan's Law in the theoretical M_{BOL} - $log\ T_e$ above, Figure 4 shows the PLC mapped into the observational M_0 - $(B\text{-}V)_0$ color-magnitude diagram. Again the entire plane is mapped. To see how the PLC relates to the more commonly referred to relations (the PL and PC relations), the reader is referred to a more detailed discussion in the sections ahead, the caption to Figure 4, and the Cepheid section in Jacoby *et al.* (1992) where an empirical analog of Figure 4 is given.

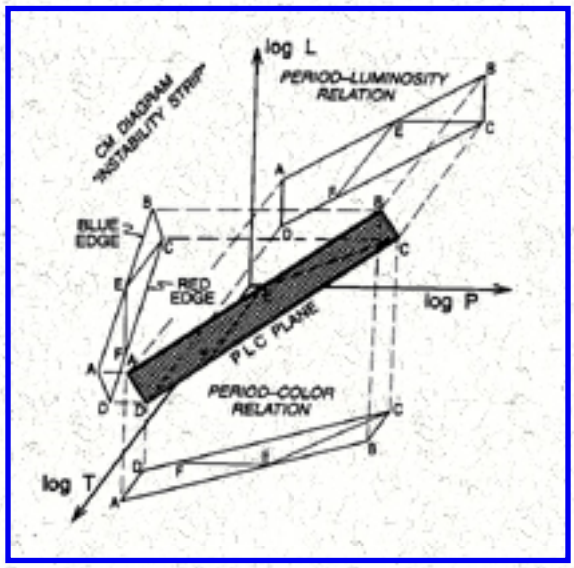

Figure 4. The Cepheid Manifold: Projections of the PLC plane (shown shaded) onto the three principal co-ordinate systems (luminosity [L], increasing up, period [log P], increasing to the right and color [(B-V)] becoming bluer to the lower left). The backward projection onto the L-P plane gives the period-luminosity relation. Projecting to the left gives the position of instability strip within the color-magnitude diagram. Projecting down gives the period-color relation.

Stars can be found evolving across many parts of the color-magnitude diagram. However, only in very narrowly defined regions do they become pulsationally unstable. Cepheid pulsation in particular occurs because of the changing atmospheric opacity with temperature in the helium ionization zone. This zone acts like a heat engine and valve mechanism, alternately trapping and then releasing energy, thereby periodically forcing the outer layers of the star into motion against the restoring force of gravity. Not all stars are unstable to this mechanism. The cool (red) edge of the Cepheid instability strip is thought to be controlled by the onset of convection, which then prevents the helium ionization zone from driving the pulsation (see Baker & Kippenhahn 1965; and Deupree 1977 for references). For hotter temperatures a blue edge is encountered when the helium ionization zone is found too far out in the atmosphere for significant pulsations to occur. Further details and extensive references can be found in the monograph on stellar pulsation by Cox (1980).

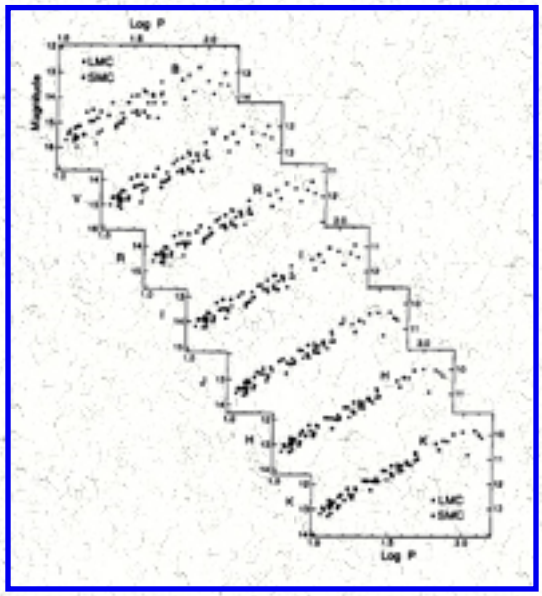

Figure 5. Magellanic Cloud Cepheid period-luminosity relations at seven wavelengths, from the blue to the infrared, constructed from a self-consistent data set (Madore & Freedman 1991). LMC Cepheids are shown as filled circles; SMC data, shifted to the LMC modulus, are shown as open circles. Note the decreased width and the increased slope of the relations as longer and longer wavelengths are considered.

5. OBSERVATIONAL CONSIDERATIONS

5.1. *General Issues*

By the 1960's the instability strip had been observed to have the following general properties: periods for Cepheids ranged from several days to a few hundred days; at constant period, the *B* magnitude total width of the PL relation was about 1.2 mag; the *V* magnitude width was measured to be about 0.9 mag; and the *(B-V)* color width was found to be about 0.4 mag, with the reddest Cepheids being the faintest at any given period. In a practical sense, this meant that in estimating distances, any individual Cepheid could deviate from the statistical ridge line by up to ± 0.6 mag in *B*; and such an error (if applied to one Cepheid) would translate into an equivalent error of about 30% in distance. Large samples can decrease the error on the apparent modulus inversely with the square root of the number; a formal error of only 10% being possible with a sample containing as few as a dozen Cepheids.

The discussion in the preceding section concerned an idealized PLC relation, expressed in its linearized form. Some of the difficulties encountered in the empirical calibration of this relation will be discussed in the present section. We concentrate on extragalactic studies. And so we do not discuss the issue of how best to determine independent distances and independent reddenings for the Galactic population of classical Cepheids: as plentiful as they are, Galactic Cepheids in the field are problematic, while only a handful of (short-period) Cepheids are contained in open clusters, which are generally sparsely populated, and often heavily obscured. The interested reader is however referred to the recent papers by Fernie (1990), Fernie & McGonegal (1983), Feast & Walker (1987) and Jacoby *et al.* (1992) for a pathway into the literature on this Galactic approach to the calibration.

Because they are nearby, and because of the large numbers of Cepheids cataloged in them (Payne-Gaposchkin 1971, Payne-Gaposchkin & Gaposchkin 1966), the Magellanic Clouds have long been the testbed for calibrations of the period-luminosity and period-luminosity-color relations. Indeed, the original discovery of these relations was made in the Magellanic Clouds (Leavitt 1906). These same large samples allowed the first estimates of the slope of the PL relation and first approximations to the period and color dependences of the PLC. Now with a number of analyses of the geometric expansion parallax to the LMC via the remnant of Supernova 1987A there are geometric distance modulus estimates of 18.50 0.13 mag (Panagia *et al.* (1991), 18.38 ± 0.07 mag (Schmidt-Kaler 1992), 18.52 ± 0.13 mag (McCall 1993), 18.61 ± 0.11 mag (Crotts *et al.* 1995), < 18.37 ± 0.04 mag (Gould & Uza 1997) for the LMC. While the precision of this measurement might be expected to improve with time as the expansion continues to be monitored, the systematics (assumptions about ring geometry and placement of the SN with respect to the main body of the LMC, etc) will soon dominate the solution. Nevertheless, it is reassuring that the majority of the determinations agree extremely well with alternative estimates of the LMC distance modulus, and that an independent check of the zero point (at the 10-15% level) is provided by the measurement of RR Lyrae distances (*e.g.*, Reid & Freedman 1994), which also are in good agreement with the Cepheids (for more recent reviews see Westerlund 1990, 1997 and references therein).

For work on the distance scale, the existence of a statistical relation between period and luminosity is of

such great utility by itself, that it is of little wonder that concern about second-order effects in the calibration (*i.e.*, those aspects above and beyond establishing the slope and zero point) were **not** of immediate import in the earliest studies. Some of these issues are: the origin of the scatter in the PL relation; the systematic effects of reddening; the systematic effects of metallicity (*e.g.*, Gascoigne 1974; Stothers 1983; Freedman & Madore 1990), companions (*e.g.*, Madore 1977; Coulson *et al.* 1986); CNO abundance, helium abundance and mass loss (*e.g.*, Lauterborn *et al.* 1971; Lauterborn & Siquig 1974; Cox *et al.* 1978; Becker & Cox 1982); magnetic fields (*e.g.*, Stothers 1982); the possibility of curvature in the PL relation (*e.g.*, Fernie 1967, Sandage & Tammann 1968, 1969); the relative disposition and the slopes of the red and blue edges of the instability strip (Fernie 1990), and the physical origin of these constraints (*e.g.*, Iben & Tuggle 1972a, b; 1975; Chiosi, Wood, Bertelli & Bressan 1991), *etc*. Unfortunately, several of the corrections to be considered are probably manifesting themselves simultaneously, and at the same level of numerical significance.

Before we can approach an empirical determination of the coefficients in the PLC (or any determination of their variation with metallicity) we must solve the reddening problem. While theory predicts a finite width to the instability strip (with temperature/color being the controlling parameter), and while metallicity is a quantity that is known to be different from galaxy to galaxy (and it is known to vary systematically within individual galaxies), only when reddening has been accounted for can we go on to look for meaningful correlations of luminosity residuals with intrinsic color and/or metallicity, for instance. To decouple and solve for the effects of metallicity, reddening, and intrinsic temperature variations, high precision photometry is a prerequisite, and at least as many independently measured quantities are needed as there are parameters to be determined.

5.2. *Reddening*

Interstellar grains, within our Galaxy, along the line of sight to a nearby galaxy, or within the galaxy being studied, will each result in light being selectively scattered and absorbed. If any one of these components of extinction is not accounted for, a Cepheid in an external galaxy will appear fainter and more distant than it actually is, and at the same time it will appear redder and cooler than it truly is. Systematic errors will thereby creep into the distance scale.

Accounting for the Galactic foreground component associated with dust in the plane of our own Milky Way is relatively straightforward and will not be discussed here in any detail. The use of foreground stars and/or reddening maps, generated from galaxy counts in combination with neutral hydrogen studies (see Burstein & Heiles 1984) appears to be quite reliable and is widely used. Since most external galaxies subtend an angular size small in comparison to expected variations of extinction across the line of sight, and since most extragalactic studies are also done at fairly high Galactic latitudes, these foreground Galactic extinction corrections are relatively small and of low variance.

Dealing with the reddening internal to the parent galaxy itself is more problematic. In the earliest studies it was simply ignored. Even if this simplification had proven true for the first few specific cases, there is no reason to believe that it would have obtained in general.

To illustrate the systematic effects of reddening on the observed PL and PLC relations, we consider the following example. Suppose for the moment that the instability strip is intrinsically very narrow both in color and in magnitude at fixed period. Now consider a sample of Cepheids drawn from this strip in a nearby galaxy, where on average the reddening is $E\ (B\text{-}V) = 0.2$ mag, with a standard deviation of ± 0.1 mag. These stars, differentially obscured, would be observed to have a period-color relation with a full (± two-sigma) color width of ~ 0.4 mag, a B period-luminosity relation with a magnitude width of 1.7 mag and a V period-luminosity relation with a width of 1.3 mag (for a ratio of $A_V / E\ (B\text{-}V) = 3.3$). As ``predicted" from a general consideration of the theoretical PLC, the deviations in the period-luminosity relation would be found to be correlated, with residuals from the period-color relation, apparently confirming the theory. But none of this correlation would be intrinsic, of course, despite it being very well defined. Unfortunately too, solutions for distances would be systematically in error since the ridge line of the data (defining the mean PL relations) would be displaced from the intrinsic strip by $A_B = 4.3\ E\ (B\text{-}V)$, always towards larger apparent distances.

The above example is extreme, but it illustrates the point that any attempt to disentangle the effects of differential reddening and true color deviations within the instability strip must rely first on a precise and *thoroughly independent* determination of the intrinsic structure of the Period-Luminosity-Color relation. In order to achieve that calibration high-quality, independent reddenings and distances to individual calibrator Cepheids must be available. The uncertainty involved in undertaking this first step will affect all future results based on those assumptions. Below we discuss old methods that have been adopted to deal with the reddening problem, and emphasize new methods that have been brought to bear with the introduction of panoramic, digital detectors operating at optical and now at near-infrared wavelengths.

5.3. *Metallicity Sensitivity of the PL Relation*

The chemical composition of a star plays a role in setting the rate of energy generation, it affects the evolution off of the main sequence, and it determines the wavelength distribution of the emergent flux. The role of metallicity in the evolution of individual Cepheids in specific, and for the forms of PL, PC and PLC, in general, has been a matter of conjecture and debate for several decades now. Stothers (1988) reviewed the theoretical aspects of this problem in great detail, concluding that at blue wavelengths the effect could be of concern to the distance scale. While the effects are generally conceded to be smaller at longer wavelengths, only recently has strict attention been paid to quantifying the effects of metallicity for near-infrared bandpasses.

Two independent physical mechanisms contribute to the effect of metallicity on the mean color of Cepheids. First of all, it is expected that the observed colors of Cepheids should vary (in a wavelength-dependent way) as a function of differing amounts of atmospheric metal-line blanketing. In addition, changes in the mean metallicity of the star as a whole are predicted to affect the interior opacities, resulting in equilibrium radius changes and different mean surface brightnesses (effective temperatures) for the same nuclear-generated luminosity. Detailed studies suggest however, that the effect of metallicity on the observed colors is largest for atmospheric line blanketing, compared to changes forced

upon the interior structure of the star.

The most recent self-consistent modeling effort is that of Chiosi *et al.* (1993). These authors produced linear nonadiabatic pulsation calculations for a grid of Cepheid models with a range of masses, various effective temperatures, and chemical compositions ranging from 1/4 to solar metallicity, for a variety of mass-luminosity relations. The theoretical fluxes were then convolved with the $UBVR_cI_c$ passbands for comparison with observations. These authors conclude that the agreement between theory and observation is best at longer wavelengths, noting a discrepancy between the observed and predicted (B-V, Log P) relations between the SMC, the LMC, and the Galaxy. Their predicted uncertainty of the true distance modulus, after correcting for reddening, is δ (m-M) = -1.7 δ Z (at log P = 1.0). Hence, for the entire range of chemical compositions represented by the low-metallicity SMC (Z = 0.004) and the solar-metallicity Galactic Cepheids (Z = 0.016), a very small abundance effect (amounting to only 0.02mag, full range) is predicted.

The predictions of Chiosi *et al.* (1993) are consistent with the results of a test of the metallicity sensitivity of the Cepheid PL relation by Freedman & Madore (1990). These authors undertook the first empirical test of the metallicity sensitivity of the PL relation by observing samples of Cepheids in three fields at differing distances from the nucleus of M31. The observational test is differential, and thus independent of any absolute metallicity calibration. From multiwavelength (BVRI) observations, true distance moduli and reddenings were determined for each of the three fields. The range in metallicity over the three fields is approximately a factor of 5. Large (0.80 mag) differences were found between the *apparent blue* moduli, whereas the maximum differences in the *apparent I-band* moduli amounted to only 0.3 mag. After correcting for reddening, a small (0.3 mag peak-to-peak) range in the true distance moduli was found, having low overall statistical significance, but still in the same sense as predicted by theory.

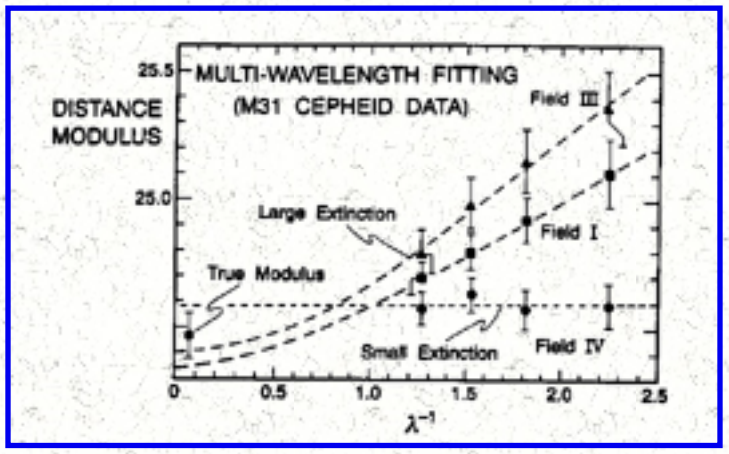

Figure 6. Multiwavelength fits of normal reddening lines to *BVRI* apparent distance moduli for M31 Cepheids (Freedman & Madore 1990). The three fields in M31 have distinctly different average reddenings associated with them, however the true modulus, as given by the intercept at $1/\lambda = 0$ is quite stable, indicating little residual sensitivity of the Cepheid PL relation to metallicity.

Despite the good agreement with the predictions of Chiosi *et al.* (1993), the results of Freedman & Madore (1990), are smaller (by about a factor of 3) than earlier predictions by Stothers (1988) for B and V-band photometry. Subsequently, the Freedman & Madore (1990) data have been reanalyzed by Gould (1994), who concludes that the M31 data are consistent with a larger metallicity dependence. However,

see Chiosi *et al.* (1993) for their cautionary remarks about the predictions from (B-V) photometry. Furthermore, a large metallicity dependence for the Cepheid PL relation does not appear to be consistent with the very good agreement of the (lower metallicity) Population II distance indicators (*e.g.* RR Lyraes and first ascent red giant branch (TRGB) stars) to be discussed later.

While the importance of metallicity effects is still not totally resolved, all theoretical models to date predict that at progressively longer wavelengths, the effects of metallicity differences should be very small. We are currently completing a five-year program in which we hve obtained JHK near-infrared array photometry of the Freedman & Madore sample of M31 Cepheids (Freedman, Madore & Sakai 1998, in preparation.) The longer wavelength baseline added to the optical data will offer much tighter constraints on this empirical metallicity calibration. As a further check of the metallicity sensitivity of the PL relation, the M31 test has been carried over to 2 fields in M101 (Kennicutt *et al.* 1998) as part of the Key Project on the Extragalactic Distance Scale. Once again the test indicates that as far as the methodology of using V and I-band data to determine extinction-corrected moduli, the metallicity effect is small, on the order of $\delta (m\text{-}M)_0 / \delta [O/H] = -0.24 \pm 0.16$ mag/dex. Even at this level of dependence it is to be emphasized that the resulting effect on the distance scale will only amount to a few percent. This is so because the LMC metallicity (-0.4 dex) is very close to the mean metallicity of the galaxies being observed in the Key Project (-0.3 dex). Obviously individual distances of galaxies with metallicities significantly larger or smaller than the metallicity of the LMC will systematically deviate (if not corrected for metallicity) but no large bias is expected in the mean. Obviously, NICMOS data would be extremely valuable in dealing with this issue empirically.

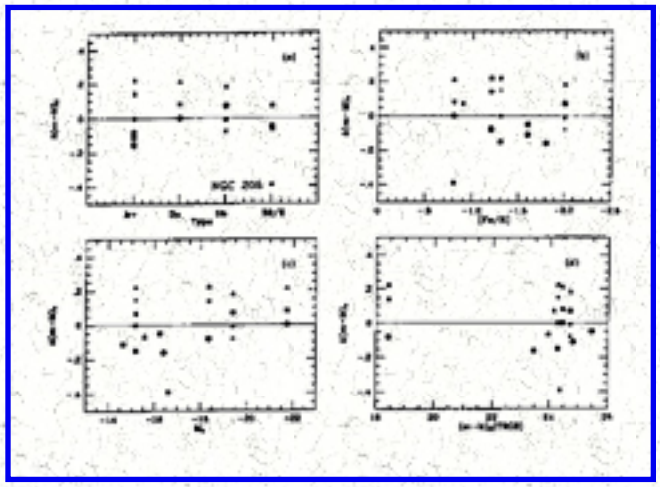

Figure 7. A differential comparison of distance moduli determined from the Population I Cepheid PL relation and the Population II TRGB magnitude as a function of Hubble type of the parent galaxy (upper left) absolute magnitude of the parent galaxy (lower left), the TRGB modulus (lower right) and finally the metallicity of the parent galaxy (upper right). Within the scatter no trends are apparent, especially with metallicity. (adapted from Lee, Freedman & Madore 1993)

6. ADVANCES DRIVEN BY NEW TECHNOLOGY

6.1. *Application of Near-Infrared Techniques*

Although the first near-infrared observations of Galactic Cepheids were made nearly 30 years ago (Wisnewski & Johnson 1968) their applicability to the distance scale was not appreciated until quite recently. In the first of a series of papers, McGonegal *et al.* (1982) unambiguously demonstrated that once periods were adopted from optical data, near-infrared observations of Cepheids provided a number

of distinct advantages.

It was, of course, anticipated that by going to the infrared concerns about total and/or differential reddening would be significantly reduced. For instance, a blue extinction of $A_B = 0.32$ mag (typical for Cepheids in the LMC, for instance) would translate to a total correction of $A_K = 0.05$ mag at 2.2 μm; the full correction in the near infrared being comparable to the uncertainty alone associated with most optical extinctions!

But it was also immediately clear from the outset (see for example Figure 5) that the infrared had other advantages directly applicable to the establishment of the Cepheid distance scale. First of all, the decrease in the observed width of the PL relation was dramatic. Even single observations of the Magellanic Cloud Cepheids, (uncorrected to mean light) produced a PL relation with remarkably small scatter (± 0.2 mag). This narrowing of the width is due to two effects: a decreased sensitivity to differential reddening, but more significantly, due to a much decreased sensitivity of the infrared surface brightness to the temperature width of the instability strip. For exactly the same reason, the amplitudes of individual Cepheids (shown in Figure 1, as plotted earlier by Wisnewski & Johnson 1968) also decrease with the wavelength of the observations. Thus, Cepheids observed at long wavelengths and at random points in their cycle are **(1)** closer to their time-averaged mean magnitudes than the equivalent observation in the blue, and **(2)** the mean magnitudes themselves are in fact coming from a narrower projection of the instability strip into the infrared plane than the equivalent blue PL relation. From *B* to *K*, a typical Cepheid amplitude drops from 1.0 mag to 0.4 mag, while the width of the PL relation decreases from 1.2 mag to 0.5 mag. As a result, for distance determinations even single, random-phase observations of known Cepheids, when made in the near-infrared, are comparable in accuracy to complete time-averaged magnitudes (derived from a dozen or more observations) in the blue.

The periods for many extragalactic Cepheids had already been determined and published from photographic studies made at blue wavelengths in many long-term studies by Hubble, Baade, Sandage, Swope, Payne-Gaposchkin, Gaposchkin and others. As a result, in only a matter of nights, it was possible to reobserve the entire galaxy sample in the near infrared and thereby provide new accurate distances, almost unaffected by absorption effects.

However, until recently, with the advent of near infrared arrays, there have been limitations in the application of the IR to the Cepheid distance scale, even for nearby Local Group galaxies. Single-channel infrared detectors, available at the outset, were aperture devices which had to be ``chopped", ``on" and ``off" the source in order to continuously monitor the intense and fluctuating terrestrial sky contribution to the signal. For Galactic Cepheids, and even for those in the Magellanic Clouds, a typical aperture of 5 arcsec could be placed over a star and chopped to a nearby reference region a few arcseconds away with relatively small uncertainty. However, for Cepheids at larger distances, the near-infrared observations of Cepheids in M31 (Welch *et al.* 1986) and M33 (Madore *et al.* 1985) show much more noise than could be attributed to photon statistics alone. The most likely source of error is crowding and confusion; that is, contamination in one of the two comparison fields where ``skies" were being measured, or contamination in the object aperture itself. Although no systematic error is expected

from this contamination, the random errors are appreciable. New observations are being obtained with near infrared InSb and HgCdTe arrays and two-dimensional image analysis is allowing more accurate infrared magnitudes to be measured in M31 and M33.

7. CCDs AND MULTIWAVELENGTH COVERAGE

Much was learned from the early near-infrared observations that could be applied to optical observations, given accurate data gathered over a sufficiently broad wavelength range. CCDs provided just that opportunity, bridging the development gap slowly being filled by the relatively small-area IR arrays. Given a wavelength sensitivity running from the *B* band (0.45 μm) to the *I* band (0.7 μm), CCDs afford the opportunity to gather seeing-limited, panoramic, digital data, which can subsequently be reduced using local sky subtraction and point-spread-function fitting techniques, to derive accurate magnitudes and colors. Crowding and confusion errors can be dealt with at the one square-arcsecond level. Use of CCDs and near-IR arrays decrease the areal confusion by about an order of magnitude over the near-infrared apertures.

CCDs also offer the advantage of a large wavelength coverage, thereby allowing an explicit determination of the reddening from the optical data itself. In this case, it is not necessary to rely purely on foreground estimates and/or on assuming that additional reddening is of negligible importance. Given a knowledge of the interstellar extinction law as a function of wavelength it is possible to fit all of the data simultaneously. Freedman (1988b) introduced this new approach to determining true moduli for extragalactic Cepheids using multiwavelength data, applying it first to single-epoch observations of Cepheids in IC 1613, and later refining it and expanding its application to data obtained for M31, M33, and NGC 300 as cited below. For a detailed discussion of the technique and its implementation the interested reader is referred to those papers. Briefly stated, one determines differential apparent moduli, scaled against the corresponding LMC PL relations. By assuming that all of the difference as a function of inverse wavelength can be attributed to selective absorption, fitting an interstellar extinction law to the data simultaneously estimates the total (foreground plus internal) absorption and the true distance modulus, relative to the LMC.

In the following, we briefly review the systematics of the PL relation as observed at wavelengths ranging from the blue to the near-infrared. To do this, we concentrate on self-consistent data sets assembled for this purpose by Madore & Freedman (1991) and plotted in Figure 5. The stars included in this compilation are Cepheids in the LMC and SMC for which there are time-averaged mean magnitudes at all seven wavelengths (excluding R for the LMC sample which largely lacks this bandpass in published Cepheid observations). Note that the slope and the dispersion of the PL relation change systematically as a function of the effective wavelength of the filter bandpass. These impressions are quantified in the equations presented at the end of Section 8. In any case, as the longer-wavelength data are considered, it is clear that both quantities (slope and dispersion) have already begun to converge on an asymptotic value (set by the period radius relation, which because of its geometrical nature is largely wavelength independent). From this point of view it makes no practical sense to observe Cepheids at

wavelengths much beyond 2 μm if the aim is to decrease the dispersion in the observed PL relation. Fortunately, this regime is still accessible from the ground and is not far into the thermal IR where background effects become extremely large.

For comparison, we show the rate of fall-off in the monochromatic extinction as a function of wavelength scaled to the blue extinction. As is well appreciated, the extinction does continue to decrease with increasing wavelength, making it sensible to extend the observations as far into the infrared as is practical. Of course, a decrease in extinction by a factor of over 5 is realized at K in comparison to B, so for most purposes this too is a reasonable wavelength at which to stop the effort.

The impact of panoramic linear detectors, such as the CCD, on the study of extragalactic Cepheids has been significant. It is now possible to obtain from the ground, high-quality light curves of Cepheids in galaxies 2 Mpc away, ranging from blue and visual wavelengths, as well as reaching out to nearly one micron with CCD detectors, and then extending to 2.2 μm with the newly available HgCdTe and InSb infrared areal detectors. With HST, the distances reached have now exceeded 20 Mpc, and NICMOS is being applied to a number of these galaxies in follow-up studies in the near infrared.

8. OBTAINING ACCURATE CEPHEID DISTANCES

Once new extragalactic Cepheids are found, at least four issues need to be adequately addressed, all of which are tightly coupled to common sets of observations: (1) Periods have to be determined, (2) Complete light curves have to be delineated, (3) Mean magnitudes must be derived, and finally, (4) Accurate colors are required for reddening determinations. Needless to say, it would be hard to derive (1) the periods (or prove that a star is in fact a Cepheid) without (2) the light curves; and vice versa. Similarly, (3) and (4), accurate mean magnitudes and colors generally depend on correct period-phasing and proper lightcurve fitting. But the requirements for accurate periods are in fact quite different from the requirements for accurate magnitudes. The number of data points required to yield a time-averaged magnitude (of specified precision) increases as the square of the lightcurve amplitude. This makes colors and mean magnitudes based on short wavelength observations more costly in observing time than their longer-wavelength counterparts. On the other hand, for fixed photometric uncertainties, periods increase in accuracy almost linearly with the time interval over which the observations are spaced. Furthermore, periods good to a few percent can be obtained using only moderately accurate photometry after only a dozen or so cycles, thereby making the time constraint a minimal one.

Finally, one must contend with the intrinsic width of the instability strip as projected into the PL relation. Increasing N, the numbers of Cepheids is the most obvious solution here. For the B-band the equivalent dispersion in magnitude in the Cepheid PL relation is ± 0.35 mag. The error in the mean apparent distance modulus decreases like $\sqrt{N}$. In the absence of reddening then it would appear that for *apparent* distance moduli alone, a dozen Cepheids will give the requisite accuracy in the mean. But of course the real problem, once again, comes when trying to deal with reddening. And an example using two band-passes only illustrates this graphically. In such a case, the ensemble-averaged extinction essentially comes from differencing the mean apparent moduli found at two different wavelengths.

Multiplying this difference by the ratio of total-to-selective extinction appropriate to those two wavelengths and subtracting the product from the mean apparent modulus gives the final true modulus. If 10% in distance is the goal (0.2 mag in true modulus), then for the filter combination *VI*, simple arithmetic shows that two to three dozen Cepheids are required to establish the mean moduli to such a degree that the reddening corrected modulus has a final error of less than 0.2 mag. Of course, either increasing the number of wavelengths and/or increasing the wavelength baseline will each reduce the final error on the mean without demanding an increase in sample size.

In closing this section, we present our adopted fiducial multiwavelength PL relations. We emphasize that these relations differ slightly from those published by other workers up to this point, because they are derived from sets of data which are now totally self-consistent. Specifically, all of the PL relations are based on the same stars in order to eliminate sample-dependent variations in the solutions. Furthermore, Cepheids with log P > 1.8 are excluded from the least-squares fits due to uncertainties in their reddenings and their evolutionary status. The LMC data set (scaled and dereddened as outlined in the next section) has been chosen as fiducial because of its large sample size, large wavelength coverage and because the LMC is very close to being face-on, thereby minimizing the effects of back-to-front geometry on the solutions. The relations are centered on $log\ P = 1.0$, the mid-point of the range of periods considered here. Errors on the quoted coefficients are given after each of the values. Following each of the PL relations, the quantity in square brackets is the rms dispersion about the mean for that relation.

$M_B = -2.43\ (\pm 0.14)\ (log\ P - 1.00) - 3.50\ (\pm 0.06)\ [\pm 0.36]$
$M_V = -2.76\ (\pm 0.11)\ (log\ P - 1.00) - 4.16\ (\pm 0.05)\ [\pm 0.27]$
$M_R = -2.94\ (\pm 0.09)\ (log\ P - 1.00) - 4.52\ (\pm 0.04)\ [\pm 0.22]$
$M_I = -3.06\ (\pm 0.07)\ (log\ P - 1.00) - 4.87\ (\pm 0.03)\ [\pm 0.18]$

[Note that the *RI* magnitudes are on the Cousins system, while our *JHK* magnitudes are on the CIT/CTIO system. There are 32 LMC Cepheids for which *BVI* photoelectric photometry is available in the range $0.2 < log\ P < 1.8$. *R* photometry is not available for many of the stars used above; however, *R* magnitudes were derived using the methodology set out in Freedman (1988b).]

Finally, we give below consistent PL solutions, based on a smaller set consisting of only 25 LMC stars, each of which has *BVRIJHK* photometry available (given the same conditions outlined above):

$M_B = -2.53\ (\pm 0.28)\ (log\ P - 1.00) - 3.46\ (\pm 0.12)\ [\pm 0.40]$
$M_V = -2.88\ (\pm 0.20)\ (log\ P - 1.00) - 4.12\ (\pm 0.09)\ [\pm 0.29]$
$M_R = -3.04\ (\pm 0.17)\ (log\ P - 1.00) - 4.48\ (\pm 0.08)\ [\pm 0.25]$
$M_I = -3.14\ (\pm 0.17)\ (log\ P - 1.00) - 4.84\ (\pm 0.06)\ [\pm 0.21]$
$M_J = -3.31\ (\pm 0.11)\ (log\ P - 1.00) - 5.29\ (\pm 0.05)\ [\pm 0.16]$
$M_H = -3.37\ (\pm 0.10)\ (log\ P - 1.00) - 5.65\ (\pm 0.04)\ [\pm 0.14]$

M_K = -3.42 (± 0.09) (*log P* - 1.00) - 5.70 (± 0.04) [± 0.13]

The effective wavelengths for each of the seven bandpasses were chosen to be appropriate for a G-star spectrum (see for example, Bessell 1979) where, for future reference, we have adopted: *B*(0.444 µm), *V* (0.550 µm), *R*(0.653 µm), *I*(0.789 µm), *J*(1.25 µm), *H*(1.60 µm), *K*(2.17 µm).

Finally, it should be noted that there are external checks on the Cepheid calibration and distance scale derived from it that have been applied to galaxies within the Local Group. An extensive review of these methods (including the use of RR Lyrae stars, red giant luminosity functions, novae and long-period variables, to name just a few) confirms (conservatively at the ± 0.2 mag level) the basic solidity of the Cepheid calibration (van den Bergh 1989, de Vaucouleurs 1991). For details, the interested reader is referred to those reviews and the many references cited therein. Because many of these independent methods that provide checks on the Cepheid distance scale use intrinsically fainter stars, it is unlikely that galaxies significantly beyond the Local Group will be of much use in further refining the agreement (or disagreement) between the various estimators. However, more extensive and more precise observations of those same (faint) distance indicators within these and other Local Group galaxies will be crucial for fine tuning the calibration, and may be especially helpful in establishing the level at which metallicity corrections are needed in Population I and Population II distance indicators alike.

9. LOCAL GROUP GALAXIES

We now quickly review the status of the individual galaxies in the Local Group for which (non-photographic) digital data on known Cepheids have been obtained in the last few years. This discussion and that in the next section update and supersede similar overviews published earlier by Madore (1985) and Walker (1987).

For the LMC, we adopt hereafter 18.5 mag for its true modulus and 0.10 mag for *E (B-V)*, and scale all other Cepheid-based distances assuming a value for the total-to-selective absorption of $R_V = A_V / E\ (B-V) = 3.3$ (appropriate for the later spectral types of Cepheids). In a later section we discuss the impact of recent parallax observations of Galactic Cepheids by the Hipparcos satellite, and conclude that these calibrations are consistent at the 10% level. All period-luminosity fits are done over the range $0.2 < \log P < 1.8$. Furthermore, as discussed in Freedman (1988b), all fits are carried out for a self-consistent set of stars in the LMC defined by the simultaneous availability of photometry at *B, V and I* wavelengths. Although the sample of Cepheids with *B* and *V* photometry alone is about a factor of two larger, the comparison of inconsistent data sets can lead to erroneous results. It should be noted that although we quote the sources of original data throughout the next two sections, *the distances and reddenings given for each galaxy here are based on a new and homogeneous application of the multiwavelength fitting procedures* discussed earlier in this review (and described in detail in Freedman *et al.* 1991). In this procedure, we have adopted the reddening law as determined by Cardelli *et al.* (1989). By definition, our multiwavelength fitting procedure does not yield information about the distance and/or reddening to the LMC, as they are adopted *ab initio*. For completeness, we also review data for Cepheids in the

Magellanic Clouds.

9.1. *The Magellanic Clouds*

For a relatively complete bibliography of modern photographic and photoelectric observations of Magellanic Cloud Cepheids, the reader is referred to Tables 2 and 4 in Madore (1985); they will not be repeated here. Moreover, Caldwell & Laney (1991) have reviewed progress in the southern hemisphere on calibrating the Cepheid PL relations. They use data available in Madore (1985), in addition to more recently published near-infrared *JHK* data available for many dozens of Cepheids observed by Welch *et al.* (1987) and also Laney & Stobie (1986a, b). Similar to Welch & Madore (1984), these latter papers concentrate, among other things, on using the near-infrared data to determine the back-to-front geometry of the two Magellanic Clouds based on the ability of near-infrared observations of Cepheids to give extremely precise distances to individual stars. In this regard, it should be noted that Visvanathan (1989) has calibrated the Cepheid PL relation at 1.05 μm and applied it to Cepheids in the SMC (Mathewson *et al.* 1986, 1988), also aiming to probe the structure of the SMC in the context of a tidal encounter/ disruption model.

9.2. *IC 1613*

Sandage (1971) published photographic light curves and periods for 25 of the confirmed Cepheids discovered, but never published, by Baade. Both single-phase, near-infrared *H*-band observations of 10 of those Cepheids (McAlary, Madore & Davis 1984) and single-phase, multiwavelength *BVRI* observations (Freedman 1988b) of 11 of them have now been published. Freedman's work incorporated the near-infrared data. Using the new fitting procedure (rather than an earlier adopted linear extinction approximation), and excluding the lower-accuracy *H* band data, yields a total mean reddening of $E(B-V) = 0.02$ mag, and a true modulus of 24.42 ± 0.13 mag, corresponding to a distance of 765 kpc. To maintain homogeneity for comparison of relative distances, this value supersedes the distance modulus 0.12 mag lower, quoted by Freedman (1988b).

It is also worth noting at this point that Freedman's (1988b) conclusions concerning the universality of the slope of the PL relation (once brought in to some degree of doubt because of the uncertainties in the faint-magnitude calibration of the photographic data on the IC 1613 Cepheids) have subsequently been bolstered by the additional analysis of 16 newly confirmed Cepheids in IC 1613, as discussed in Carlson & Sandage (1990).

In comparison to any other member of the Local Group, IC 1613 offers the best opportunity for a ground-based telescope to provide a definitive calibration of the multiwavelength period-luminosity relation for Classical Cepheid variables. It is nearby and therefore offers the opportunity for accurate photometry; it has very low foreground (and internal) extinction and yet it is distant enough that back-to-front effects are negligible. Finally, IC 1613 (and its Cepheid population) is metal poor, both in an

absolute sense and with respect to the Galactic Cepheids in clusters. Comparison of a low-metallicity calibration through IC 1613 with the high-metallicity calibrations through the LMC and Milky way, respectively, may shed additional light on the metallicity sensitivity of the Cepheid PL relation zero point.

9.3. *NGC 6822*

One of the most extensive studies of the dwarf irregular Local Group galaxy NGC 6822 is the photographic work of Kayser (1967). This study built on the original work of Hubble (1925) who found several Cepheids and a number of bright irregular variables in this galaxy. Unfortunately, NGC 6822 is fairly close to the Galactic plane (b = -18 degrees), resulting in large, and still somewhat uncertain, foreground reddening estimates. Published estimates for the reddening to the Cepheids in NGC 6822 range from $E\ (B\text{-}V)$ = 0.19 to 0.42 mag.

Results on the Cepheid distance to NGC 6822 have been appearing slowly. Both Hodge (1977), and then van den Bergh & Humphreys (1979) have reported photoelectric *BV* observations of the 65-day Cepheid, V7 in NGC 6822. Multiwavelength *BVRI* CCD data have been obtained by the authors, but are as yet unpublished; while Schmidt, Spear & Simon (1986), Schmidt & Spear (1987), Schmidt & Simon (1987), and Schmidt & Spear (1989) have published some CCD observations of Cepheids in NGC 6822, which were obtained for other reasons. Of late, the only directed study of the Cepheid distance to NGC 6822 is the paper by McAlary *et al.* (1983) on near-infrared *H*-band aperture photometry of 9 Cepheids. Unfortunately, an independent determination of the foreground/internal reddening was not attempted because only one wavelength was involved in the new study. Visvanathan (1989) observed three Cepheids in NGC 6822 once each at 1.05 μm and derived a true modulus of 23.26 mag (scaled to an LMC true modulus of 18.5 mag). On the other hand, random-phase *I*-band CCD data (Lee, Freedman & Madore 1993) yield a true modulus of 23.59 mag.

Pending complete publication of the new CCD data, we can use the photographic observations of Kayser (1967) in combination with the *H*-band observations of McAlary *et al.* (1983) to provide a multiwavelength fit and solve for the true distance modulus and reddening to NGC 6822. In this application we have rederived all apparent moduli with respect to our internally self-consistent set of LMC Cepheid data. Excluding Kayser's variable No. 30 (which falls many sigma above the mean B PL relation), we find $(m\text{-}M)_B$ = 24.66 ± 0.06 mag, $(m\text{-}M)_V$ = 24.50 ± 0.08 mag and $(m\text{-}M)_H$ = 23.77 ± 0.17 mag, resulting in $(m\text{-}M)_0$ = 23.66 mag with $E\ (B\text{-}V)$ = 0.26 mag. The reddening is well within the range of previous estimates quoted above and is remarkably close to Kayser's original estimate of 0.27 mag. Despite this formal solution, it was clear that the Cepheids in NGC 6822 could profit from a modern investigation at several wavelengths. Accordingly, Gallart *et al.* (1996) using single-phase (multiwavelength) CCD data of the Cepheids in NGC 6822 have derived a new estimate of distance and reddening. They have also compared their result with the the distance calculated using the tip of the red

giant branch as a distance indicator. A distance modulus of $(m\text{-}M)_0 = 23.49 \pm 0.08$ mag and a reddening of $E\ (B\text{-}V) = 0.24 \pm 0.03$ mag are derived.

9.4. *M33*

Hubble (1926) discovered 35 Cepheids in the inner regions of M33 and determined their periods. These photographic data were later recalibrated by Sandage (1983). Sandage & Carlson (1983a) added identifications, periods and photographic mean magnitudes for 13 new Cepheids in an outer region of this galaxy, while Kinman, Mould & Wood (1987) then surveyed the main body of M33 using photographic plates taken at the prime focus of the KPNO 4m in search of long-period variables, and in the process discovered 54 new Cepheids. All four of these publications include finder charts for their variables.

Building on these discovery papers, single phase *H*-band observations (Madore *et al.* 1985) were made of 15 Cepheids in M33. These were then augmented by and incorporated into a multiwavelength study of 19 Cepheids (Freedman, Wilson & Madore 1991) using CCD observations to obtain light curves and therefore time-averaged magnitudes and colors. It was the *H*-band study of the M33 Cepheids that first noted the basic limitation due to crowding and confusion on the application of aperture techniques to the infrared Cepheid distance scale. *JHK* array imaging of individual Cepheids in M33 and M31 is being done by the authors using the Palomar 200-inch, so some of those early limitations should soon be lifted. Until those data are available, the CCD observations alone indicate that for M33, $A_B = 0.41$ mag and the true modulus is 24.63 ± 0.09 mag, corresponding to a linear distance of 840 kpc.

9.5. *M31*

Baade & Swope (1963, 1965) and Gaposchkin (1962) used 200-inch plate material to catalog Cepheid variables in M31. With the exception of the outermost Field IV (for which there is both *B* and *V* data) only blue photographic magnitudes are available, making reddening estimates for the Cepheids both circumstantial and rather unreliable. Nearly a quarter of a century later Welch *et al.* (1986) obtained single-phase *H*-band observations of 22 Cepheids in M31. More recently, Freedman & Madore (1990) have published multiwavelength PL relations for 38 Cepheids in three of the Baade & Swope M31 fields resulting in independent reddenings and true distance moduli for each of the regions. A consistent true distance modulus of 24.44 ± 0.10 mag (corresponding to 770 kpc) is determined here with mean reddenings ranging from $E\ (B\text{-}V) = 0.00$ mag in Field IV to 0.25 mag in Field III. Those data are shown plotted in Figure 6.

10. BEYOND THE LOCAL GROUP

To discover Cepheids in galaxies, and then confidently determine their periods, light curves, mean magnitudes and colors is an extremely demanding task. So it is perhaps not too surprising that although

Cepheids in galaxies as far away as M81 were known to Baade in the early 1960's, up until the 1980's the only major galaxy outside of the Local Group for which a definitive study had been published of its variable star content was the solitary, late-type spiral galaxy, NGC 2403 (Tammann & Sandage 1968). Only in the last decade have CCD surveys begun to come to the fore, as the last of the photographic surveys for Cepheids in galaxies easily resolved from the ground, are now being published. CCDs have small fields of view, but they have significantly higher quantum efficiency than photographic emulsions, especially at longer wavelengths. Accordingly, they are in fact allowing significant progress to be made in searching for Cepheids in the few remaining galaxies near enough to be resolved from the ground. Progress on those fronts is now reviewed.

10.1. *NGC 2403*

Morphologically very similar to M33 (and its southern counterpart NGC 300) NGC 2403 is a highly resolved late-type spiral galaxy often associated with M81 and a handful of lower luminosity spiral and irregular galaxies (*e.g.*, de Vaucouleurs 1975). Many dozens of photographic plates taken by Mount Wilson and Palomar observers were searched for variables by Tammann & Sandage (1968) resulting in the discovery of 17 Cepheids. Due to plate limitations, only the brightest Cepheids in the outer parts of the galaxy were found. Even so, only the brightest parts of the blue light curves were securely calibrated and only fragmentary information was available in the visual bandpass. Nevertheless, good periods were determined by these authors and (assuming no extinction within NGC 2403 itself) an apparent modulus was estimated from the brightness of the apparently least reddened Cepheid seen at maximum light. These data have been re-analyzed by Madore (1976) and then by Hanes (1982) and again by Rowan-Robinson (1985) with different sets of assumptions, and consequently diverging conclusions. New data were obviously required before significant progress could be made beyond arcane arguments concerning methodology.

I-band CCD observations of 8 of the known Cepheids in NGC 2403 are discussed by Freedman & Madore (1988) who derive a tentative true modulus of 27.51 mag. Their adopted error of ±0.24 mag includes the uncertainty for the still undetermined amount of reddening internal to NGC 2403 itself. Given what we now know about the difficulties inherent in doing near-infrared aperture photometry in confusion-limited cases, the modified *J*-band observations reported by McAlary & Madore (1984) and the conclusions drawn therein, are thus superseded.

10.2. *M81*

Baade (1963) was aware that Cepheids had been detected in M81 but it was another 20 years before any results were published. Because of the high surface brightness of the disk of M81, photometry of individual stars is very difficult, making the detection of variable stars such as Cepheids extremely taxing, especially near the plate limit. Nevertheless, Sandage (1984) succeeded in determining the periods for two Cepheids in M81 using *B*-band photographic plate material. Freedman & Madore (1988)

obtained *I*-band CCD photometry of these stars (based on finder charts and periods made available by Sandage (1987, private communication), and derived a true modulus of 27.59 ± 0.31 mag adopting a foreground Galactic extinction of A_B = 0.15 (Burstein & Heiles 1984). This modulus corresponds to a distance of 3.30 Mpc which is still uncertain at the 15% level in as much as the sample is small and no corrections for reddening internal to M81 itself were included. HST observations by Freedman *et al.* (1994) yield a reddening-corrected distance of 3.6 ± 0.3 Mpc, based on 30 Cepheids discovered in two fields (one along the major axis of M81, the other positioned along the minor axis).

10.3. *M101*

Sandage & Tammann (1974) attempted to find Cepheids in their 200-inch photographic plate material on M101. Their failure led them to conclude that M101 has a distance modulus in excess of 29.3 mag. Later, using CCD detectors Cook *et al.* (1986) did succeed in detecting at least two Cepheids at $R \sim 23$ mag (with preliminary periods of 37 and 47 days) in a relatively uncrowded outer region of this galaxy. Given the uncertainties in the absolute zero point of the calibration of the Cepheid PL relation and the unknown extinction internal to M101 itself these data give an apparent *R*-band modulus of 29.38 mag. Other fields in M101 also observed by this group (Cook *et al.* 1989), and their results based on 4 Cepheids (Alves & Cook 1995) give a true distance modulus of 29.08 ± 0.13 mag (6.4 ±0.4 Mpc).

More recently Kelson *et al.* (1996) have used *HST* to image an outer field in M101 and discovered 29 Cepheids, from which they derive $E(B\text{-}V) = 0.03$ mag and a true distance modulus of 29.34 ±0.17 mag, corresponding to a distance of 7.4 ± 0.6 Mpc. This latter distance compares very favorably with the planetary nebula luminosity function distance 7.7 ± 0.5 Mpc derived by Feldmeier *et al.* (1996).

10.4. *NGC 300*

Graham (1984) conducted a photographic study of NGC 300 using the Tololo 4m reflector and was able to discover 18 Cepheids, determine their periods, and estimate mean *B* and *V* magnitudes. Madore *et al.* (1987) subsequently observed 2 of these Cepheids at *H*. Walker (1988) later criticized Graham's photoelectric calibration sequence and suggested a correction to the photographic photometry of the Cepheids. Visvanathan (1987) observed three Cepheids in NGC 300 at 1.05 μm, and derived a true modulus of 25.80 maag (scaled to our adopted LMC modulus). Finally, Freedman *et al.* (1991) present *BVRI* CCD observations of 16 Cepheids in NGC 300 giving revised periods and time-averaged magnitudes and colors. A true distance modulus of 26.67 mag, corresponding to a distance of 2.16 Mpc, is derived from a multiwavelength analysis of the CCD data of the 10 Cepheids with complete light curves.

10.5. *NGC 247* and *NGC 7793*

Catanzarite, Freedman, Madore & Horowitz (1998, in preparation) have found 9 Cepheids in NGC 247,

which turns out to be located at a distance that is nearly a factor of two larger than that of NGC 300. The significantly larger distance, with the ensuing crowding problems and brighter absolute magnitude cut-off in the observational data made this object far harder to determine a Cepheid-based distance than was originally anticipated. The requisite data for NGC 7793 have also been obtained and are currently being reduced.

10.6. *WLM*

A photographic study of the Wolf-Lundmark-Melotte galaxy has been published by Sandage & Carlson (1985a) where 15 Cepheids are identified and periods determined (ranging from 3.3 to 9.6 days). The CCD study of WLM published by Ferraro *et al.* (1989) unfortunately included none of the Sandage & Carlson Cepheids, but the CCD photometry does indicate that the photographic photometry is too bright by +0.4 mag in both *B* and *V* (as derived from the intercomparison of the two studies given in their Table 2.

Applying the *B* offset to the photographic data for the Cepheids in WLM and rederiving the apparent modulus as discussed above we find $(m\text{-}M)_B = 25.19$. Adopting $A_B = 0.09$ mag (Burstein & Heiles 1984), gives a true modulus of 25.10 mag. From preliminary reductions of *I*-band CCD observations of 5 WLM Cepheids, Lee, Freedman & Madore (1993) find a true modulus of 24.89 ± 0.15 mag, corresponding to a linear distance of 0.95 Mpc.

10.7. *IC 10*

Saha *et al.* (1996) reported the discovery 4 Cepheids in this galaxy and derive a true distance modulus of 24.59 ± 0.30 mag (corresponding to a distance of 830 Mpc) after correcting for $E\ (B\text{-}V) = 0.94$ mag. Wilson *et al.* (1996) then obtained *JHK* observations of these same Cepheids and derived a slightly revised true modulus of 24.57 ± 0.21 mag, giving a distance of 820 kpc. The largest uncertainty at this point must be the adopted foreground reddening correction which is considerable. A TRGB/Cepheid study of IC 10 (Sakai, Madore & Freedman 1998) is nearing completion, and should throw some light on this problematic object.

10.8. *NGC 3109*

From photographic material Demers *et al.* (1985) report discovering 5 Cepheids with periods in the range 10 to 23 days in the nearly edge-on, Magellanic-type irregular galaxy NGC 3109. Sandage & Carlson (1988) also using photographic material, but with better plate scale, were able to observe deeper into the luminosity function and determine the periods for 29 Cepheids. The periods of their Cepheids ranged from 6 to 31 days, confirming only 2 out of the 5 earlier-reported periods. Using the data from Sandage & Carlson, and adopting a foreground extinction of $A_B = 0.14$ mag from Burstein & Heiles (1984), we derive a true modulus of 25.94 mag for NGC 3109, corresponding to 1.54 Mpc. No

correction for extinction internal to NGC 3109 itself has been applied.

10.9. *Pegasus* = *DDO 216*

Hoessel *et al.* (1990) report the discovery of 31 variable stars in Pegasus, with 7 being likely Cepheids. Based on these observations they derive a distance modulus of 26.22 ± 0.20 mag, corresponding to a geometric distance of 1.75 Mpc.

10.10. *Leo A* = *DDO 069*

Hoessel *et al.* (1994) report the discover of 14 variable stars in Leo A of which only 5 had sufficient phase coverage for them to be classified as Cepheids. Based on these stars (corrected for foreground Galactic extinction) the authors derive a true distance modulus of 26.74 mag, corresponding to a distance of 2.2 Mpc, placing Leo A at the outermost edge of the Local Group.

10.11. *GR8* = *DDO 155*

Tolstoy *et al.* (1995) found a total of six variables in the dwarf irregular galaxy GR8, only one of which was classified as a Cepheid. After correcting for Galactic extinction the single star gave a distance modulus of $(m\text{-}M)_0$ = 26.75 ±0.35 mag, corresponding to a linear distance of 2.24 Mpc.

10.12. *Sextans A* and *Sextans B*

In a photographic survey of Sextans A, Sandage & Carlson (1983b) discovered 5 Cepheids whose periods ranged from 15 to 25 days. In a later paper Sandage & Carlson (1985b) recalibrated the Sextans A photometry, and added data on the adjacent dwarf-irregular galaxy Sextans B, in which they discovered 4 Cepheids having periods ranging from 7 to 28 days. However, CCD data for stars in Sextans A (Hoessel *et al.* 1983) after transforming from the original Gunn system to the BV system give a zero-point difference between the two data sets amounting to 0.2 mag. Walker(1987) then used a CCD with standard Johnson filters to study this problem further, and concluded that the Sandage & Carlson B-band data are too faint by 0.16 mag in the color range appropriate to Cepheids. With the original Sextans A data transformed to the Sextans B photometric scale as described by Sandage & Carlson (1985b), and then further corrected using Walker's offset, we derive true moduli of 25.59 and 25.64 mag for Sextans A and B, respectively, after adopting foreground extinctions of A_B = 0.06 and 0.05 mag (Burstein & Heiles 1984). The above true moduli correspond to 1.31 and 1.34 Mpc, respectively. Finally, it should be noted that for Sextans A, Visvanathan (1987) reports a true modulus of only 25.35 mag, based on single-phase 1.05 µm observations of three Cepheids.

10.13. *NGC 2366* = *DDO 042*

Tolstoy *et al.* (1996) found 6 Cepheids out of a total of 13 variables stars in this M81 Group galaxy, NGC 2366. After correcting for foreground Galactic extinction they derive $(m\text{-}M)_0 = 27.68 \pm 0.20$ mag, corresponding to a distance of 3.44 Mpc.

10.14. *M83 (= NGC 5236), IC 5152, and the Phoenix Dwarf*

Caldwell & Schommer (1990) have been monitoring the luminous southern spiral M83 for Cepheids, while Caldwell *et al.* (1988) report actually having discovered Cepheids in two southern dwarf irregular galaxies, IC 5152 and the Phoenix Dwarf, as well as in M83. No details have yet been published.

10.15. *The Centaurus Group*

Finally, it should be reported that at least two groups are attempting to discover Cepheids in the Centaurus Group. Walker (private communication) has been obtaining CTIO prime-focus CCD frames of galaxies in this cluster, but his coverage is presently insufficient to securely identify variables, and therefore no periods have yet been reported. On the other hand, Tammann *et al.* (1991) have a Key Project underway at ESO which has nine half nights used in early 1991 to begin a search for Cepheids in the Centaurus Group late-type galaxies NGC 5236, NGC 5264 and .

11. THE HUBBLE CONSTANT

Of course, while distances to individual galaxies are of value in their own right, there is a more compelling reason for undertaking this extremely time-consuming task of Cepheid discovery and calibration. That goal is the Hubble constant, a measure of the size-scale and indeed the time-scale of the Universe. This goal was deemed sufficiently important that the design of the *Hubble Space Telescope* was in large measure constrained to meet the minimum requirements needed to undertake this task from space: to discover Cepheids in galaxies well beyond the Local Group, out to and including the Virgo and Fornax clusters.

Even so, one or more secondary distance indicators are needed to get to ``cosmologically significant'' distances where the pure Hubble flow can be reliably measured. And it is generally accepted that these secondary distance indicators are best calibrated by the Cepheid PL relation. At the moment secondary methods with small measured internal dispersions are the best contenders for confidently extending the distance scale, with the intent of determining the value of the Hubble constant and placing a credible uncertainty. They are: the Tully-Fisher relation, Type II SN, Type Ia SN, the surface brightness fluctuation technique and the Faber-Jackson relation. The planetary nebula luminosity function, although showing great promise as a precise distance indicator, has not been pressed to distances any further than those already directly probed by Cepheids themselves. The latter three, because they apply primarily to early-type spirals, S0 galaxies or ellipticals might seem to be outside of the sphere of influence offered by the Cepheid calibration, but this is not strictly true. With the availability of *HST* a volume of space at

least one thousand times larger than is regularly available to ground-based telescopes is now accessible. This volume includes several groups of galaxies that are known to contain both early-type systems and late-type spirals. Confirmed group membership then allows Cepheid distances to be brought into the calibration of galaxies that do not themselves contain Cepheids. This has in fact been the case in several attempts to calibrate these same relations from the ground. Specifically, M31 and M81 (which have Cepheid-based distances) with their significant bulge luminosity have been used to calibrate the PNLF (Ciardullo *et al.* 1989) and an application of the Faber-Jackson relation (Dressler 1987). For the surface-brightness-fluctuation technique the apparent association of M32 again with M31 has been used as a calibrating path. For the future, obvious groups with a mix of Hubble types, worthy of detailed distance determinations are the Centaurus (NGC 5128) Group, and the Leo I (M96 = NGC 3368) Group; with the NGC 2841 Group, the NGC 1023 Group and the NGC 2997 Group offering some interesting potential as well.

12. THE FUTURE

Any future ground-based attempts to detect Cepheids in external galaxies must carefully consider the question of how the periods are going to be unambiguously determined. The rapid success enjoyed by the recalibration of the extragalactic distance scale using infrared detectors was in no small part due to the fact that enormous amounts of telescope time had already been invested in discovering those Cepheids and determining their periods. Unlike all previous investigations we are now confronted by a new problem in the application of Cepheids to the extragalactic distance scale. When the light curves are sparsely sampled over time intervals that are only a few cycles in duration there is a tight coupling between the accuracy of the period determinations and the photometric accuracy of the observations. Co-ordinated ground-based observations are difficult to schedule, and even more difficult (if not impossible) to guarantee. With space observations there is however the immense advantage that the exposures can be optimally scheduled to minimize aliasing effects and also provide for uniform coverage of the phased light curve. Details of the methodology employed by the Key Project will soon be given in Madore & Freedman (1998).

13. CONTRASTING ASPECTS OF THE PL AND PLC

A point of some confusion which needs clarification when discussing Cepheids as distance indicators resides in the difference between the PLC and the PL relation. As discussed earlier, the PLC is simply a restatement of Stefan's Law, and it is therefore applicable to all stars on an individual basis. The PL and PC relations, on the other hand, are statistical relations for ensembles of stars; and they are in turn the result of constraints on Stefan's Law. That constraint is manifest in nature as a strip in which stars are unstable to pulsation. Here we expand on and illustrate this statement of differences.

A PLC relation exists for all stars. That is, for all combinations of temperature and luminosity one can calculate a period, since the PLC embodies exactly the same (universally applicable) principles as does Stephan's Law, from which it is derived. To use the PLC formalization, one must of course observe a color, correct it to an intrinsic color, and then independently determine a fundamental period in order to

calculate a luminosity. But while all stars may have mathematically and physically well-defined fundamental-mode periods, not all stars are unstable to these oscillations, and so their pulsational periods often are not manifested directly.

Much as Nature has provided us with a useful and powerful constraint on Stephan's Law, through the hydrogen burning main sequence, Nature has also provided a different constraint on Stephan's Law (*i.e.*, a constraint on the ubiquitous PLC relation) by defining a narrow zone in which stable pulsation can and does occur. This alternate ``constraint'' manifests itself as the Cepheid instability strip. *The Cepheid instability strip itself, should not be confused with the period-luminosity-color relation*. The Cepheid instability strip defines a range of luminosities, colors, and periods over which pulsation is a stable mode for the star and is therefore an observable. But this constraint does not control the detailed correlations between period, temperature and luminosity, nor does it control the interdependence of the observed parameters for individual stars. In much the same way, the main sequence is a strip of stable hydrogen burning, where stars are constrained to spend a large fraction of their luminous lifetimes. While the gross details of the main sequence are controlled by a single parameter (the mass of the star) the individual stars in this narrowly defined range (the main sequence) still obey the two-parameter Stephan's Law.

The Cepheid constraint, in the form of an instability strip, controls the *statistical* properties of the *ensemble* of Cepheid variable stars. As such, physical laws *external to Stephan's Law* are responsible for the now famous group statistical trends of the period-luminosity and period-color relations. But these trends are incomplete (and even sometimes misleading) descriptors for individual stars: that is to say *the properties of individual stars can never be accurately defined by the constraints on the PLC relation, but only by the PLC relation itself.*

To illustrate how fundamentally different these two concepts (of the underlying equations and the overlaying constraints) are, the interested reader is referred to an earlier paper on the subject (Madore & Freedman 1991). However, the flavor of the argument can be had from considering Figure 8. The solid slanting lines in each figure represent the lines of constant period for the same underlying PLC relation. The heavy pair of lines cutting the constant-period lines represent two extreme examples of hypothetical boundaries to the instability strip inside of which stars are allowed to pulsate. If we now project each of these diagrams into alternate representations of the data, using the period as the abscissa, we get the corresponding period-luminosity and period-color relations as given in Figure 9 and 10. In the period-luminosity representation of the data contained in Figure 9, (where the instability strip is essentially vertical in the CM diagram), there is a strong *statistical* trend of luminosity with period. However, in the corresponding period-color plot (Figure 10), there is no correlation at all, in a statistical sense; yet for individual stars the period, luminosity and color are in any case perfectly correlated through the period-luminosity-color relation. Conversely, in Figure 9, there is no statistical Period-Luminosity relation; there is a very strong Period-Color relation, and yet again precisely the same PLC relation is generating the data. Only the constraints have changed.

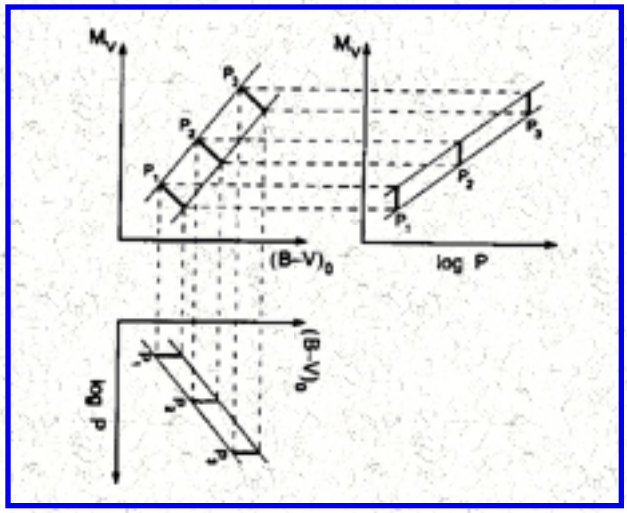

Figure 8. Projections of the Instability Strip. The Cepheid instability strip is shown plotted in the upper left-hand panel. Lines of constant period (P_1, P_2, P_3, *etc.*) are shown as thick lines crossing between the red and blue edges of the instability strip, which act as constraints on the underlying PLC relation which would otherwise fill the plane, as in Figure 3. The broken horizontal lines show how the instability strip and the lines of constant period map over into the period-luminosity plane, while the vertical lines show the mapping down into the period-color plane (which can be viewed in its normal orientation by rotating the diagram 90 degrees counterclockwise.

The distribution of observed data points (drawn from the underlying PLC) may be constrained both by observational selection effects and/or by different physics, without necessarily violating the two-parameter period-luminosity-color relation. Accordingly, differences in the statistical correlations (PL, PC, *etc.*) do not, of necessity, signal deeper-seated differences in the properties of the individual stars. On the other hand, differences in the bulk properties of an ensemble may be taken as fair warning that the detailed physics is changing too. In fact, it is difficult to understand why and how the two properties could be decoupled.

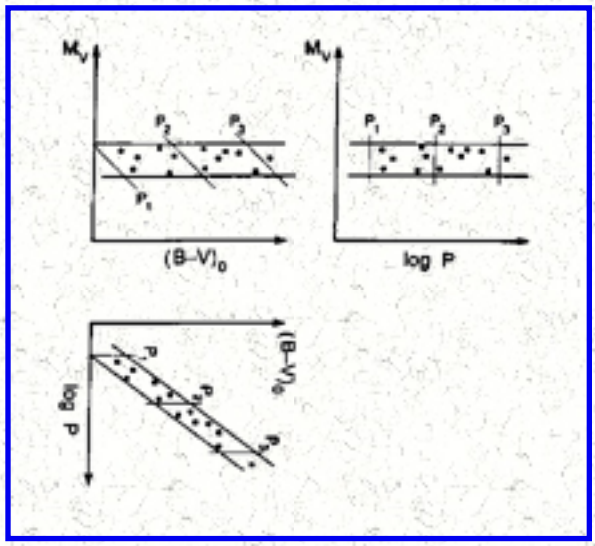

Figure 9. The same as Figure 8 except now a different instability strip is imposed on the underlying universal PLC. This instability strip is horizontal in the CM diagram resulting in a definite statistical correlation of color with period (lower panel, rotated by 90 degrees), but *no trend of luminosity with period* (right-hand panel).

It is, of course, historically very important that the instability strip is naturally oriented in such a way as to give not only a statistical PL, but also a statistical PC relation, for it was in attempts to utilize both of these relations (and to understand the ``scatter'' about their means) that ultimately led to the empirical formulation of a PLC (Sandage 1958).

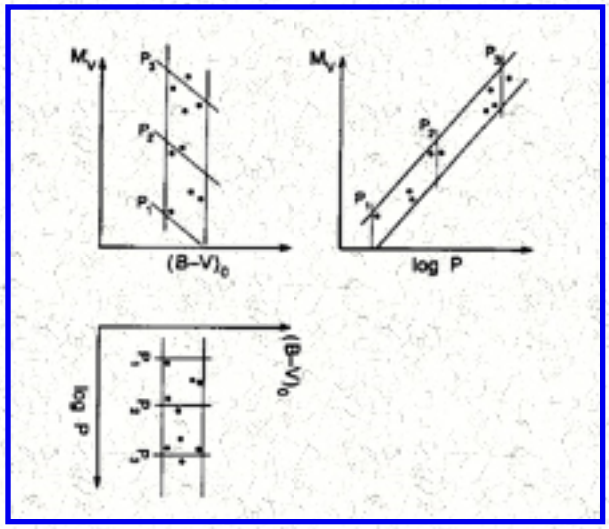

Figure 10. The same as Figure 8 except now a second instability strip is imposed on the underlying universal PLC. This instability strip is vertical in the CM diagram resulting in a definite statistical correlation of luminosity with period (right-hand panel), but showing *no trend of color with period* (lower panel, rotated by 90 degrees).

14. A REDDENING-FREE FORMULATION OF THE PL RELATION

The absolute calibration of colors and/or magnitudes of Cepheids is obviously wrought with many traps and uncertainties in methodology and procedure. One very appealing way to proceed is in an *implicit* formulation and calibration of the problem. Rather than explicitly solving for the reddening/extinction star by star, one can begin quite differently: First adopt a standard reddening line for the color system being employed, then form linear combinations of the magnitudes and colors so that the numerical quantity formed cancels the reddening (star by star) without ever explicitly determining it. Then this formulation can be used both for the calibration objects and for the target Cepheids. Forming this reddening-free magnitude directly parallels the more common reddening-free application to colors, such as $Q = (U-B) - X\,(B-V)$ as defined by Johnson (1963). An example follows.

Suppose that the observed magnitude of the Cepheid is V and its apparent color is $(B-V)$. As in the standard procedure, where individual reddening corrections are made, we assume that the ratio of total-to-selective absorption is known from independent determinations, and that its value is $R = A_V / E\,(B-V)$. Then it naturally follows that a reddening free quantity W (called the Wesenheit function by Madore 1982) can be formed where $W \equiv V - R\,(B-V)$. A simple expansion of the relevant terms shows that for small amounts of reddening the numerical value of W is independent of extinction, and equal to the value that would be calculated if the intrinsic magnitudes and colors were known (which they now need not be). That is, by definition,

$$W = V_0 + A_V - R\,[\,(B-V)_0 + E\,(B-V)\,]$$

$$W = V_0 + R\,E\,(B-V) - R\,(B-V)_0 - R\,E\,(B-V)$$

$$W = V_0 - R\,(B-V)_0 \equiv W_0$$

There exists some confusion in the literature as to the real motivation and physical justification for

creating W for Cepheids. *W* in fact is a reddening-free quantity for stars, not exclusively for Cepheids. It is strictly defined by the properties of the interstellar medium, not by any properties of the stars to which it is to be applied. One is not at liberty, for example, to change the value of *R* from its normal value of 3.3, unless that correction derives from an independent study of the extinction law itself. Accordingly, with the exception of the small known dependence of *R* on *(B-V)* and *E (B-V)* itself, (manifest as non-linear curvature terms at large values of these quantities; true for all applications of reddening corrections, not just W) one cannot manipulate the form of W at all.

The reason for some of the confusion dates back to a similar realization of the PLC introduced by van den Bergh (1975), also called *W*. In that first appearance of a linear combination of *V* and *(B-V)* the complete reddening independence of the function was not fully implemented, as will become clear now. In the following discussion we will use W_{BFM} and $W_{vdB} = V - \beta (B-V)$ to distinguish between the differing definitions used by Madore (1982) and van den Bergh (1975), respectively.

For Cepheids one can begin to see what W_{BFM} is, both in terms of its parent relationship, the period-luminosity-color relation, and in terms of its own definition. Adopting a linearized form of the period-luminosity-color relation we have,

$$V = V_0 + A_V$$

$$V = M_V + mod_0 + A_V$$

$$V = \alpha \log P + \beta (B-V)_0 + \gamma + mod_0 + A_V$$

where mod_0 is the true distance modulus. By definition,

$$W_{BFM} \equiv V - R\,(B-V)$$

so, by substituting the period-luminosity-color relation into the definition of W_{BFM} we get

$$W_{BFM} = \alpha \log P + \beta (B-V)_0 + \gamma + mod_0 + A_V - R\,(B-V)$$

or, expanding the reddening terms, regrouping and cancelling, we get

$$W_{BFM} = \alpha \log P + [\beta - R]\,(B-V)_0 + \gamma + mod_0$$

since, by definition, A_V equals $R\,E\,(B-V)$. For Cepheids, the W_{BFM} can be reformulated as a period-luminosity-color relation. Here it must be emphasized that the zero point γ and the slope of the period dependence α in the W_{BFM} formulation of the period-luminosity-color relation are identical to their

counterparts in the *V* formulation; only the coefficient multiplying the intrinsic color changes from β to [β - *R*].

Here now is the point of confusion. van den Bergh (1969) noted the numerical similarity of $R = 3.2$ to the then espoused value of $\beta = 2.7$, and at that point he chose his definition of $W_{vdB} \equiv V - \beta (B\text{-}V)$ which is quite a different approach. W_{BFM} has the advantage of being a strictly-defined, reddening-free magnitude adopting a well-determined quantity *R*, which does not attempt to anticipate the *a priori* unknown value of β. Furthermore, residual scatter in the W_{BFM} - *log P* relation is also thereby distinctly of interest in its own right. Unlike scatter in the observed PL or PC relations, scatter in the W_{BFM} - *log P* relation cannot be due to reddening effects, be they differential or total. One is not at liberty to adjust the coefficient *R* for various samples of Cepheids (to minimize the scatter in the residual, for example) unless there is *independent* evidence that the ratio of total-to-selective absorption is different for that particular galaxy. The remaining scatter in a W_{BFM} - *log P* plot will be due to a combination of intrinsic (color?) correlations and photometric errors. As is so often the case it will be an understanding of the photometry and its quality that will ultimately limit our understanding of the intrinsic interrelations.

In order to illuminate the differences between the W_{BFM} and W_{vdB} , Figure 11 portrays the mapping of the PLC from its projection onto the traditional color-magnitude diagram (as an instability strip) and then into the three ``period-luminosity'' planes.

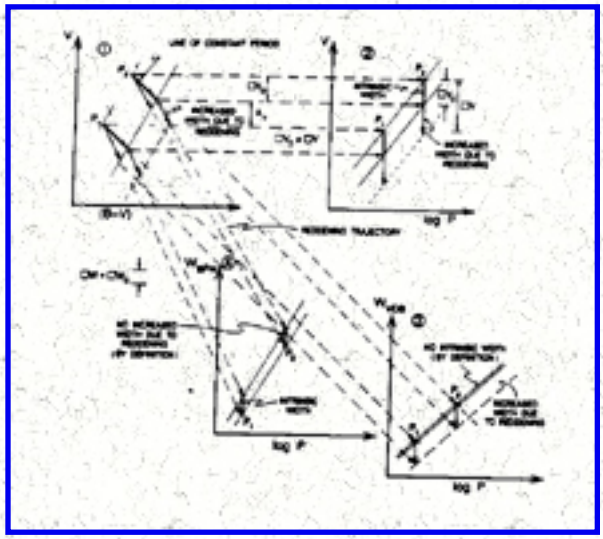

Figure 11. Projecting the observed instability strip, in the presence of reddening. (1) In the upper left panel the instability strip superimposed on the PLC is shown projected into the color-magnitude plane. Lines of constant period (P_1 and P_2) are shown as thick solid lines slanting down to the right. The blue and red edges of the instability strip are shown as thinner solid lines sloping down to the left. Arrows indicated the magnitude and direction of reddening which acts to increase the apparent width of the distribution by systematically scattering points to redder colors and to fainter magnitudes. A dashed line parallel to but fainter than the red edge of the instability strip illustrates the bounds of this effect. (2) The upper right panel is constructed from the first panel by projecting the instability strip and the reddening vectors into the Period-Luminosity plane. There is a systematic increase in the width of the apparent PL relation due to extinction, as in the CM diagram. (3) If the slopes of the lines of constant period are known *a priori*, then the projection of the instability strip into the W_{vdB} - *log P* plane can be performed. By definition, the intrinsic width goes to zero in this projection, but because the slope of the lines of constant period are not exactly parallel to the reddening trajectory, extinction does project into this plane and will widen the relation, and systematically shift the ridge line. (4) Since reddening trajectories are, in general, already determined *a*

priori, it is possible to project the instability strip into the W_{BFM} - *log P* plane where (by definition) extinction effects are eliminated. In this case, however the intrinsic width does still contribute to the dispersion, but the disposition of the individual stars within this strip is not effected by reddening.

The upper left-hand panel shows a portion of the Cepheid instability strip in a color-magnitude diagram. The upwardly slanting solid lines give the red and blue edges of the strip, while the heavy downward-slanting lines labeled P_1 and P_2 are representative lines of constant period. Arrows indicate the slope of a reddening/extinction line. The upwardly sloping broken line indicates the apparent red edge of the instability strip as defined by stars reddened away from the intrinsic line.

The horizontal broken lines leading from Panel 1 to Panel 2 show the first mapping of the instability strip into the *V-log P* plane. The sloping lines of constant period in Panel 1 now become vertical, with downward extensions due to reddening increasing the apparent dispersion at fixed period.

Panel 3 to the lower right shows the effect of forming W_{vdB} given *a priori* knowledge of the value of β the slope of the lines of constant period in the PLC. As can be seen, the projected width in the W_{vdB} - *log P* plane is non-zero in the presence of reddening. While the intrinsic width of the instability strip does project to zero (by definition, once β is known from independent sources) there is residual widening due to reddening

Panel 4 shows the effect of forming W_{BFM}. Since the slope of a reddening line is well known from independent studies, differential reddening has no effect on the width at constant period. The only factor contributing to the width in W_{BFM} is the intrinsic width of the PLC (and as mentioned earlier photometric errors in the magnitudes and colors, which broaden all of the above relationships and projections).

Given Figure 11, it is perhaps worth noting that in the presence of differential reddening it is clearly inappropriate to determine the value of β by minimization of residuals, as would be the case in an unrestricted application of a multi-linear regression fit to PLC data, for instance. For the example at hand, one can see immediately by inspection that a slope somewhere between the true value of β and the reddening slope R would give the minimum residuals plotted as a function of period. The numerical value of that parameter for any given set of Cepheids is however of no universal significance.

15. COMMENTS ON REDDENING DETERMINATIONS

It should, by now, go without saying that the removal of reddening is essential to any study that aspires to a calibration of the intrinsic PLC relation for Cepheids. What is all too often forgotten in the process is that the systematics of this first step will not only affect the calibration, they may well predetermine it. Some authors have claimed that color-color plots for Cepheids can be accurately calibrated and confidently used to determine reddenings to Galactic and extragalactic Cepheids. We examine in some

detail now one such case, that of Feast and his collaborators (hereafter referred to as the South African Group). Their calibration is as widespread as its implications, and therefore we discuss it in some detail.

The South African calibration of the reddening determination begins with Galactic Cepheids (Dean *et al.* (1978). It has then been applied to Magellanic Cloud Cepheids (Martin *et al.* 1979), where they derive a form of the PLC. And then they have further generalized the dereddening procedure for all extragalactic Cepheids of arbitrary metal abundance (Caldwell & Coulson 1985). Beginning with the specific case of the Galactic calibration the South African Group accept at least four crucial assumptions. Assumption (1): There exists a relation between $(B\text{-}V)_0$ and $(V\text{-}I)_0$ that is *dispersionless*. Assumption (2): A shape for this relation is obtained by following single stars through their pulsation cycle. Assumption (3): Since no single star cycles through all of the intrinsic colors expected for Cepheids, in practice a variety of trajectories need to be superposed by moving the narrow color-color loops formed by individual stars (of differing periods) back along reddening lines until they overlap and form an *empirically non-linear* but continuous *(imposed minimum dispersion)* sequence. Assumption (4): A zero point can be fixed by placing stars of independently known reddening (*e.g.*, Galactic cluster Cepheids and very near-by field objects) into this relation. And finally, Assumption (5): Metallicity corrections can be found that consist of simple zero-point shifts on the colors as deduced by the authors from published theory. This formalism and calibration has been adopted in one form or another by the South African Group for all of their subsequent analysis of Magellanic Cloud data and their calibration of the PLC as they have applied it to the extragalactic distance scale (including most recently Laney & Stobie 1994).

We now illustrate the dangers inherent in each of these assumptions. We start with the generally accepted, linear form of the PLC. It is written twice below: once with the color $(B\text{-}V)_0$, and then again with the color $(V\text{-}I)_0$ as the temperature indicator:

$$M_V = \alpha \, logP + \beta \, (B\text{-}V)_0 + \gamma$$

$$M_V = \delta \, logP + \varepsilon \, (V\text{-}I)_0 + \eta$$

We then equate these two expressions and regroup like terms, eliminating M_V, thereby leading to the following equation, applicable to the color-color plane:

$$(B\text{-}V)_0 = [(\delta - \alpha) / \beta] \, logP + [\varepsilon / \beta] \, (V\text{-}I)_0 + [(\eta - \gamma) / \beta]$$

By claiming that for Cepheids there is a unique and dispersionless relation between any two intrinsic colors (despite empirical evidence to the contrary, Cousins 1978a, b) the South African Group is explicitly ignoring the period dependence in the above equations. The tacit assumption then is that both colors are insensitive to gravity effects, and therefore the combination of the equations given above are forced by them to be degenerate in period (*i.e.*, $\alpha = \delta$). The consequences of such an assumption are two-fold: not only are the derived reddenings wrong at the level that surface-gravity difference effects from

star to star are manifest in the time-averaged colors, but the inferred intrinsic colors are deceiving. If the South African calibration tracks the ridge line of the true instability strip in the color-color plane then the following statements can be made: Obviously the stars residing on the constant period lines intrinsically to the blue of the mean will systematically have their reddenings underestimated by this method (while stars whose intrinsic colors have them on the red side of the instability strip will have their reddenings overestimated). But moreover, as Figure 12 illustrates, should the relative slope of the constant-period line be less than the slope of the reddening line in the color-color plot, then the inferred intrinsic position of the stars within the instability strip will be totally inverted from their true mapping!

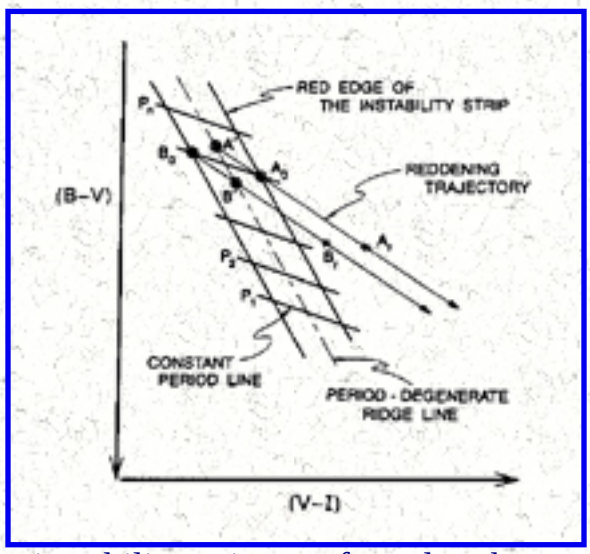

Figure 12. Projection of the PLC into the *(B - V) - (V - I)* color-color plane. As shown by the foregoing equation involving (B-V), (V-I) and log(P) in Section 15, the projection of the Cepheid PLC into the color-color plane results in a finite region crossed by lines of constant period and bounded by the blue and red edges of the instability strip. Representative reddening trajectories are shown passing through the ends of a typical constant-period line such that their projection back onto the central ridge line illustrates the reddening errors made if one erroneously adoptes a dispersionless relation between these two colors. Notice how a Cepheid that intrinsically resides on one (red/blue) edge of the instability strip gets forced to the opposite (blue/red) edge by this incorrect procedure.

While ignoring the period dependence in a second PLC relation may be a convenient and simplifying first approximation to a difficult problem, continuing on to add higher-order non-linear (curvature) terms, and also use theoretical displacements of the origin (attributed to metallicity effects) seems to be, at the very least, somewhat premature.

Furthermore, the validity of Assumption (2) is questionable. It explicitly equates the instantaneous, time-dependent behavior (of luminosity and color) of an *individual* Cepheid of fixed mass, period, and dynamically evolving surface gravity (as it cycles through radius, luminosity and temperature with phase) with the time-averaged properties of *an ensemble of* stars each having different masses, different mean surface gravities, temperatures and periods. However, there is no *a priori* justification for assuming that the behavior of a single star during its cycle is anything more than qualitatively indicative of the way in which the (time-averaged properties of the) instability strip are mapped in luminosity and color when changing from star to star. For example, no one seriously considers determining the slope of the color term β, in the PLC by looking at how an individual star changes its luminosity with color (as a function of phase). Likewise, no one should seriously use the color-color trajectory of individual Cepheid to calibrate the complex mapping of a variety of stars and their PLC into the color-color plane.

Despite the small formal uncertainties in the resulting PLC fit determined by this methodology (see

Feast 1991 for a recent example) it should be emphasized that almost all methods which ``correct" for differential absorption within the PL relation will give rise to a PLC of smaller (apparently intrinsic) scatter. Furthermore, the determination of the color term β in the PLC depends sensitively and explicitly on there being accurate individual reddenings for each of the stars entering the calibration. For the reasons outlined above, we do not believe that an accurate value of β has yet been determined precisely because the systematics of determining reddenings have yet to be fully appreciated or adequately addressed.

Because of its inherent complexity we are not in a position to solve the reddening problem at this time; however, its impact on the distance scale can be minimized by accepting that reddening is a systematic problem, and realizing that it can be dealt with effectively by at least three available means, which involve (1) moving as far to the infrared as is practical, so as to reduce the extinction problem to the level of other systematic and random errors, (2) combining multiwavelength (visual to near-infrared) data for significant numbers of Cepheids in a given galaxy, and determining the ensemble-averaged extinction (and true modulus) using an independently calibrated wavelength-dependent extinction law, or (3) using reddening-free formulations which are designed to cancel out any and all extinction on a star-by-star basis, without ever attempting to determine the amount explicitly. Each of these alternatives is dealt with in some detail in this review and its other appendices.

It is clear however that if an *explicit* solution for individual reddenings is ever to be found, it will most likely come through an investigation of extragalactic, not Galactic, Cepheids. The LMC has acted as the focal-point for calibration purposes for some years now, primarily because it has a large population of Cepheids with known periods, and because it is sufficiently close that accurate photometry can be obtained for its stars with relative ease. However, the LMC Cepheids do individually suffer from some degree of extinction internal to the LMC itself, and also varying amounts of foreground Galactic extinction. The SMC has a similarly large population of Cepheids. Although it is somewhat further away than the LMC, it is not excessively so. And while it is generally accepted that in comparison to the LMC the extinction is less internal to and in front of the SMC, it is now known (primarily from studies of the Cepheids!) that the back-to-front geometry of the SMC is such that appreciable differential modulus residuals are affecting the magnitudes. Any empirical correlations between reddening-corrected colors and extinction-corrected magnitudes would have this (geometric) noise to contend with.

We suggest then that the best place for future work on the intrinsic calibration problem is not the Magellanic Cloud system, but the Local Group galaxy IC 1613. The foreground reddening to IC 1613 is, by all estimates, very low and probably quite uniform, considering the high Galactic latitude and small angular size of this galaxy as compared to either of the Magellanic Clouds. In a like way to the SMC the extinction internal to IC 1613 also appears to be quite small. With the surveys of Sandage (1971) and Carlson & Sandage (1990) now complete, there is also a sizable population of Cepheids in IC 1613 to work with. Of course crowding is more of a problem for photometry of individual Cepheids in IC 1613 as compared to the LMC, for example; but considering the success had with photoelectric photometers

using aperture sizes in excess of 10 arcsec when working on LMC / SMC Cepheids it is realistic to expect that point-spread-function fitting routines (effectively working on one-arcsec scales) will be able to do at least as well. And the quality of *BVRI* light curves obtained for Cepheids in NGC 300 (Freedman *et al.* 1992), at a distance about three times further than IC 1613, seems to bear out this expectation. Of course, IC 1613 is only one galaxy, representing a single cut of metallicity, still the Cepheid calibration is at that stage where even one solid observational study can contribute a great deal to the effort.

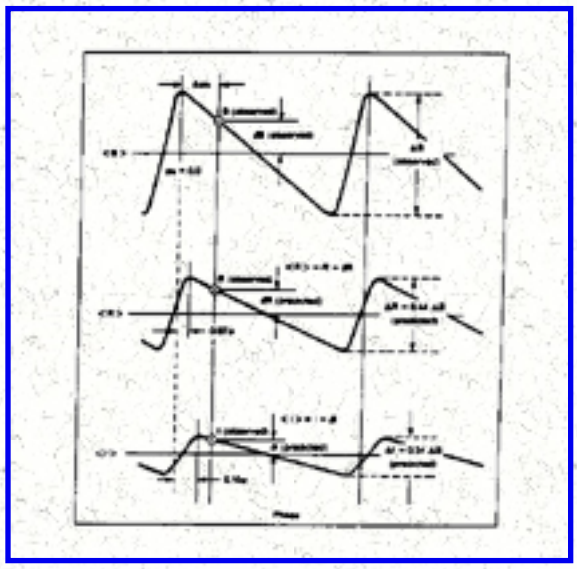

Figure 13. Cepheid light curves as a function of observed wavelength. A schematic illustration of the relative decrease in amplitude and shift in phase associated with observing Cepheids at progressively longer wavelengths (adapted from Freedman 1988a).

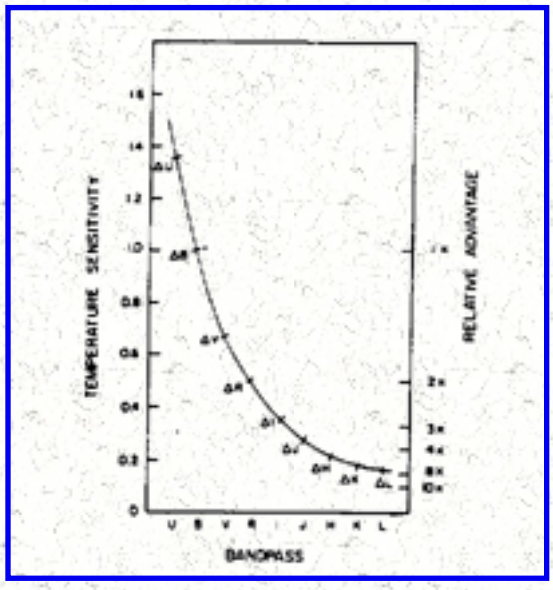

Figure 14. Amplitudes and/or instability strip width for Cepheids as a function of increasing wavelength (adapted from Freedman, Grieve & Madore 1985). The large relative amplitudes (large strip widths) at blue and ultraviolet wavelengths are due to the higher sensitivity of monochromatic surface brightness to temperature variations at short wavelengths; low amplitudes (small instability strip widths) in the red and near-infrared are dominated by the small percentage changes in surface area, driven by the radial pulsation.

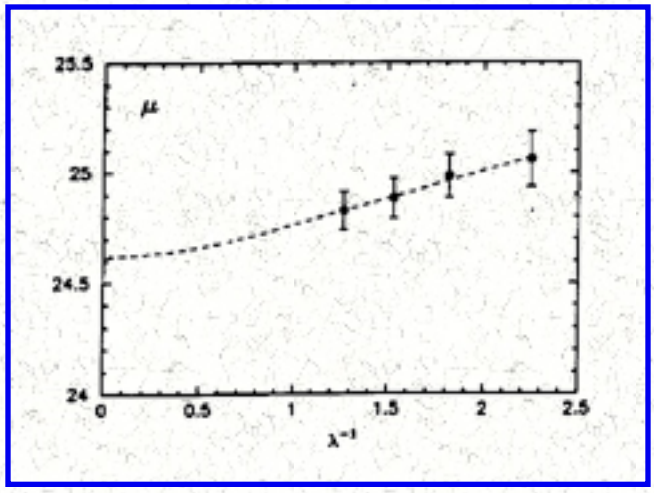

Figure 15. BVRI apparent distance moduli for Cepheids in M33, plotted as a function of inverse wavelength (1/ λ in inverse microns) from Freedman, Wilson & Madore (1991). The broken line is a fit of a Galactic extinction law to the data, with E (B-V) = 0.10 mag.

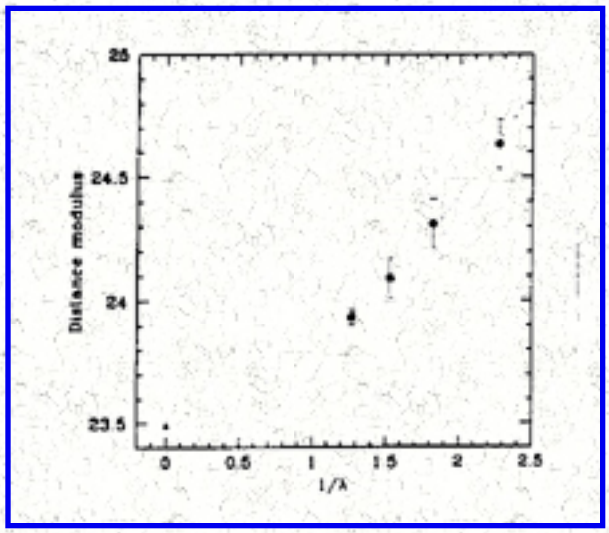

Figure 16. BVRI apparent distance moduli plotted as a function of inverse wavelength for Cepheids in NGC 6822. The filled triangle marks the true modulus = intercept of the fit at the origin 1/ λ = 0.0 for E (B-V) = 0.21 ± 0.03 mag (from Gallart *et al.* 1996).

16. COMPARISONS WITH OTHER DISTANCE INDICATORS

As recently as a decade ago, the range of published Cepheid distances to nearby galaxies was sufficiently large that by adopting one or another calibration could result in differences in the Hubble constant of almost a factor of two. Fortunately, a decade later, distance determinations to nearby galaxies have been obtained with new CCD data using a number of independent techniques (Cepheids, RR Lyraes, TRGB, and even type II supernovae in the case of SN 1987 in the LMC). Now that photometry with linear detectors is available for a variety of methods, and corrections for reddening can be applied, the distances to nearby galaxies have converged to *full range* differences of less than 0.3 mag (*i.e.*, 15% in distance, Freedman & Madore 1993). Moreover, the excellent agreement of individual distances gives no indication of large remaining systematic errors.

However, as noted by Freedman & Madore (1993), although the Cepheid and RR Lyrae distances agree to within their stated errors, the differences are systematic (in the sense that the RR Lyrae distances are smaller than the Cepheid distances). This effect has been noted and discussed by Walker (1992), Hazen & Nemec (1992) and Reid & Freedman (1994) in the case of the LMC, and Saha *et al.* (1992) in the case of IC 1613. Most recently, this effect has been discussed by van den Bergh (1995). As yet unresolved

are the slope and zero points of the relation between absolute magnitude and the metallicity for RR Lyrae stars, as well as the metallicity sensitivity of the Cepheid PL relations as a function of wavelength. However, the fact that the Population I Cepheid distances now agree as well as they do (to within 0.15 to 0.30 mag) with the Population II RR Lyrae and TRGB distances, is consistent with the predictions of a small Cepheid PL dependence on metallicity by Chiosi *et al.* (1993), and the observational result of Freedman & Madore (1990).

17. THE KEY PROJECT

The Cepheid distance scale provides the zero-point calibration for most of the relative distance indicators in use today: the Tully-Fisher relation for spiral galaxies, the surface-brightness fluctuation method for elliptical galaxies, the planetary nebula luminosity function, Types I and II supernovae, brightest stars in galaxies, and the globular cluster luminosity function (for a recent overview see Jacoby *et al.* 1992). The Cepheid distance scale also lies at the heart of the *HST Key Project on the Extragalactic Distance Scale* (Freedman 1994a,b,c; Kennicutt *et al.* 1995) and in several other *HST* distance scale programs (*e.g.*, Sandage *et al.* 1994; Saha *et al.* 1994, 1995; and Tanvir *et al.* 1995).

The Key Project on the Extragalactic Distance Scale has been designed to use Cepheid variables to determine (Population I) primary distances to a representative sample of galaxies in the field, in small groups, and in major clusters. The galaxies were chosen so that each of the secondary distance indicators with measured high internal precisions could be accurately calibrated in zero point and intercompared on an absolute basis. These data will then be used as secondary calibrations and applied to independent galaxy samples at cosmologically significant distances. Cepheid distances to the Virgo and Fornax clusters provide an alternative route to the secondary calibrations. The intention is to derive a value for the expansion rate of the Universe, the Hubble constant, to an accuracy of 10% (for additional details see Kennicutt *et al.* 1995, Freedman, Madore & Kennicutt 1997).

17.1. *Goals*

A measurement of the Hubble constant to 10% provides an immense challenge given the history of systematic errors in the extragalactic distance scale. For this reason, the Key Project has been designed to allow many independent cross-checks of both the primary and secondary distance scales. The goals of the Key Project are described in more detail in Kennicutt *et al.* (1995) and Freedman *et al.* (1994a). Briefly, there are four primary goals: (1) To discover Cepheids, and thereby measure accurate distances to spiral galaxies located in the field and in small groups that are suitable for the calibration of several independent secondary methods. (2) To make direct Cepheid measurements of distances to three spiral galaxies in each of the Virgo and Fornax clusters. (3) To provide a check on potential systematic errors in the Cepheid distance scale via independent distance estimates to the nearby galaxies, M31, M33 and the Large Magellanic Cloud (LMC). And (4) to undertake an empirical test of the sensitivity of the zero point of the Cepheid PL relation to metallicity as described previously.

17.2. *First Results*

Prior to the 1994 repair mission, the Key Project team was still able to undertake a search for new Cepheids in the nearby galaxy M81. These observations were undertaken to provide a test of the new discovery algorithms (Madore & Freedman 1998) which were designed to optimally detect Cepheids with a range of (unknown) periods, using a minimum of spacecraft time, and further restricted by the small (60-day) observing windows available only once in any given year. 30 Cepheids were discovered in two fields searched in M81 and a reddening-corrected distance modulus of 27.80 ± 0.20 mag was derived (Freedman *et al.* 1994b). Previous ground-based attempts to discover variables in this galaxy yielded only two confirmed Cepheids, one of which was intentionally targeted by the Key Project as a test of the search procedure. This Cepheid was recovered and confirmed to have a period in agreement with the more extensive ground-based determination derived from decades worth of data.

Immediately following the December 1993 repair mission, BVR images of the Virgo spiral galaxy M100 were obtained as part of a collaboration between the WFPC2 IDT and the H_0 Key Project teams. ALLFRAME photometry was obtained for over 30,000 stars. By overlaying the position of the mean Cepheid instability strip on the resulting color-magnitude diagrams, it was possible to demonstrate that stars were present with the magnitudes and colors expected for Cepheid variables at the distance of the Virgo cluster. Given this success, a sequence of 12 V and 4 I exposures was begun in April 1994. Twenty high signal-to-noise Cepheid variables were found, from which a reddening corrected distance of 17.1 ± 1.8 Mpc (or a distance modulus of 31.16 ± 0.20 mag) was determined to M100 (Freedman *et al.* 1994a). Allowing for the uncertainty in the position of M100 with respect to the Virgo cluster core, in addition to the uncertainty in the Virgo cluster recession velocity, a preliminary value of the Hubble constant of $H_0 = 80 \pm 17$ km/sec/Mpc was determined. A discussion of the random and systematic errors is found in Freedman *et al.* (1994a). Recently, a new determination of the distance to M100 has been made based on a larger sample of over 50 Cepheids and an improved calibration (Ferrarese *et al.* 1996). A value of 15.8 ± 1.5 Mpc is obtained, in good agreement, to within the measurement uncertainties, with the earlier value.

Other galaxies currently being analyzed as part of the HST Key Project include NGC 925 (Silbermann *et al.* 1996) in the NGC 1023 Group; NGC 3351 in the Leo I group (Graham *et al.* 1997); two fields in M101, discussed above in the context of extending the metallicity test (Kelson *et al.* 1996; Stetson *et al.* 1998, in preparation; Kennicutt *et al.* 1998, in preparation); NGC 7331 (Hughes *et al.* 1998, in preparation), a Tully-Fisher calibrator in the field; NGC 4414 (Turner *et al.* 1998, in preparation), a distant and fairly inclined early-type spiral useful for calibrating a number of secondary methods including type Ia supernovae. Recently, NGC 1365, a galaxy in the Fornax cluster (Silbermann *et al.* 1998; Madore *et al.* 1998, in preparation) has been observed for Cepheids, and the results of that survey are discussed in the closing sections of this lecture series. Other galaxies completed at the time of writing include NGC 3621 (Rawson *et al.* 1998) and NGC 2090 (Phelps *et al.* 1998).

18. OTHER GROUND-BASED WORK

18.1. *Galactic Cluster and LMC Calibration*

While currently the most commonly adopted route for calibrating the zero point of the Cepheid PL relation is through the Large Magellanic Cloud, a more traditional approach is to use individual Cepheids in Galactic clusters. Following this route, main sequence fitting and B-star reddenings can provide (in principle) individual moduli, absolute magnitudes and intrinsic colors for the member Cepheid(s). In practice this approach has turned out to be limited in a number of ways: very few clusters have known Cepheids as bona fide members, those examples generally only cover periods up to about ten days, and many of the clusters are either very sparse or behind considerable amounts of (perhaps variable) extinction, or both.

While sample size and the period distribution of that sample is not likely to be changed considerably, the treatment of the reddening and measurement of the true distance moduli can be re-examined with new technology. In a long-term collaboration Persson *et al.* (1996) have embarked on a project at Las Campanas and Palomar of infrared imaging of the main sequences of all Galactic clusters containing classical Cepheids. These clusters include NGC 7790, NGC 129, NGC 6649, NGC 6664 and Lynga 6. A parallel study of many of these clusters is also underway by Fry & Carney (1997, private communication).

Finally, in addition to the recalibration of Galactic clusters, multiple epochs of JHK photometry are being obtained for a sample of over 90 Cepheids in the LMC. This sample will serve as a fiducial calibrating sample for anticipated NICMOS observations of Cepheids. Also, at Las Campanas we have been obtaining JHK observations of the known Cepheids in IC 1613 and NGC 300.

18.2. *Recent Ground-Based Searches for Cepheids*

Easily accessed only from the southern hemisphere, the South Polar (Sculptor) Group contains the last of the relatively nearby spiral galaxies to be searched for Cepheids from the ground. Three of its members (NGC 247, NGC 300 and NGC 7793) are of the proper type and inclination to become Tully-Fisher calibrators, given independent distance measurements. Using the CTIO 4m and the Las Campanas 2.5m we have been following up the Cepheids discovered in NGC 300 (Graham 1984, Madore *et al.* 1987) and monitoring NGC 247, NGC 7793 (and NGC 253) for new variables. Based on *BVRI* CCD data of 10 Cepheids Freedman *et al.* (1992) determined a distance to NGC 300 of 2.1 ± 0.1 Mpc.

19. HELIUM CORE FLASH AND THE TIP OF THE RED GIANT BRANCH AS A PRIMARY DISTANCE INDICATOR

19.1. *Introduction*

In his 1930 *Harvard Observatory Monograph:* ``Star Clusters," Harlow Shapley outlined various methods for the estimation of distances to Galactic globular clusters. Noteworthy among these methods is the one that assumes that the apparently brightest (giant) stars are all of the same absolute magnitude. Tested for consistency in those cases where more than one method of distance determination could be made (with RR Lyrae stars, for instance), and roughly corrected for foreground contamination (choosing the magnitude of the sixth-brightest star as a robust estimator), Shapley went on to map out the size scale of the Galaxy as defined by the old Population II globular cluster system. Although the exact details of his approach are now known to be flawed, the method as applied was of sufficient precision that a revolutionary view of the size of our Galaxy was obtained, and the Milky Way as an island universe started to take on a tangible reality of its own.

Before pursuing the historical path relating to the successful application of brightest red giant stars as *extragalactic* distance indicators we digress slightly in the next section to present a set of criteria that any extragalactic distance indicator might be judged by. It will rapidly become clear that many of these criteria are probably mutually exclusive in a practical sense (ultra-luminous, locally calibrated and theoretically understood), but ideals are seldom realized in full measure in the real world. Nevertheless, we can establish metrics for relative performance.

CATALOGUE OF GLOBULAR CLUSTERS

N. G. C.	Ellip-ticity	Orien-tation	Photographic Magnitude				Adopted Modulus
			Var.	Bright	6th	30th	
104	8	-55	. . . .	13.09	12.4	13.4	14.17
288	9	. . . .	. . . .	14.80	14.5	15.1	15.81
362	8	+65:	15.5	14.12	13.5	14.8	15.55
1261	9.5	. . . .	. . . .	. . . .	. . . .	. . . .	16.72
1851	9	-75	. . . .	. . . .	. . . .	. . . .	15.78
1904	9	+ 5	. . . .	15.29	15.01	15.72	16.54
2298	8	+39:	. . . .	. . . .	. . . .	. . . .	17.12
2419	9	-56	. . . .	. . . .	. . . .	. . . .	17.41
2808	8	+84	. . . .	14.9	14.3	15.4	16.05

3201	9	. . . .	14.52	13.52	13.3	13.8	14.81

Figure 17.A reproduction of part of Shapley's original 1930 table showing the first use of the brightest red giants in globular clusters to determine distances.

20. THE IDEAL DISTANCE INDICATOR

In an extragalactic context the requirements for an ideal distance indicator are indeed demanding:

1. High luminosity is a pre-requisite, given the enormous distances that must be bridged in passing out of the Milky Way, beyond the Local Group and eventually into regions of pure and undisturbed Hubble flow.

2. The ideal distance indicator (be it derived from a luminosity or a measure of size) needs to have the lowest possible intrinsic dispersion. Low-precision distance indicators all eventually run afoul of bias at large distances where only the largest and/or intrinsically brightest objects fall into limiting-case samples. Blindly calibrated against the mean these exceptional objects always end up underestimating distances, if not properly corrected for selection effects.

3. A secure empirical calibration requires that examples of the distance indicator be found locally so that detailed and repeated tests can be made at high signal-to-noise, before applications are made at the limits of detectability.

4. In order to anticipate problems, predict trends, and understand exceptions, a firm theoretical basis for the distance indicator is required. In the consideration of many distance indicators a theoretical understanding is all too often lacking.

5. Lacking a detailed theoretical understanding of the distance indicator, one might require that a demonstrable empirical proof that the luminosity (or size) being used is insensitive to (or at least can be easily corrected for) known effects. Age differences, chemical composition variations, population size, environment differences and, of course, interstellar reddening are just a few of the known outstanding variables that should be considered.

6. The ideal distance indicator should also be universally available. It should be found in spiral galaxies, ellipticals and irregulars, if clusters, groups and the field are to be equally sampled without bias. This universality constraint obviously weighs heavily against Population I distance indicators, because of the lack of any significant star formation in elliptical and S0 galaxies at the present time.

7. Singular events are to be avoided. The hope is to find a distance indicator that has more than an occasional or unpredictably fleeting presence in a galaxy, but rather that it is abundant and

always found whenever and wherever it is needed. Follow-up observations or applying new technology is problematic for one-time, historical events. Supernovae of all types suffer from this problem.

8. Finally, the identification of the ideal distance indicator should be unambiguous. Two, three or more types and sub-types of the distance indicator, each having subtle differences in their properties inevitably require additional observations to resolve differences. Cepheids (Classical Population I versus Population II W Virginis stars) suffered from this flaw early in the history of their calibration; supernovae suffer from the (growing) diversity of types to this very day (compare the observations required, as the singular event is unfolding, to definitively distinguish between a supernova of SN Type II as opposed to a supernova of SN Type Ia [Branch-Normal], for example).

21. SOME HISTORY CONCERNING THE RED GIANT BRANCH

Following Shapley's brave application of brightest red giants to the Galactic distance scale, continued applications were ironically being made at the same time as new observational data were being assimilated (sometimes by the very same people) which were showing that the method was fatally flawed. Flawed in the optical, that is. Late into the 1960's and 70's Arp in his review and even Harris (1974) in his doctoral thesis used the apparent B-band luminosities of the brightest (few) red giants as statistical indicators of distances to globular clusters. And this proceeded in the face of compelling evidence (and theory) that the giant branch morphology was a sensitive function of age and most especially a function of metallicity (see Figure 18 for examples). Bolometric corrections, driven primarily by atmospheric line-blanketing effects in the optical resulted in differences of up to 2 mag between the absolute magnitudes of the brightest red giant stars in metal-rich (line-blanketed) systems as compared to those in metal-poor globular clusters. It was not until the detailed and calibrated studies of the color-magnitude diagrams (CMDs) of Galactic globular clusters by Arp, Sandage, Wildey and others, using more modern photometric systems, that the absolute UBV magnitudes of the brightest giants in globular clusters were found to be less than ideal as distance indicators. The detailed morphology of the giant branch, (especially its height above the horizontal branch) and its terminal color were found to depend critically on the mean metallicity of the system.

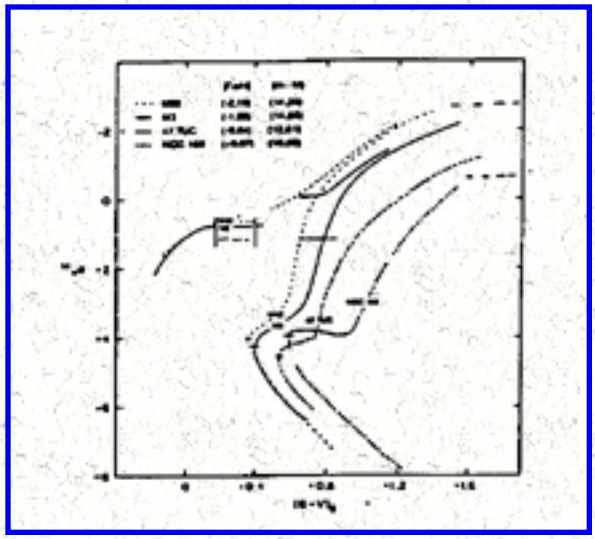

Figure 18. A schematic representation of the effect of metallicity on the morphology of the red giant branch when observed at optical (UBV) wavelengths.

The application of the then new CCD detectors to unexplored wavelengths led Mould & Kristian (1986) to reconsider the tip of the red giant branch as a potential distance indicator. With admittedly sparse statistics, they noted in a series of papers that the dominant feature in the CMDs of Local Group galaxy halos was the presence of a giant branch population of stars, showing a wide range of colors, but generally terminating at high-luminosity at a well-defined and fairly constant magnitude. Of the four galaxies that they initially imaged (M31, M33, NGC 147 and NGC 205) only M31 had an independent and reasonably secure distance published (based on Cepheids), while the distance to M33 was still under considerable debate. At the conclusion of their 1986 paper, Mould & Kristian reasonably called for more work before the TRGB method could be considered a mature distance indicator. Their requests included: (1) The examination of a larger sample of Local Group galaxies, and (2) an absolute calibration through Galactic globular clusters based directly in the Cousins I-band system.

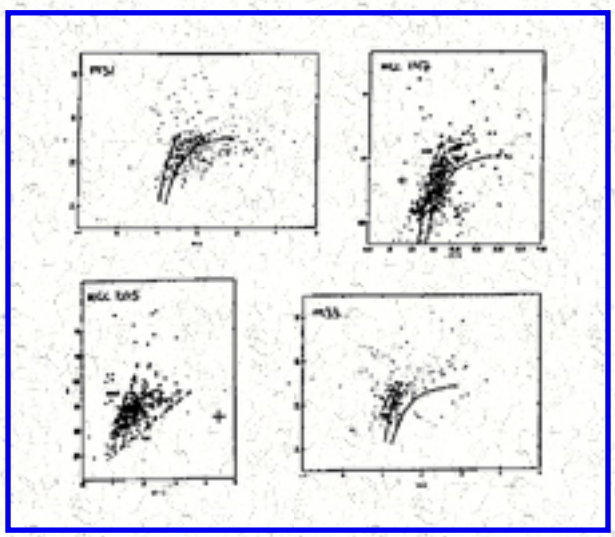

Figure 19. A sampling of early color-magnitude diagrams for Local Group galaxies and their halos.

Answering the call for a direct calibration of the method using Galactic globular clusters Da Costa & Armandroff (1990) published a grid of standard globular cluster giant branches observed in the Kron-Cousins VI system. And they found ``acceptable agreement'' between the bolometric magnitudes of the brightest giants and the theoretical predictions for the luminosities of helium core flash. At the same time, considerably more observational work was being undertaken which supported the use of the TRGB

as a distance indicator in the I band. Freedman (1988) made the first combined CCD-based determination of a TRGB distance and a Cepheid-based distance for IC 1613. While confusion over the disparate Cepheid distance moduli to M33 finally resolved itself with the application of multiwavelength CCD observations of the variable stars in that galaxy (Freedman, Wilson & Madore 1991), the result again confirmed the TRGB calibration. A comprehensive review and survey of published results pertaining to the comparison of tip distances in comparison to RR Lyrae and Cepheid distances was given by Lee, Freedman & Madore (1993), and the interested reader is referred to that paper for additional details and references.

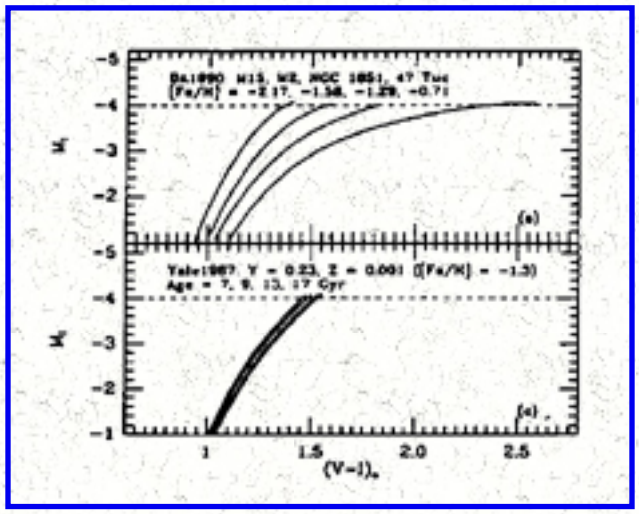

Figure 20. Sensitivity of the TRGB to age and metallicity effects (adapted from Lee, Freedman & Madore 1993). The upper panel shows fiducial giant-branch lines for a series of Galactic globular clusters having a range of metallicities. Note how the terminal I-band magnitude is a very weak function of chemical composition. The lower panel shows the (negligible) effect of age (7-17 Gyr) on the RGB peak luminosity, based on Revised Yale isochrones calculated for [Fe/H] = -1.3 dex.

The TRGB method, as applied by Lee, Freedman & Madore (1993) is based on a calibration established for the metallicity range of -2.2 < [*Fe / H*] < -0.7 dex, derived by using empirical loci of the red giant branches for four Galactic globular clusters given in the paper by Da Costa & Armandroff (1990). Da Costa & Armandroff estimated distances by adopting the metallicity-M_V magnitude relation for RR Lyraes based on the theoretical horizontal branch models for Y_{MS} = 0.23 of Lee, Demarque & Zinn (1990). At present, the exact calibration at the higher end of metallicity range (*i.e.*, metallicities exceeding the most metal-rich Galactic clusters) and its practical effects on TRGB distances to composite systems still remains uncertain.

22. CONCERNS AND TECHNICAL ISSUES

There are of course a number of procedural concerns that must be attended to in both calibrating and then applying the TRGB Method to extragalactic distance determinations. We briefly discuss the most important of these in this section. Some of these problems can be anticipated and dealt with in the design phases of the observing program (for example, crowding, signal-to-noise, *etc.*); some require careful post-processing (the removal of cosmic rays, background galaxies, *etc.*), or require complementary observations (to distinguish AGB stars, and deal with high-metallicity effects). Others will hopefully diminish in importance with additional time and effort (such as zero point uncertainties).

22.1. *Detecting the Tip*

Until recently, the apparent magnitude of the TRGB was simply estimated by visual inspection of the color magnitude diagram. Lee, Freedman & Madore (1993) introduced a quantitative edge-detection method (the Sobel filter) to both identify the position and estimate the uncertainty of the TRGB observed luminosity. When this filter is convolved with the luminosity function, the output response function peaks where the discontinuity is the largest. Further refinements to this method have subsequently been introduced by Sakai, Madore & Freedman (1996a, b).

22.2. *Asymptotic Giant Branch Stars*

Normal globular clusters have asymptotic giant branch stars. These evolutionarily-advanced stars are found at magnitudes above and below the TRGB, loosely paralleling the red giant branch to the blue and exceeding the first ascent red giant branch stars at higher luminosities. In mixed-age populations intermediate-mass stars can also evolve up the AGB sequence populating those luminosity intervals above the TRGB with even brighter and often very much redder stars than normally found in old, metal-poor, pure Population II systems.

AGB stars can be a source of additive noise in the luminosity function near the TRGB, as they can be slightly brighter than M_I ~ -4.0 mag. Fortunately, the AGB luminosity function is known to be flat and/or only rather slowly rising, thus making it extremely unlikely to be misidentified with the much more abrupt TRGB signature (when the edge-detection filter is passed through the luminosity function, it would respond more prominently to the pronounced discontinuity of the RGB tip). The AGB problem can also be minimized by observing the red giant branch population preferentially in the outermost halos of the galaxies where intermediate-age populations are less likely to be present. Furthermore, the added advantage of working in the lower-surface density halos is that crowding effects are also minimized.

22.3. *Red Supergiants*

Depending on the mix of Pop I and II, very massive stars can add contamination to the reddest portions of the CMD by contributing evolved supergiant stars. These objects are in proportion to the recent star formation rate and are spatially co-located with their immediate progenitors, the blue (plume) main sequence stars. Avoiding regions of easily identified active star formation reduces this contaminant effectively to zero. Nevertheless, these red supergiants are both rare (in comparison to TRGB stars) and show no characteristic discontinuity in their gradually increasing apparent luminosity function. They can add noise to the TRGB detection, but they are not likely to be mis-identified with it. This is especially true given that the blue population effectively predicts their presence and rough numbers.

22.4. *High-Metallicity Populations*

At high metallicity (beyond [Fe/H] = -0.7 dex) bright stars suffer noticeable line blanketing even in the I-band (*e.g.*, Bica *et al.* 1994). However, the effect is to make these high-metallicity tip stars fainter than their low-metallicity counterparts. This would be a problem (which could be calibrated in principle) for

the determination of distances to pure, high-metallicity systems, but whether such ``pure" systems do exist or even could exist is unlikely. In terms of detection thresholds, mixed-metallicity populations (that is, any system that has low-metallicity stars as the precursor population to the next generation of higher-metallicity red giants) would first reveal their (bluer, brighter) low-metallicity stars, and thereby define the jump in TRGB luminosity function at a magnitude corresponding to the low-metallicity calibration independent of the fainter (high-metallicity population) tip stars mixed in below.

Although the magnitude of the TRGB has been shown both observationally and theoretically to be extremely stable at M_I ~ -4.0 mag, this stability has only been solidly demonstrated and calibrated in the metallicity range defined by Galactic globular clusters (i.e., -2.1 < [*Fe / H*] < -0.7 dex). At the higher metallicity end of this range, little data have been obtained to demonstrate whether the constancy of the TRGB magnitude prevails, or if not, how it changes in detail. Of course, one can reduce this uncertainty by restricting TRGB observations to the halos of galaxies where color gradients suggest lower metallicities. And, in practice, for most irregular galaxies, and the outer regions of spiral galaxies, the available lower-metallicity calibration will be sufficient.

22.5. *Crowding*

Crowding will limit the discovery and the photometry in all TRGB applications. However, given even a rough estimate of the expected distance, the local surface brightness (in the halo) will predict the expected crowding at the magnitude corresponding to the tip. Using computer simulations, Madore & Freedman (1995) showed that the TRGB method could be applied out to 3 Mpc [*(m - M)* ~ 27.5 mag] from the ground, and from space at least a factor of four further in distance [*(m - M)* ~ 30.5 mag], being limited primarily by integration time rather than crowding in the latter case.

22.6. *Sufficient Signal*

While this may seem to be a simple matter of combining aperture and integration time to reach the requisite signal-to-noise ratio, other factors preempt extended integration. Variable seeing is a critical issue for ground-based attempts to go to the limit of this method; while the limiting case of using HST encounters a variety of subtle but important issues relating to charge-transfer efficiency, fixed pattern noise, extensive cosmic ray removal, *etc.* when extremely long intergations are called for. Given these limitations, with its present detectors, HST may be considered to have an operating range of ~ 10 Mpc for applying the TRGB method; beyond that, extreme care should be taken in the acquisition, processing, and interpretation of the data.

22.7. *Background Galaxies and Quasars*

Background galaxies as a source of noise can be dealt with in a variety of ways. First they can be resolved. In most cosmological models, galaxies are not expected to be much less than an arcsec for the magnitudes of interest in our applications, where I < 25 mag. Based on simple profile-fitting, galaxies can therefore be discriminated from stars and eliminated early in the analysis process. Very distant,

point-like objects are not expected to have any abrupt discontinuity in their apparent luminosity function and could at worst contribute a ``background" noise component which can be further reduced by color selection, eliminating the very bluest contaminants (certain quasars) and the very reddest (background ellipticals).

22.8. *Cosmic Rays*

Careful planning and post-processing can deal with cosmic-ray events in the CCD images used to detect the TRGB. Median-filtering of multiple exposures, combined with image-profile fitting selection, set to reject ``sharp" events can reduce cosmic-ray noise to an acceptable level of contamination.

22.9. *RR Lyrae Distance Scale*

The absolute magnitude of the TRGB rests on the globular cluster distance scale, which in turn depends on the calibration of the absolute magnitudes of the horizontal branch RR Lyrae stars. And that calibration, in form and zero point, is still controversial (see, for example, Sandage & Cacciari 1990, Renzini 1991, and Carney *et al.* 1992, for the full range of opinions). We have adopted the calibration of Da Costa & Armandroff (1990) which is $M_V\,(RR) = 0.17\,[Fe\,/\,H] + 0.82$ mag. As discussed in Walker (1992), Saha *et al.* (1992), and Freedman & Madore (1993), the fainter ($M_V\,(RR) \sim 1.0$ mag) alternative calibration disagrees with the Cepheid distance scale to overlapping galaxies at the 0.2-0.3 mag level. Our currently adopted zero point is ~ 0.8 mag, and falls between the aforementioned extremes.

23. AN OVERVIEW OF THE THEORETICAL UNDERPINNINGS: CORE HELIUM IGNITION

The evolution of a post-main-sequence low-mass star up the red giant branch is one of the best-understood phases of stellar evolution (*e.g.*, Iben & Renzini 1983). For the stars of interest to us in the context of the TRGB, a helium core forms at the center of the star, supported by degenerate electron pressure. Surrounding the core, and providing the entire luminosity of the star is a hydrogen-burning shell. The ``helium ash" from the shell rains down on the core increasing its mass systematically with time. The temperature of the (basically isothermal) core and therefore the luminosity generation rate at its surface are simple functions of core mass and core radius. In analogy with the white dwarf equation of state and the consequent scaling relations that interrelate core mass (M_c) and core radius (R_c) for degenerate electron support, the core (= shell) temperature (T_c) and the resulting shell luminosity are simple functions of M_c and R_c:

$$T_c \sim M_c\,/\,R_c$$

$$L_c \sim M_c^{7}\,/\,R_c^{5}$$

meaning that as the core mass increases (and the radius shrinks) the luminosity increases due to both effects. That is, the star secularly ascends the red giant branch to ever-increasing luminosities, *and higher core temperatures*. And it is the latter increase that stops the progression in luminosity: When T_c exceeds a physically well-defined temperature (set by nuclear physics), helium in the core will ignite. While this does provide a new and additionally powerful source of energy, helium core ignition does not make the star brighter, but rather it all but eliminates the shell source by explosively heating and thereby lifting the electron degeneracy within the core. This dramatic change in the equation of state is such that the entire internal structure of the star is rearranged so quickly that the core flash (which generates the equivalent instantaneous luminosity of the entire galaxy) is internally quenched in a matter of seconds, inflating the core and settling down to a helium core-burning main sequence, far removed in luminosity and effective temperature from the RGB. This phase change marks the TRGB. And nuclear physics fundamentally controls the stellar luminosity at which the RGB is truncated, essentially independent of the chemical composition and/or residual mass of the envelope sitting above the core. This is the underlying power of the TRGB: it is a physically based and theoretically well understood distance indicator.

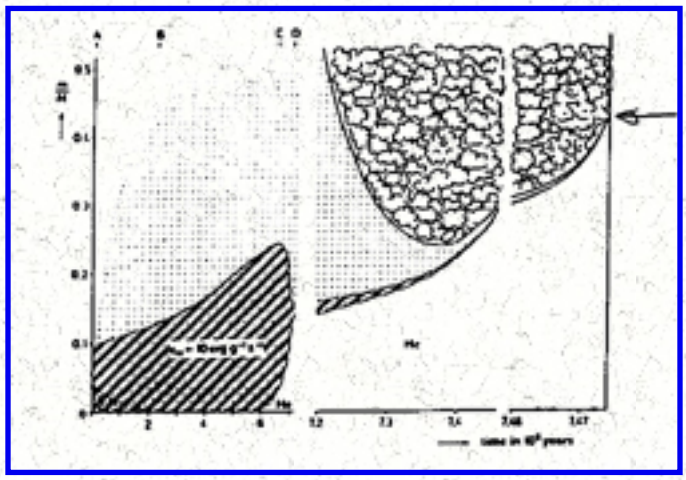

Figure 21. A schematic representation of the time evolution of the interior of a low-mass star from core hydrogen burning (A-B-C) through shell-hydrogen burning (D), ending with abrupt core Helium ignition at 7.47 x 10^9 years (arrow). Adapted from Thomas (1967).

24. RECENT APPLICATIONS OF THE TRGB METHOD

24.1. *Ground-based Studies: The Local Group*

A comparison of 10 galaxies with estimated TRGB distances with those having primary distances estimated using Cepheids or RR Lyrae stars was presented by Lee, Freedman & Madore (1993). These galaxies covered a wide range of morphological types (dwarf ellipticals: NGC 147, NGC 185 and NGC 205, an early-type spiral: M31, a late-type spiral: M33, and several irregulars: NGC 3109, NGC 6822, IC 1613 and WLM), covering a range of luminosity, metallicity, and distances up to *(m - M)* = 25.5 mag. The results of this comparison with Cepheid and RR Lyrae distances were extremely encouraging: the difference in the *relative* distances amounts to less than ± 10% *(rms)*, or 5% in distance.

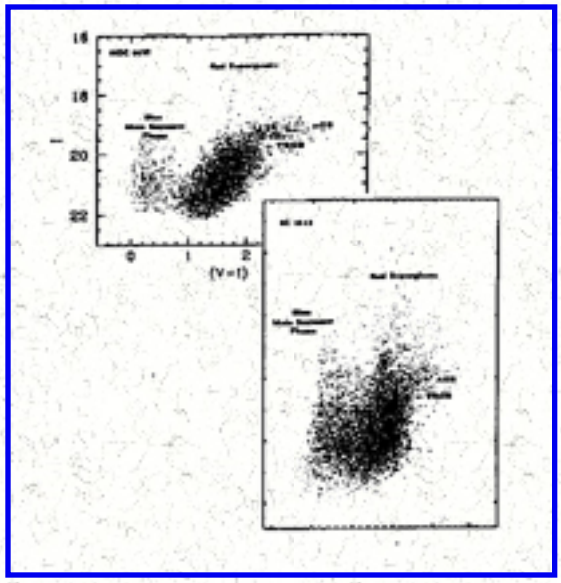

Figure 22. A montage of modern I - (V - I) color-magnitude diagrams for the two Local Group galaxies IC 1613 (lower right) and NGC 6822 (upper left). While red and blue supergiants are marked along with the AGB population, it is clear that the dominant contributor is the RGB with its broad and distinctive upper luminosity plateau marking the TRGB. The NGC 6822 data are adapted from the thesis of Gallart (1996).

Motivated by this result, we undertook a number of follow-up studies including simulations (Madore & Freedman 1995) to investigate the sources of error and factors limiting the application of this method. Then, using the combined facilities of the Palomar 5m and Las Campanas 2.5m we have begun a complete survey of TRGB distances to all galaxies in the Local Group and as far beyond it as aperture and seeing conditions will permit. To date, the results for two galaxies slightly peripheral to the Local Group, Sextans A and Sextans B have been submitted for publication. These objects were chosen to allow a further comparison with the Cepheid distance scale, given that Cepheids have been observed in both of these galaxies and the derived distances indicated that the TRGB would be readily detected from the ground. And indeed it was, with both galaxies showing the tip at I ~ 21.7 mag. Other galaxies currently being under study are NGC 3109, WLM, M33, and the various dwarf elliptical companions to M31.

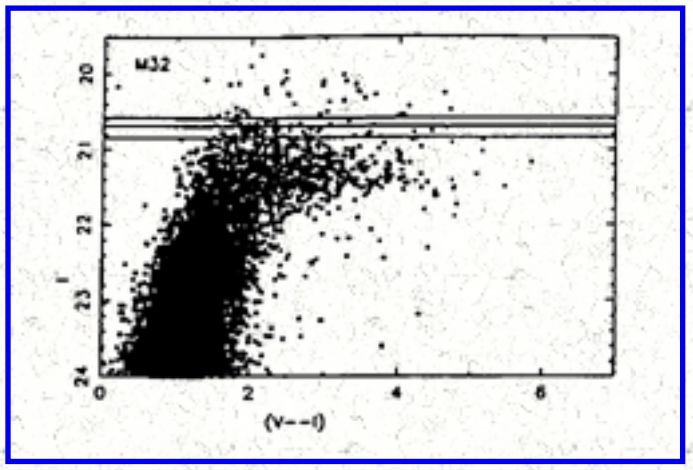

Figure 23. The I - (V - I) color-magnitude diagram for stars in M32 as derived from WFPC-2 HST observations by Grillmar *et al.* (private communication). Note that while the reddest (metal-rich) bright giant stars are found progressively at fainter magnitudes the bluest (metal-poor) giants still define the brightest tip. The horizontal lines mark the expected magnitude for the TRGB based on three apparent Cepheid moduli derived for various fields in M31, which is thought to be the parent galaxy of M32, and therefore at the same distance.

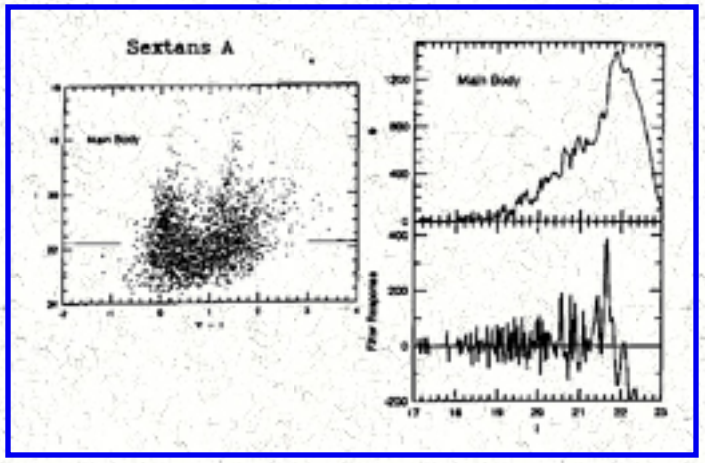

Figure 24. Sextans A: The left panel shows the I - (V - I) color-magnitude diagram for the main body of the dwarf irregular galaxy Setxans A. The horizontal lines at I ~ 21.7 mag mark the derived apparent magnitude level of the TRGB. The upper right panel shows the apparent I-band luminosity function for the stars in Sextans A; the lower right panel shows the Sobel response function identifying the position of the discontinuity in the luminosity function (Sakai, Madore & Freedman (1996a).

24.2. *HST Applications: Inside 10 Mpc*

A number of researchers have already begun to use HST to apply the TRGB method to determining distances beyond the seeing/resolution limit of ground-based telescopes. For instance, the halo of the peculiar elliptical radio galaxy NGC 5128 (= Cen A) has been resolved by Soria *et al.* (1996) and their I-(V-I) color-magnitude diagram shows the TRGB at I = 24.1 mag, thereby providing a distance of 3.6 ± 0.2 Mpc. Similarly, Elson (private communication) reports the detection of the TRGB in the southern hemisphere lenticular galaxy NGC 3115, and quotes a preliminary distance of ~ 10 Mpc. And most recently, Sakai *et al.* (1997) report the detection of the TRGB in the giant elliptical galaxy NGC 3379 (= M105) at a distance of 11.5 ± 1.6 Mpc. This latter application is of special interest given that NGC 3379 is a member of a group (the Leo I Group) which has two spiral galaxy members which have had independent Cepheid-based distances derived. Tanvir *et al.* (1995) find a distance of 11.9 ± 0.9 Mpc for NGC 3368 (= M96), while Graham *et al.* (1997) derive a slightly lower modulus for their target spiral NGC 3351, corresponding to a distance of 10.0 ± 0.3 Mpc. While the differences in these Population I distances may indicate back-to-front geometry, they agree, individually and in the mean, to within ~ 10% of the Population II TRGB distance.

At the time of writing the authors were aware of two HST proposals to pursue applications of the TRGB method in the Virgo cluster. One proposal by Harris and collaborators was to image two low-metallicity dwarf galaxies directly; those exposures are still to be taken. On the other hand, early reports indicate that Ferguson *et al.* apparently have detected the red giant population *between* galaxies in the Virgo cluster core. However, at these large distances, very long integration times are essential to achieve the required signal-to-noise needed to detect stars at $I > 27$ mag, and consequently no color information is yet in hand.

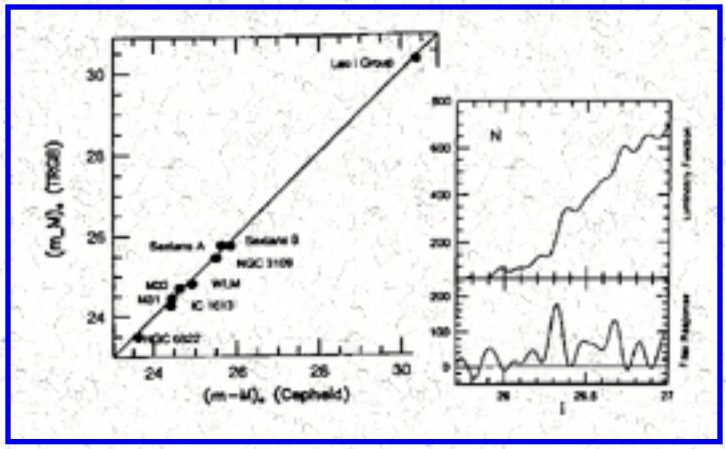

Figure 25. NGC 3379 and the Comparison of Cepheid Distances with the TRGB. The right panel shows both the I-band luminosity function (upper) and the tip response function (lower) for the HST observation of stars in the giant elliptical galaxy NGC 3379 (Sakai *et al.* (1997). The left panel shows a comparison of the NGC 3379 TRGB distance (marked by the Leo I Group) with the corresponding Cepheid-based distance to the group. Other Cepheid-TRGB comparisons are also shown for closer galaxies, Sextans A, NGC 3109, M33, *etc.*

25. THE SCORECARD

As a concluding summary we return to the list proffered at the beginning of the article as criteria that a successful extragalactic distance indicator might aspire to, and try to assess the TRGB in that context.

Luminous:

Indeed the luminosity generated by the helium core flash is enormous, being comparable to the instantaneous output of the rest of galaxy. Sadly, the duration of this burst is only a few seconds, and even more tragically, virtually all of that energy is absorbed internally within the star as it restructures itself en route to quiescent helium core burning on the horizontal branch. Nevertheless, the luminosity at which the upward evolution of the red giant star is terminated by core ignition is still quite luminous by stellar standards. In the I band the TRGB magnitude is as bright as a 5-day Cepheid variable.

Dispersionless:

By extragalactic standards, it is fair to say that any distance indicator that can claim a precision of ±0.20 mag (or 10% in distance) qualifies as being an excellent distance indicator. The TRGB method boasts an externally defined dispersion of less than ± 0.1 mag, comparable to Cepheid distance moduli.

Calibrated:

For the metallicity range -2.2 < [Fe/H] < -0.7 dex, the I-band color-magnitude diagrams for Galactic globular clusters calibrate the zero point of the TRGB method to the same level that the RR Lyrae distance scale is now known. As the RR Lyrae zero point is improved, the TRGB zero point will also get better with time.

Understood:

To first order, nuclear physics determines the bolometric luminosity at which all low-mass stars terminate.

Insensitive:

Theory predicts (and observations confirm) that the bolometric (I-band) magnitude is insensitive to chemical composition variations in the range -2.2 < [Fe/H] < -0.7 dex, and for ages in the calculated range 7-17 Gyr.

Abundant:

The halos of all galaxies are synonymous with Population II stars. If there is a measurable surface brightness defining these halos then the red giant branch stars must be present in abundance.

Ubiquitous:

Every galaxy (elliptical, spiral or irregular) must have had a first generation of stars. The low-mass and low-metallicity members of that generation of stars must now be populating the red giant branch, and defining the tip.

Unambiguous:

At the color and approximate magnitude level expected for TRGB stars other populations of stars do little more than add noise to the distinctive discontinuity in the red-giant-branch luminosity function. However, care should be taken that the TRGB is truly triggering the edge detector by having a fair sample of luminosity function well sampled below the tip before incompleteness in the photometry sets in. All too often that may prove to be a luxury in limiting applications, but the warning still stands.

26. CONCLUSIONS

The tip of the red giant branch (TRGB) method is as precise and as accurate as the Cepheid PL relation. Moreover, an extremely useful feature of the TRGB method is that it is applicable to any galaxy containing a detectable population of old, metal-poor, low-mass stars. In practice, this means that nearly all nearby galaxies, regardless of Hubble type and/or inclination, can now be placed on a common distance scale out to the crowding and the flux limits of CCD detectors and telescopes. These distances will allow, for the first time, a complete sample of accurate, uniformly-measured distances to all galaxies within the Local Group and out to distances of ~ 10 Mpc.

27. IMPLICATIONS OF THE HIPPARCOS OBSERVATIONS OF GALACTIC CEPHEIDS

Hipparcos parallaxes have recently become available for a sample of Galactic Cepheids, and we have used these new distances to calibrate the Cepheid period-luminosity (PL) relation at six wavelengths (*BVIJHK*). Comparing these calibrations with previously published multiwavelength PL relations we find agreement to within 0.07 ± 0.14 mag, or 4 ± 7% in distance. Unfortunately, the current parallax errors for the fundamental pulsators (ranging in signal-to-noise = $\pi / \sigma\pi$ from 0.3 to 5.3, at best) preclude an unambiguous interpretation of the observed differences, which may arise from a combination of true distance modulus, reddening and/or metallicity effects. We explore these effects and discuss their

implications for the distance to the Large Magellanic Cloud (LMC) and the Cepheid-based extragalactic distance scale. These results suggest a range of LMC moduli between 18.44 ± 0.35 and 18.57 ± 0.11 mag; however, other effects on the Cepheid PL relation (*e.g.*, extinction, metallicity, statistical errors) are still as significant as any such reassessment of its zero point.

27.1. *Introduction*

Feast and Catchpole (1997 = FC97 hereafter) have recently published the first results on parallaxes to Galactic Cepheids based on measurements from the Hipparcos satellite. They list data for the 26 highest signal-to-noise Cepheid parallaxes; and after an extensive series of reductions (see their Table 2) they conclude that the best fit PL relation for the visual bandpass is M_V = -2.81 *log (P)* - 1.43, with a standard error on the Hipparcos zero point of ± 0.10 mag, adopting the slope from prior work on LMC Cepheids. The authors go on to apply this V-band solution to determining the distance modulus of the LMC corrected for *E (B-V)* = 0.074 mag. Adding a metallicity correction of +0.042 mag and adopting $< V >_0$ - *log (P)* from Caldwell & Laney (1991) gives $(m\text{-}M_V)_0^{LMC}$ = 18.70 ± 0.10 mag. In this *Letter* we go beyond the V-band PL relation and explore the implications of the Hipparcos data for the multiwavelength calibrations of the Cepheid PL relation from the blue (B-band) out into the near infrared (2.2 μm K-band).

28. COMPARISON WITH V-BAND PERIOD-LUMINOSITY RELATIONS

In Figure 26 we compare differentially four calibrations (heavy dotted lines) of the V-band Cepheid PL relation with the FC97 Hipparcos-based relation (solid horizontal lines). The first two comparisons (in the upper two panels) are with the relations given by Madore & Freedman (1991; hereafter MF91), derived from self-consistent sets of LMC Cepheid data whose stars either had complete *BVRI* observations (MF91.1 containing 32 Cepheids) or complete *BVRIJHK* observations (MF91.2 containing 25 stars).* These first two solutions indicate the sensitivity of slopes and zero points to sample selection, which are considerable, but within the quoted statistical uncertainties: ± 0.11 and ± 0.20, respectively for the slopes, and ± 0.05 and ± 0.09 mag, for the zero points. So as to make the subsequent comparisons consistent, the original Sandage & Tammann (1968) calibration (ST68.1 in the lower left panel) has been placed on the modern Hyades/Pleiades Galactic cluster distance scale by applying a single offset of +0.13 mag derived from the average difference between the absolute magnitudes of the Cepheids used in the 1968 calibration updated to Feast and Walker (1987), their Table 2. This distance scale corresponds to a Hyades modulus of 3.27 (see Pel 1985) and uses the Pleiades main sequence, at a modulus of 5.57 (van Leeuwen 1983) to effectively correct for the over-metallicity of the Hyades with respect to the older Galactic clusters in which the Cepheid calibrators are found.** Finally, the FW87 calibration itself is plotted in the lower left panel. In all panels the dashed horizontal lines represent the fiducial Hipparcos calibration flanked by thin parallel lines at ± 0.10 mag.

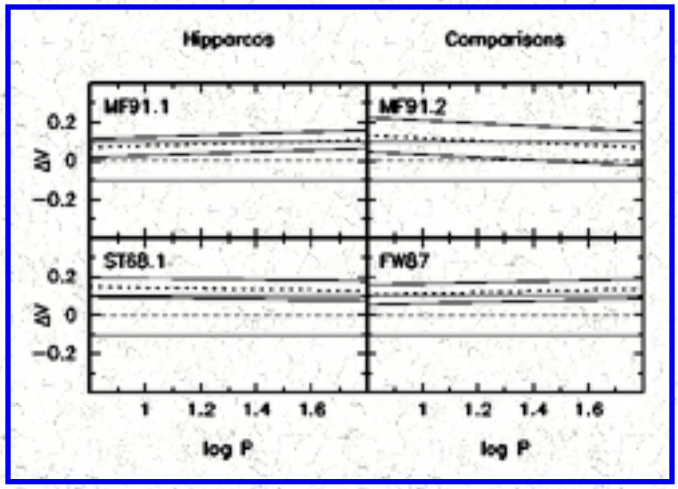

Figure 26. Differential comparison of recently published V-band PL relations (heavy lines) relative to the Hipparcos calibration (thin lines). Plotted is the difference [*V* - *V*(Hipparcos)] versus log P, in the sense that if Hipparcos is brighter the difference shown is positive.

The error bars of all of the plotted previously published relations overlap with errors quoted for the Hipparcos solution (a formal uncertainty was not given by ST68, so we have arbitrarily assigned them an error of ± 0.05 mag). However, the offsets are not randomly distributed, with each of the solutions appearing to be systematically fainter in *V* with respect to the Hipparcos calibration by about 0.1 mag. We discuss the significance and possible implications of this difference in the following sections.

---

* Tanvir (1997) has suggested that there may be small corrections (ranging from 0.02 to 0.09 mag) to the published I-band magnitudes of these LMC Cepheids arising from the originally sparse sampling and consequent averaging of their light and color curves. For the past five years we have been obtaining new VI CCD observations of the LMC calibrators at Las Campanas and now also at Siding Springs Observatories. These new data are designed to address those concerns.

** At the February 14, 1997 meeting of the Royal Astronomical Society in London on February 14, 1997 F. van Leeuwen and C.S. Hansen Ruiz reported a true distance modulus of 5.29 ± 0.06 mag for the Pleiades cluster, based on Hipparcos trigonometric parallaxes. Following the Venice Meeting in June 1997 the value had changed only slightly to 5.33 ± 0.06 mag (C. Turon, private communication). If adopted, this Pleiades modulus would make the Galactic-cluster-based calibrations approximately 0.3 mag fainter than the FC97 solution plotted in Figure 27. At this point in time, the Galactic cluster zero point appears to be in a state of flux, and we will not comment on it further, except to note that the Hipparcos calibration will undoubtedly converge on a more accurate zero point than we have access to at this precise moment.

29. MULTIWAVELENGTH PERIOD-LUMINOSITY RELATIONS

In Madore & Freedman (1991) we published fiducial PL relations in seven bandpasses: *BVRIJHK*. These were all based on selecting self-consistent sets of previously published LMC Cepheid data, scaled to an LMC true distance modulus of 18.50 mag and applying a single line-of-sight reddening correction

using $E(B\text{-}V) = 0.10$ mag. Thirty-two stars were available for a calibration of *BVRI* PL relations; 25 stars were used for an alternative set of *BVRIJHK* calibrations. In the following we compare those multiwavelength PL relations with the Hipparcos sample of Galactic Cepheids, individually corrected for foreground reddening and scaled to their geometric parallax distances. We have collected from the literature multiwavelength (*BVIJHK*) mean magnitudes for as many of the Hipparcos-calibrating Cepheids as have been published (notably for the infrared Wisniewski & Johnson 1968, Welch *et al.* 1984, Laney & Stobie 1992 and reference therein). These form rather disjoint subsets. After eliminating the suspected overtone pulsators listed by FC97, the total available sample with parallaxes drops from 26 to 20. Of these only 7 have mean magnitudes published at all six wavelengths, while 10 and 13 Cepheids, respectively have either *BVIJK* or *BVJK* magnitudes in common. We have analyzed these four groups of stars independently, but self-consistently, in the following way.

Using the Hipparcos parallaxes and Galactic reddenings adopted by FC97 from Fernie, Kamper & Seager (1993) scaled to the various wavelengths using the extinction law of Cardelli *et al.* (1989), we derived absolute magnitudes for each of the Cepheids in each of the observed wavelengths. (We note that these corrections for interstellar extinction are not inconsiderable, ranging up to 2 mag in *B* for several stars). The resulting PL relations are shown in the six panels of Figure 27. Error bars are one-sigma uncertainties from the quoted parallaxes. Note the highly correlated nature of the individual data points about the fiducial lines. And too, we remind the reader that the computation of distances and their related errors from observed parallaxes is non-trivial (Brown *et al.* 1997), as distances are not linearly related to parallaxes, and parallax errors can subtly bias samples. A full treatment of this issue is beyond the scope of this paper, but we note that selection biases at least are minimized for stars having the smallest reported errors. As discussed by Brown *et al.*, given the true parallax distribution the expected biases follow naturally; however, corrections to the *observed* parallaxes require assumptions about the true distribution, and detailed modeling. Fortunately for this application the Cepheid sample is not parallax-selected; the objects being chosen in advance based on their optical variability, periods and apparent magnitudes.

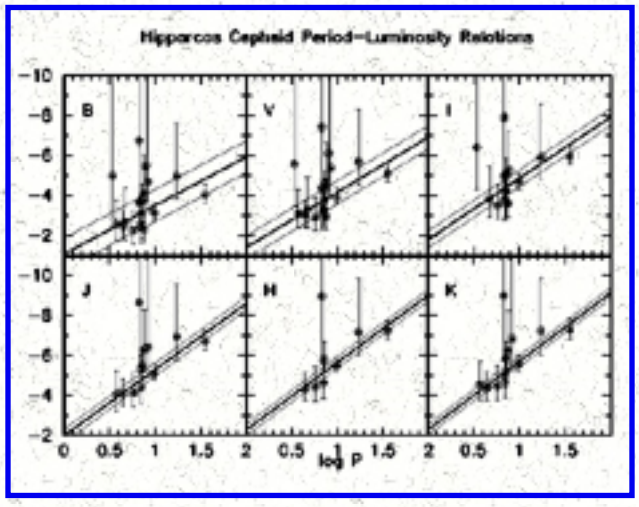

Figure 27. Multiwavelength Period-Luminosity relations for Cepheids with Hipparcos parallaxes, plotting all stars that have data available at the particular wavelength, as noted in the upper left corner of each panel. In each panel the solid sloping line is not a fit to the data, but rather it is the published calibration of Madore & Freedman (1991) flanked by thin parallel lines representing the 2-σ limits quoted by them as being the intrinsic width of the instability strip at each wavelength.

The differences between these individual (trigonometric) absolute magnitudes and the predicted *BVIJHK* magnitudes derived from the mean PL relations of MF91 (solid lines in Figure 27) are each plotted in

Figure 28 against the corresponding B-band residual. The *(B-V)* intrinsic color residuals are plotted against the B-band residuals in the upper right panel. The individual residuals at a given wavelength contain random contributions from the parallax uncertainties, reddening errors, and finally the intrinsic (temperature-induced) magnitude residuals which reflect the finite width of the Cepheid instability strip. The observed residuals are however extremely large (nearly 5 mag peak-to-peak) and are almost certainly dominated by the (achromatic) errors in the parallaxes, given the strict unit-slope correlation of the mag-mag residuals, and the total lack of any correlation between the magnitude-color residuals (Figure 28).

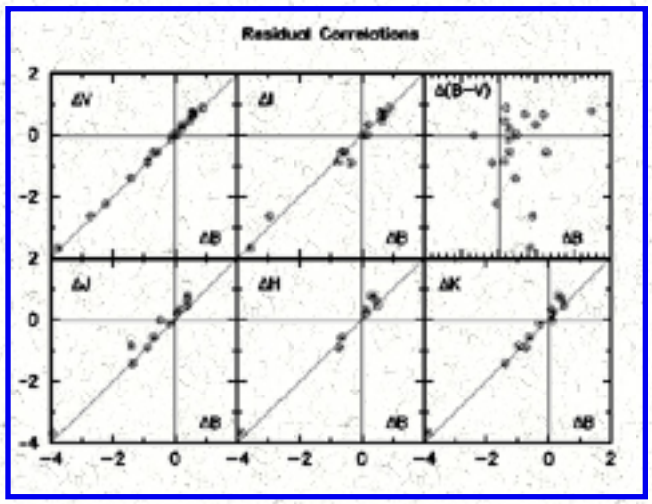

Figure 28. B-band residuals from the multiwavelength Period-Luminosity relations in Figure 27 are sequentially plotted as a function of residuals from each of the other five PL relations and (upper right panel) against the (B-V) color residuals. The total lack of correlation in the latter instance is unexpected except in the limit where the residuals are dominated by distance errors in the derived parallaxes. This latter situation is apparently the case given the strong (unit-slope) correlations of the residuals in each of the other panels, regardless of wavelength.

Wavelength-dependent offsets between the six mean solutions independently will reflect **(1)** errors in the adopted true distance to the LMC (which set all of the zero points in the MF91 multiwavelength PL relation calibrations), **(2)** reddening errors in the adopted extinction to the LMC sample of calibrating Cepheids, and finally **(3)** intrinsic differences between the LMC and Galactic Cepheids, for example, due to metallicity.

Our first solution considers the largest data set (in terms of parallaxes) but the one that is most restricted in terms of wavelength coverage: it consists of 19 Cepheids observed in *B* and *V*. Weighted by the square of the signal-to-noise ratio in the Hipparcos parallax, the residuals were summed and averaged at each of the two wavelengths giving mean offsets between the LMC calibration and the Galactic Cepheids. The variance in each mean offset was then calculated from the average of the squares of these same residuals again inversely weighted by the variance in the individually quoted parallaxes. The differences are $\delta B = +0.23 \pm 0.35$ mag and $\delta V = +0.16 \pm 0.28$ mag, in the sense that the LMC Cepheid calibration appears to be too faint with respect to the Galactic calibration. (Further restricting the sample to only those 12 stars with $\pi / \sigma\pi > 2.0$ changes δB to $+0.22 \pm 0.24$ mag and δV to $+0.15 \pm 0.17$ mag.)

If the (statistically marginal, but apparently systematic) differences in the *B* and *V* solutions were to be ascribed to reddening alone, then the Galactic data and the LMC calibration can be reconciled by invoking an increase of $\delta E\,(B\text{-}V) = 0.07$ mag in the adopted mean reddening to the LMC Cepheid sample. This is consistent with a similar suggestion regarding the LMC Cepheid calibration made

recently by Bohm-Vitense (1997) based on different data. This reddening solution has the consequence that it would also require the distance modulus of the LMC to be revised *downwards* by -0.06 mag to 18.44 mag; the uncertainty on this offset being at least as large as the uncertainty in the individual moduli (± 0.3 mag), depending on the degree of correlation in those cumulative uncertainties. This particular path, of a reddening solution, cannot be considered definitive. Other possibilities are: **(1)** the LMC true modulus should be increased by (0.23 + 0.16) / 2 = +0.20 mag, without any change to the foreground reddening, or **(2)** that there are differential metallicity corrections amounting to -0.23 and -0.16 mag that need to be applied at the *B* and *V* wavelengths, respectively. Of course, any suitably contrived linear combination of the above three effects could also be invoked. More constraints on the problem are obviously needed.

An alternative possibility is that some of the wavelength-dependent effects seen in the comparison of Galactic (high metallicity) data with the LMC (lower metallicity) data could be due to chemical composition differences between the two samples. Taken at face value the dependence of the apparent *V* modulus on metallicity would be very large, $\delta V / \delta[Fe/H] = 0.16 / 0.15 = 1.1$ (± 1.9) mag/dex, assuming that the full offset in *V* noted in the above comparison is due to metallicity, and adopting a metallicity underabundance of 1.4x between the LMC and the Solar neighborhood (see, for example, FW87). However, we note that this effect is basically indistinguishable from reddening in its form (as evidenced by our first set of solutions), and that the offset (whatever its origin) when treated as reddening leads to a true distance modulus for the LMC that is unchanged, from previous assumptions, at 18.50 mag. Given this apparent degeneracy between reddening and metallicity, and the current large uncertainties in the parallaxes, assessing the dependence on metallicity from these data alone will remain problematic.

To obtain added leverage on the solution, moving to the infrared has numerous well known advantages, as first articulated in McGonegal *et al.* (1982): reddening effects are known to decrease with wavelength, in a well defined and calibrated manner; and simultaneously, metallicity effects are also expected to decrease in amplitude with increased wavelength.

Our second solution is based on 13 Cepheids each having *BVJK* data in common. This four-color solution gives a derived reddening *increase* for the LMC Cepheid sample of +0.04 ± 0.08 mag, with no formal offset in the derived 18.50 ± 0.13 mag true modulus for the LMC. Our next approximation employs 10 Cepheids each now having *BVIJK* mean magnitudes. Here the formal solution for the true modulus for the LMC is 18.53 ± 0.14 mag, with a corresponding increase in the mean reddening of +0.06 ± 0.07 mag. Finally, we have analyzed a sample of 7 Galactic Cepheids, each having *BVIJHK* photometry, to obtain one last solution: $\delta E(B-V) = 0.07 \pm 0.07$ mag with $(m-M)_{LMC} = 18.57 \pm 0.11$ mag. The fit to this final set of observations is shown in Figure 29; the χ^2 weighted residual fitting surface being shown as an inset. The individual apparent moduli discussed here, and their errors, are summarized in Table 1.

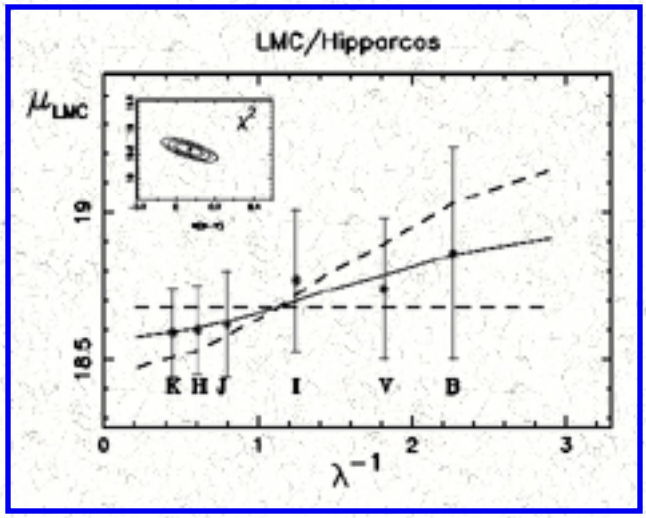

Figure 29. Apparent modulus plots for LMC Cepheids observed at *BVIJHK* scaled to the Hipparcos zero point and using the published multiwavelength PL solutions of Madore & Freedman (1991). The solid line is a weighted χ^2 fit of a reddening line to the data; the broken line indicates the one-sigma limits on that solution. Inset (top left) shows the χ^2 surface indicating the minimization solution for the modulus and reddening and the interdependence of their associated errors.

Table 1. Multiwavelength Reddening Solutions

No. Stars	$\mu_B \pm \sigma$	$\mu_V \pm \sigma$	$\mu_I \pm \sigma$	$\mu_J \pm \sigma$	$\mu_H \pm \sigma$	$\mu_K \pm \sigma$
19	18.73 ± 0.35	18.66 ± 0.28	. . .	. . .	. . .	. . .
13	18.71 ± 0.36	18.64 ± 0.24	. . .	18.44 ± 0.23	. . .	18.54 ± 0.13
10	18.74 ± 0.36	18.67 ± 0.24	18.71 ± 0.20	18.44 ± 0.24	. . .	18.57 ± 0.14
7	18.86 ± 0.36	18.74 ± 0.24	18.77 ± 0.24	18.62 ± 0.18	18.60 ± 0.15	18.59 ± 0.15

Finally, if we now adopt the metallicity correction of $\delta V = 0.04$ mag advocated by FC97 and assume that the effects at JHK are negligible, (and eliminate *B* and *I* from the solution given that metallicity corrections for these filters are not well defined at this time) we find for this 4-color solution $\delta E\ (B\text{-}V) = 0.06 \pm 0.11$ mag with $(m\text{-}M)_{LMC} = 18.57 \pm 0.11$ mag. This is virtually indistinguishable from the full *BVIJHK* solution given above.

30. SUMMARY OF HIPPARCOS RESULTS

We have used the Hipparcos parallaxes of nearby Galactic Cepheids to explore corrections to the multiwavelength Period-Luminosity relations for LMC Cepheids. The latter are based on an LMC data set scaled to a true distance modulus of 18.50 mag and an adopted foreground reddening of $E\ (B\text{-}V) = 0.10$ mag. Although the current uncertainties in the parallaxes are large and still dependent upon the

specific subsets of the Cepheids chosen for the comparison, the agreement is good, indicating that to within ± 0.14 mag (or, 7% in distance) the previously adopted zero point is substantially correct. Based on different subsamples of data either having *BV*, *BVJK*, *BVIJK* or *BVIJHK* photometry, LMC moduli, ranging from 18.44 to 18.57 mag are derived. These results, summarized in Table 2, differ from the value of 18.70 mag of FC97, which are based solely on the reddening-corrected V photometry of Caldwell & Laney (1991), externally adjusted for metallicity. The Hipparcos data alone do not allow us to discriminate between metallicity effects and the physically distinct possibility of added reddening to the LMC.

Table 2. Multiwavelength Reddening Solutions

Filters	No. Stars	$E\ (B\text{-}V) \pm \sigma$	$\mu_{LMC} \pm \sigma$
BV	19	0.17 ± . . .	18.44 ± 0.35
BVJK	13	0.14 ± 0.08	18.50 ± 0.13
BVIJK	10	0.16 ± 0.07	18.53 ± 0.14
BVIJHK	7	0.17 ± 0.07	18.57 ± 0.11
V_CJHK	8	0.16 ± 0.11	18.57 ± 0.11

To alleviate the ambiguity posed by the need to simultaneously solve both for reddening and metallicity effects on the Cepheid distances we are currently deriving OB-star reddenings along the individual lines of sight to several dozen LMC Cepheids. This will allow us to decouple the reddening determinations from metallicity effects, and go beyond the use of a single mean (foreground + internal) reddening for the LMC calibrating Cepheid sample. Preliminary reductions indicate that the variance from field to field is large (ranging from $E\ (B\text{-}V) = 0.00$ up to 0.40 mag) while still indicating that an average value of $< E\ (B\text{-}V) > = 0.10$ mag is appropriate for the LMC calibrating Cepheids. Details will be presented in Madore, Freedman & Pevunova (1998 in preparation).

We close by noting that at least three other very recent determinations of the true modulus to the LMC fall on either side of the value 18.50 mag adopted by MF91 in setting a zero point for the Cepheid distance scale. Both Reid (1997) and Gratton *et al.* (1997) derive large LMC moduli (18.65 ± 0.10, and 18.63 ± 0.06 mag, respectively) using Hipparcos-based calibrations of the Galactic globular cluster and RR Lyrae distance scale. On the other hand, Gould & Uza (1997) have re-analyzed the SN 1987A supernova ``light echo'' and derive *an upper limit* of $\mu_{LMC} < 18.37 \pm 0.04$ mag for the LMC true distance modulus; although they note that if the ring is slightly elliptical ($b / a \sim 0.95$) this upper limit increases to < 18.44 ± 0.05 mag. A value of 18.56 ± 0.05 mag has been derived by Panagia *et al.* (1996) from the same data. Until these differences are fully understood and resolved, and given the remaining uncertainties in the Hipparcos Cepheid parallax data, we prefer to adopt a true distance modulus of

18.50 mag for the LMC, but now bounded by an uncertainty of ± 0.15 mag, defined to fully encompass the above range of recently published values. This value is consistent with other estimated distances to the LMC based on a wide variety of methods (for a comprehensive modern review see Westerlund 1997). Viewed in that perspective, the Hipparcos data confirm the Cepheid distance scale at better than the ± 10% level (95% confidence).

31. IMPLICATIONS OF A CEPHEID DISTANCE TO THE FORNAX CLUSTER

Thirty-seven long-period Cepheid variables have been discovered in the Fornax cluster spiral galaxy, using the Hubble Space Telescope. The resulting V and I period-luminosity relations give a true modulus of $\mu_0 = 31.28 \pm 0.07$ mag, corresponding to a distance of 18.0 ± 0.6 Mpc. A Cepheid distance to the Fornax cluster offers several means of estimating the Hubble constant. First, associating this distance with the Fornax cluster as a whole gives a local Hubble constant of $H_0 = 73\ (\pm 7)_{random}\ [\pm 18]_{systematic}$ km/sec/Mpc. Second, the Fornax cluster provides a means of calibrating a wide variety of secondary distance indicators. Recalibrating the Tully-Fisher relation using NGC 1365 and 6 nearby spiral galaxies, applied to 15 clusters out to 100 Mpc gives $H_0 = 76\ (\pm 2)_r\ [\pm 8]_s$ km/sec/Mpc. A broad-based set of differential moduli established from Fornax out to Abell 2147, nearly a factor of ten in distance further, gives $H_0 = 72\ (\pm 1)_r\ [\pm 7]_s$ km/sec/Mpc. With the addition of two Type Ia supernova calibrators in Fornax and correcting the supernova peak luminosities for decline rate, gives $H_0 = 68\ (\pm 5)_r\ [\pm 8]_s$ km/sec/Mpc, out to a distance in excess of 500 Mpc. Seven Cepheid-based distances to groups of galaxies out to and including the Virgo and Fornax clusters yield $H_0 = 70\ (\pm 3)_r\ [\pm 16]_s$ km/sec/Mpc. These major distance determination methods agree to within their statistical errors. The resulting value of the Hubble constant, encompassing all those determinations which are based directly on Cepheids or tied to secondary distance indicators, is found to be $H_0 = 72\ (\pm 3)_r\ [\pm 12]_s$ km/sec/Mpc, out to cosmologically significant distances.

31.1. *Introduction*

Hubble (1929) announced his discovery of the expansion of the Universe nearly 70 years ago. Despite decades of effort, and continued improvements in the actual measurement of extragalactic distances, convergence on a consistent value for the absolute expansion rate, as parameterized by the Hubble constant, H_0, was not forthcoming. However, progress in the last few years has been rapid and dramatic (see, for instance, Freedman, Madore & Kennicutt 1997; Mould, Sakai, Hughes & Han 1997; Tammann & Federspiel 1997). This accelerated pace has occurred primarily as a result of the improved resolution of the Hubble Space Telescope (and its consequent ability to discover classical Cepheid variables at distances a factor of ten further than can routinely be achieved from the ground), giving accurate zero points to a number of recently refined methods which can measure precise relative distances beyond the realm of the Cepheids. These combined efforts are providing a more accurate distance scale for local

galaxies, and are indicating a convergence among various secondary distance indicators in establishing an absolute calibration of the far-field Hubble flow.

Soon after the December 1993 HST servicing mission it was clear that the measurement of Cepheids in the Virgo cluster (part of the original design specifications for the telescope) was feasible (Freedman *et al.* 1994a). And although the subsequent discovery of Cepheids in the Virgo galaxy M100 (Freedman *et al.* 1994b) and subsequent refinements (Ferrarese *et al.* 1996) were important steps in resolving outstanding differences in the extragalactic distance scale (Mould *et al.* 1995), the Virgo cluster is complex both in its geometric and its kinematic structure, and there still remain large uncertainties in both the velocity and distance to this cluster. Virgo clearly was, and still is, not an ideal test site for an unambiguous determination of the cosmological expansion rate or the calibration of secondary distance indicators. In this paper we discuss the implications of a Cepheid distance to the next major clustering of galaxies, the Fornax cluster, which is a much less complicated system than Virgo.

32. NGC 1365 AND THE FORNAX CLUSTER

The Fornax cluster is comparable in distance to the Virgo cluster (de Vaucouleurs 1975), but it is found almost opposite to Virgo in the skies of the southern hemisphere. The Fornax cluster is less rich in galaxies than Virgo (Ferguson & Sandage 1988), but it is also substantially more compact than its northern counterpart (Figure 30). As a result of its lower mass, the influence of Fornax on the local velocity field is less dramatic than that of the Virgo cluster. And because of its compact nature, questions concerning the membership of individual galaxies in Fornax are less problematic, while the back-to-front geometry is far less controversial than any of these same points raised in the context of the Virgo cluster complex. Clearly, Fornax is a much more interesting site for a test of the local expansion rate. < p style="font-family: cursive" align=justify> **Figure 30.**A comparison of the distribution of galaxies as projected on the sky for the Virgo cluster (right panel) and the Fornax cluster (left panel). M100 and NGC 1365 are each individually marked by arrows showing their relative disposition with respect to the main body and cores of their respective clusters. Units are arcmin.

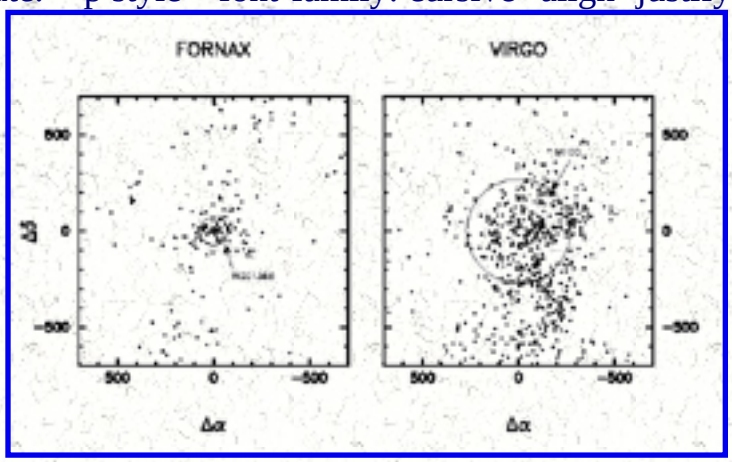

Although the goals of the Key Project on the Extragalactic Distance Scale (Kennicutt *et al.* 1995) are far broader than simply investigating the distances to a few nearby clusters, there are several important reasons to secure a distance to the Fornax cluster. It is both a probe of the local expansion velocity field, and Fornax is a major jumping-off point for a variety of secondary distance indicators which can be used

to probe a volume of space at least 1,000 times larger. To obtain a distance to the Fornax cluster, the Key Project is configured to monitor three member galaxies; the first of these, discussed here, is the Seyfert 1 galaxy NGC 1365, a strikingly picturesque, two-armed, barred-spiral galaxy with an active galactic nucleus. In the coming year, two additional galaxies, NGC 1425 and NGC 1326A, are slated for imaging with HST.

At least three lines of evidence independently suggest that the first galaxy to be observed, NGC 1365 is a physical member of the Fornax cluster. First, NGC 1365 is almost directly along our line of sight to Fornax. The galaxy is projected only ~ 70 arcmin from the geometric center of the cluster, whereas the diameter of the cluster is ~ 200 arcmin (Ferguson 1989; see Figure 30). In addition, NGC 1365 is also coincident with the Fornax cluster in velocity space. The systemic (heliocentric) velocity and velocity dispersion of the main population of galaxies in Fornax are well defined: 30 spirals/irregular galaxies give V = 1,415 km/sec and σ = ± 347 km/sec, 70 E/SO galaxies give V = 1,473 km/sec with σ = ± 335 km/sec, and the combined sample gives σ = ± 340 km/sec. The observed velocity of NGC 1365 (+1,636 km/sec) is only +181 km/sec larger than the mean velocity of the Fornax cluster as a whole, which based on 100 galaxies is found to be 1,455 ± 34 km/sec (Schroder 1995; Schroder & Richter 1997; Han & Mould 1990; NED); with the mean velocity of the spirals agreeing with the mean for the ellipticals to within 60 km/sec). The velocity off-set of NGC 1365 is only half of the cluster velocity dispersion. Finally, we note that for its rotational velocity, NGC 1365 sits only 0.02 mag from the central ridge line of the *apparent* Tully-Fisher relation relative to other cluster members defined by recent studies of the Fornax cluster (Bureau *et al.* 1996; Schroder 1995).

On the other hand, it is often noted that NGC 1365 is impressively large in its angular size, and that it is very bright in apparent luminosity as compared to any other galaxy in the immediate vicinity of the Fornax cluster. However, corrected for an inclination of 44 degrees, the 21cm neutral hydrogen line width of NGC 1365 is found to be ~ 575 km/sec (Bureau *et al.* 1996; Mathewson *et al.* 1992). Using the Tully-Fisher relation as a *relative* guide to intrinsic size and luminosity, this rotation rate places NGC 1365 among the most luminous galaxies in the local Universe; brighter than M31 or M81, and comparable to NGC 4501 in the Virgo cluster or NGC 3992 in the Ursa Major cluster. We therefore conclude that NGC 1365 is in all respects apparently normal, (albeit large and luminous) and that its distance is indicative of the ensemble distance to the other spiral and elliptical galaxies constituting the Fornax cluster proper.

33. HST OBSERVATIONS

Using the *Wide Field and Planetary Camera 2* on HST, we have obtained a set of 12-epoch observations of NGC 1365. These observations were begun on August 6, and continued until September 24, 1995. The observing window of 44 days was selected to maximize target visibility, without necessitating any roll of the targeted field of view. Sampling within the window was prescribed by a power-law

distribution, tailored to optimally cover the light and color curves of Cepheids with anticipated periods in the range 10 to 60 days (see Freedman *et al.* 1994a for additional details). Contiguous with 4 of the 12 V-band epochs, I-band exposures were also obtained so as to allow reddening corrections for the Cepheids to be determined. Each V-band epoch made use of the F555W filter and consisted of two exposures split between orbits (and allowing for cosmic ray rejection); a total of 5,100 sec of V-band data were obtained at each epoch in the course of the monitoring program. The I-band exposures (F814W) totaled 5,400 sec each, again cosmic-ray split and accumulated over two orbits.

All frames were pipeline pre-processed at the *Space Telescope Science Institute* in Baltimore and subsequently analyzed in Pasadena using ALLFRAME (a suite of special-purpose stellar photometry packages (Stetson 1994). A second independent reduction is being performed using the DoPhot photometry package. At this juncture, we are still allowing for the possibility of a 10% systematic offset in the true modulus derived from the two packages (Table 3); the results discussed here are based solely on the ALLFRAME analysis. Zero-point calibrations for the photometry were adopted (Holtzmann, J. *et al.* 1995; Hill *et al.* 1997), which agree to 0.05 mag on average. Details on the DoPHOT and ALLFRAME reduction and analysis of this data set are presented elsewhere (Silbermann, *et al.* 1997). We are also currently undertaking artificial star tests on these frames to quantify the uncertainty due to crowding.

Table 3. ERROR BUDGET ON THE CEPHEID DISTANCE TO NGC 1365

Source of Uncertainty on the Mean	Description of Uncertainty	Percentage Error	
LMC	**CEPHEID PL CALIBRATION**		
[A] **LMC True Modulus**	Independent Estimates = 18.50 ± 0.10 mag	5%	
[B] **V PL Zero Point**	LMC PL σ_V = (0.27) / $\sqrt{}$ 31 = ± 0.05 mag	3%	
[C] **I PL Zero Point**	LMC PL σ_I = (0.18) / $\sqrt{}$ 31 = ± 0.03 mag	2%	
[SC] **Systematic Uncertainty**	[A] + [B] + [C] combined in quadrature		6%
NGC 1365	**CEPHEID TRUE DISTANCE MODULUS**		
(D) **HST V-Band Zero Point**	On-Orbit Calibration: ± 0.05 mag	3%	
(E) **HST I-Band Zero Point**	On-Orbit Calibration: ± 0.05 mag	3%	
(M1) **Cepheid True Modulus**	(D)(E) are uncorrelated, but coupled by reddening law: σ_{μ_0} = ± 0.15 mag	7%	
(F) **Cepheid V Modulus**	NGC 1365 PL σ_V = (0.32) / $\sqrt{}$ 37 = ± 0.05 mag	3%	
(G) **Cepheid I Modulus**	NGC 1365 PL σ_I = (0.31) / $\sqrt{}$ 37 = ± 0.05 mag	3%	
(M2) **Cepheid True Modulus**	(F)(G) are partially correlated, giving σ_{μ_0} = ± 0.06 mag	3%	

(P1) **V-Band Ap. Corr.**	Silberman *et al.* (1998) give ± 0.067 mag	3%	
(P2) **I-Band Ap. Corr.**	Silberman *et al.* (1998) give ± 0.061 mag	3%	
(M3) **Cepheid True Modulus**	(P1)(P2) are uncorrelated, but coupled by reddening law: σ_{μ_0} = ± 0.15 mag	7%	
[Z] **Metallicity**	M31 metallicity gradient test gives σ_{μ_0} = ± 0.08 mag	4%	
	M101 calibration gives +0.14 mag of $\delta \mu_0 / \delta [Fe / H]$ = -0.25 mag/dex	7%	
[H] **Reduction Package**	Systematic differences in aperture corrections (achromatic)	4%	
(J) **Random Errors**	(M1) + (M2) + (M3) combined in quadrature		10%
[K] **Systematic Errors**	[SC] + [Z] + [H] combined in quadrature		10%
	D = 18.6 Mpc ± 1.9 (random) ± 1.9 [systematic]		

Note: There are 32 Cepheids in the LMC with published VI photometry (Madore & Freedman 1991.) The measured dispersions in the period-luminosity relations at V and I are ± 0.27 and ± 0.18 mag, respectively.

34. CEPHEIDS IN NGC 1365

Representative light curves for 9 of the 52 Cepheid candidates discovered in NGC 1365 are given in Figure 31. The phase coverage in all cases is sufficiently dense and uniform that the form of the light curves is clearly delineated. This allowed 37 of these variables to be unambiguously classified as high-quality Cepheids with their distinctively rapid brightening, followed by a long linear decline phase. Periods, obtained using modified Lafler-Kinman algorithm (Lafler & Kinman 1965), are judged to be statistically good to a few percent, although in some cases ambiguities larger than this do exist as a consequence of the narrow observing window and the restricted number of cycles (between 1 and 5) covered within the 44-day window.

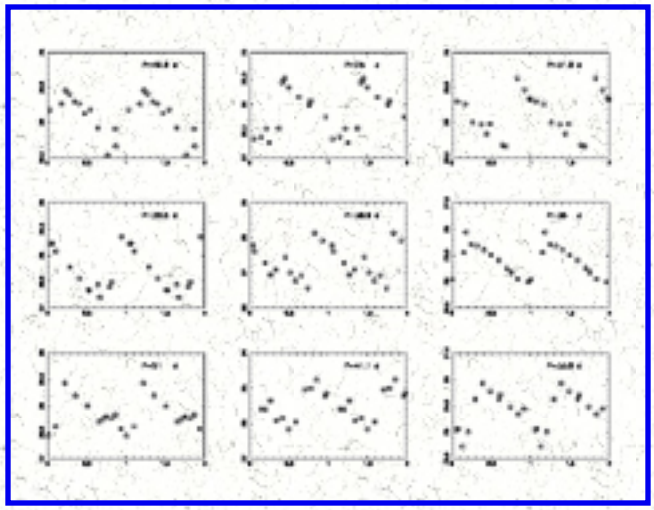

Figure 31. Representative V-band light curves for 9 of the 37 Cepheid variables found in the Fornax cluster galaxy, NGC 1365. Magnitudes are plotted along the vertical axis. Two repeated cycles in phase are plotted along the horizontal axis.

The resulting V and I period-luminosity relations for the complete set of 37 Cepheids are shown in the upper and lower panels of Figure 32, respectively. The solid line is a minimum χ^2 fit to the fiducial PL relation for LMC Cepheids (Madore & Freedman 1991), corrected for $E\ (B\text{-}V)_{LMC} = 0.10$ mag, scaled to an LMC true distance modulus of $\mu_0 = 18.50$ mag, and shifted into registration with the Fornax data. [Recent results from the Hipparcos satellite bearing on the Galactic calibration of the Cepheid zero point (Feast & Catchpole 1997; Madore & Freedman 1997) indicate that the LMC calibration is confirmed at the level of uncertainty indicated in Table 4, with the possibility that a small (upward) correction to the LMC reddening is in order.] The derived apparent moduli are $\mu_V = 31.67 \pm 0.05$ mag and $\mu_I = 31.57 \pm 0.04$ mag. Correcting for a derived total line-of-sight reddening of $E\ (V\text{-}I)_{N1365} = 0.10$ mag (based on the Cepheids themselves) gives a true distance modulus of $\mu_0 = 31.43 \pm 0.06$ mag. This corresponds to a distance to NGC 1365 of 18.0± 0.6 Mpc. The quoted error *at this step in the analysis* quantifies only the statistical uncertainty generated by photometric errors in the ALLFRAME data combined with the intrinsic magnitude and color width of the Cepheid instability strip.

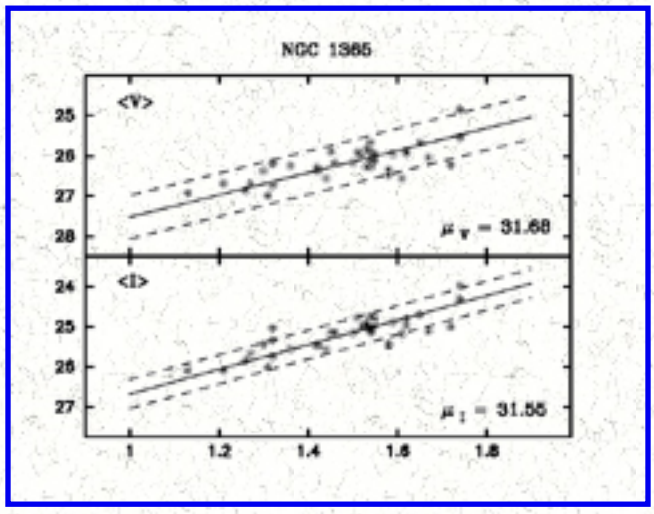

Figure 32. V and I-band Period-Luminosity relations for the full set of 37 Cepheids monitored in NGC 1365. The fits are to the fiducial relations given by Madore & Freedman (1991), shifted to the apparent distance modulus of NGC 1365. Dashed lines indicate the expected intrinsic (2-sigma) width of the relationship due to the finite temperature width of the Cepheid instability strip.

Table 4. ERROR BUDGET ON THE HUBBLE CONSTANT

Source of Uncertainty on the Mean	Description of Uncertainty	Percentage Error	
FORNAX CLUSTER	**EXPANSION VELOCITY AND INFERRED DISTANCE**		
(L) **Velocity Dispersion**	± 31 km/sec = ± 310 / $\sqrt{}$ *N*-1 (No. of gals = 111) at < *V* > = 1,267 km/sec	2%	
(M) **Geometry of Cluster**	± 0.4 Mpc at 18.6 Mpc	2%	
[N] **Virgocentric Flow**	± 22 km/sec on -44 km/sec along the Local Group line of sight	2%	
[O1] **Bulk Flow**	± 300 km/sec	24%	
Random Errors	(J) + (L) + (M) combined in quadrature		10%
Systematic Errors	[K] + [N] + [O1] combined in quadrature		26%
	H_0= 68 km/sec/Mpc ± 7 (random) ± 18 [systematic]		
LOCAL FLOW	**M81, M101, NGC 1023, NGC 2090, NGC 3621, NGC 7331, LEO, VIRGO, FORNAX**		
(P) **Random Motions**	± 4 km/sec/Mpc = ± 12 / $\sqrt{}$ *N*-1 (No. of samples = 9)	6%	
[O2] **Bulk Flow**	± 300 km/sec at *V (max)* = +1,400 km/sec	21%	
Random Errors	(P) = total observed scatter on the mean		6%
Systematic Errors	[SC] + [Z] + [O2] combined in quadrature		23%
	H_0 = 72 km/sec/Mpc ± 4 (random) ± 17 [systematic]		
DISTANT FLOW	**I. TULLY-FISHER: 16 CLUSTERS TO 10,000 km/sec**		
(S) **Observed Scatter**	± 0.04 mag = ± 0.16 / $\sqrt{}$*N*-1 (No. of clusters = 16)	2%	
[R] **TF Zero Point**	σ *(mean)* = ± 0.13 mag = ± 0.40 / $\sqrt{}$*N*-1 (No. of calibrators = 11)	6%	
[O3] **Bulk Flow**	± 300 km/sec evaluated at 10,000 km/sec	3%	
Random Errors	(S)		2%
Systematic Errors	[SC] + [Z] + [R] + [O3] combined in quadrature		11%
	H_0 = 76 km/sec/Mpc ± 2 (random) ± 8 [systematic]		
DISTANT FLOW	**II. HYBRID METHODS: 17 CLUSTERS TO 11,000 km/sec**		

(U) **Observed Scatter**	± 0.02 mag = ± 0.06 / $\sqrt{N-1}$ (No. of clusters = 17)	2%	
[O4] **Bulk Flow**	± 300 km/sec evaluated at 11,000 km/sec	3%	
[T] **FORNAX Distance**	[SC] + [Z] combined in quadrature	9%	
Random Errors	(U)		2%
Systematic Errors	[T] + [Z] combined in quadrature		10%
	H_0 = 72 km/sec/Mpc ± 1 (random) ± 7 [systematic]		
DISTANT FLOW	**III. Type Ia SN: 20 EVENTS OUT TO 20,000 km/sec**		
(T1) **Peak Luminosity**	± 0.11 mag = ± 0.45 / $\sqrt{N-1}$ (No. of SNIa = 16)	6%	
(V1) **Random Motions**	± 300 km/sec at 5,000 km/sec	6%	
[O5] **Bulk Flow**	± 300 km/sec at 20,000 km/sec	2%	
[Q1] **SNIa Zero Point**	σ *(mean)* = ± 0.18 mag = ± 0.45 / $\sqrt{N-1}$ (No. of calibrators = 7)	9%	
Random Errors	(T1) + (V1) combined in quadrature		8%
Systematic Errors	[SC] + [O5] + [Q1] combined in quadrature		12%
	H_0 = 68 km/sec/Mpc ± 5 (random) ± 8 [systematic]		

35. THE HUBBLE CONSTANT

We now discuss the impact of a Cepheid distance to the Fornax cluster in estimating the general expansion rate of the Universe. Below we present and discuss three independent estimates, where the analysis is based both on the new Fornax distance and the distances to other Key Project galaxies. At the end we intercompare the results for convergence and consistency. The first estimate is based solely on the Fornax cluster, its velocity and its Cepheid-based distance. This scrutinizes the flow sampled in one particular direction at a distance of ~ 20 Mpc. We then examine the inner volume of space, leading up to and including both the Virgo and Fornax clusters. This has the added advantage of averaging over different samples and a variety of directions, but it is still limited in volume (to an average distance of ~ 10 Mpc), and it is subject to the usual caveats concerning bulk flows and the adopted Virgocentric flow model (Table 4). The third estimate comes from using the Cepheid distance to Fornax to lock into secondary distance indicators, thereby allowing us to step out to cosmologically significant velocities (10,000 km/sec and beyond) corresponding to distances greater than 100 Mpc. Local flow uncertainties then are replaced by largescale flow uncertainties; while the systematically secure Cepheid distances are replaced by currently more controversial secondary distance indicators. This is done in order to increase volume and the sample. Averaging over the sky, and working at large redshifts, alleviates the flow problems. Examining consistency between independent the secondary distance estimates, and then averaging over their far-field estimates should provide a systematically secure value of H_0 and, more importantly, a measure of its external error. Comparison of the three ``regional'' estimates (Fornax, local

and far-field) then can be used to provide a check on the systematics resulting from the various assumptions made independently at each step.

36. THE HUBBLE CONSTANT AT FORNAX

36.1. *Uncertainties in the Fornax Cluster Distance and Velocity:*

1. **Distance** - The two panels of Figure 30 show a comparison of the Virgo and Fornax clusters of galaxies drawn to scale, as seen projected on the sky. The comparison of apparent sizes is appropriate given that the two clusters are at approximately the same distance from us. In the extensive Virgo cluster (right panel), the galaxy M100 can be seen marked ~ 4 degrees to the north-west of the elliptical-galaxy-rich core; this corresponds to an impact parameter of 1.3 Mpc, or 8% of the distance from the LG to the Virgo cluster. The Fornax cluster (left panel) is more centrally concentrated than Virgo, so that the back-to-front uncertainty associated with its three-dimensional spatial extent is reduced for any randomly selected member. Roughly speaking, converting the total angular extent of the cluster on the sky (~ 3 degrees in diameter (7)) into a back-to-front extent, the error associated with any randomly chosen galaxy in the Fornax cluster, translates into a few percent uncertainty in distance; and that uncertainty in distance will soon be reduced when the two additional Fornax spirals are observed with HST in the coming year.

2. **Velocity** - Here, we note that the infall-velocity correction for the Local Group motion with respect to the Virgo cluster (and its associated uncertainty) becomes a minor issue for the Fornax cluster. This is the result of a fortuitous combination of geometry and physics. We now have Cepheid distances from the Local Group to both Fornax and Virgo. Combined with their angular separation on the sky this immediately leads to the physical separation between the two clusters proper. Under the assumption that the Virgo cluster dominates the local velocity perturbation field at the Local Group **and** at Fornax, we can calculate the velocity perturbation at Fornax (assuming that the flow field amplitude scales with $1/ R_{Virgo}$ and characterized by a R^{-2} density distribution (Schechter 1980). From this we then derive the flow contribution to the measured line-of-sight radial velocity, as seen from the Local Group. Figure 33 shows the distance scale structure (left panel) and the velocity-field geometry (right panel) of the Local Group-Virgo-Fornax system. Adopting an infall velocity of the Local Group toward Virgo of +200 km/sec (10) with an uncertainty of ± 100 km/sec, the flow correction for Fornax is only -44 ± 22 km/sec.

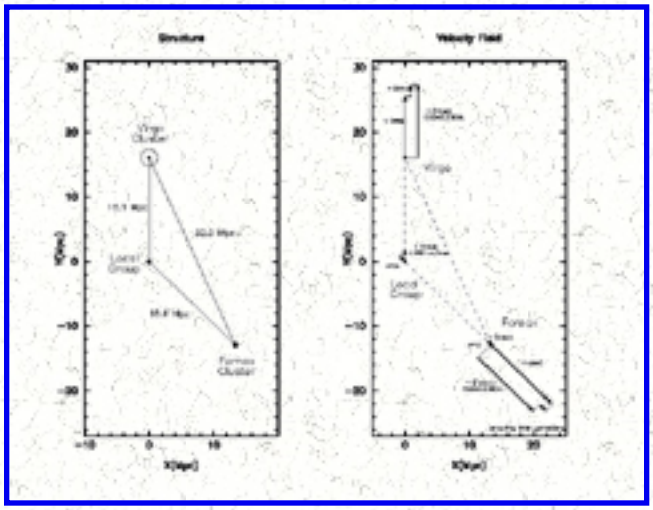

Figure 33. Relative geometry (left panel), and the corresponding velocity vectors (right panel) for the disposition and flow of Fornax and the Local Group with respect to the Virgo cluster. The circles plotted at the positions of the Virgo and Fornax clusters have the same angular size as the circles minimally enclosing M100 and NGC 1365 in the two panels of Figure 30.

3. ***H_0* at Fornax, and its Uncertainties** - Correcting to the barycentre of the Local Group (-90 km/sec) and compensating for the -44 km/sec component of the Virgocentric flow, derived above, we calculate that the cosmological expansion rate of Fornax is 1,321 km/sec. Using our Cepheid distance of 18.0 Mpc for Fornax gives $H_0 = 73\ (\pm 7)_r\ [\pm 20]_s$ km/sec/Mpc. The first uncertainty (in parentheses) includes random errors in the distance derived from the PL fit to the Cepheid data, as well as random velocity errors in the adopted Virgocentric flow, combined with the distance uncertainties to Virgo propagated through the flow model. The second uncertainty (in square brackets) quantifies the currently identifiable systematic errors associated with the adopted mean velocity of Fornax, and the adopted zero point of the PL relation (combining in quadrature the LMC distance error, a measure of the metallicity uncertainty, and a generous estimate of the possible differences in the true modulus that might be generated from adopting different stellar photometry packages). Finally, we note that according to the Han-Mould model (Han & Mould 1990), the so-called ``Local Anomaly'' gives the Local Group an extra velocity component of approximately +73 km/sec towards Fornax. If we were to add that correction our local estimate, the Hubble constant would increase to $H_0 = 77$ km/sec/Mpc.

Given the highly clumped nature of the local universe and the existence of large-scale streaming velocities, there is still a lingering uncertainty about the total peculiar motion of the Fornax cluster with respect to the cosmic microwave background restframe. Observations of flows, and the determination of the absolute motion of the Milky Way with respect to the background radiation suggest that line-of sight velocities ~ 300 km/sec are not uncommon (Coles & Lucchin 1995). The uncertainty in absolute motion of Fornax with respect to the Local Group then becomes the largest outstanding uncertainty at this point in our error analysis: a 300 km/sec flow velocity for Fornax would result in a systematic error in the Hubble constant of ~ 20%. We shall however be able to look from afar, and revisit this issue, following an analysis of more distant galaxies made later in this section.

37. THE NEARBY FLOW FIELD

We now step back somewhat and investigate the Hubble flow between us and Fornax, derived from galaxies and groups of galaxies inside 20 Mpc, each having Cepheid-based distances and expansion velocities individually corrected for a Virgocentric flow model (Kraan-Korteweg 1986). Figure 34 captures those results in graphical form. At 3 Mpc the M81-NGC 2403 Group (for which both galaxies of this pair have Cepheid distance determinations) gives H_0 = 75 km/sec/Mpc after averaging their two velocities. Working further out to M101, the NGC 1023 Group and the Leo Group, the calculated values of H_0 range from 62 to 99 km/sec/Mpc. An average of these independent determinations including Virgo and Fornax, gives $H_0 = 70\ (\pm\ 3)_r$ km/sec/Mpc. This determination, as before, uses a Virgocentric flow model with a 1/ R_{Virgo} infall velocity fall-off, scaled to a Local Group infall velocity of +200 km/sec, which was determined *ab initio* by minimizing the velocity residuals for the galaxies with Cepheid-based distances.

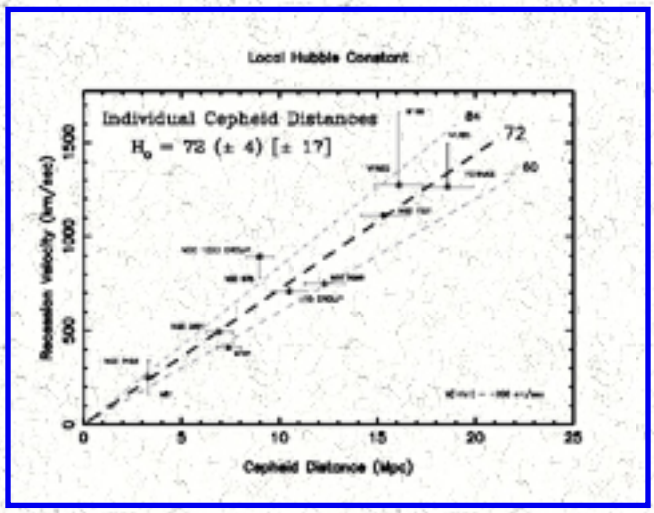

Figure 34. The velocity-distance relation for local galaxies having Cepheid-based distances. Circled dots mark the velocities and distances of the parent groups or clusters. The one-sided ``error'' bars with galaxy names attached mark the velocities associated with the individual galaxies having direct Cepheid distances. The broken line represents a fit to the data giving $H_0 = 70 \pm 3$ km/sec/Mpc. The 95% confidence interval on the observed scatter is ± 16 km/sec/Mpc, and is shown by the thin diverging broken lines; the solid lines indicate one-sigma limits.

The foregoing determination of H_0 is again predicated on the assumption that the inflow-corrected velocities of both Fornax and Virgo are not further perturbed by other mass concentrations or large-scale flows, and that the 25,000 Mpc^3 volume of space delineated by them is at rest with respect to the distant galaxy frame. To avoid these local uncertainties we now step out from Fornax to the distant flow field. There we explore three applications: **(i)** Use of the Tully-Fisher relation calibrated by Cepheids locally, and now including NGC 1365 and about two dozen additional galaxies in the Fornax cluster. Ultimately these calibrators are tied into the distant flow field at 10,000 km/sec defined by the the Tully-Fisher sample of galaxies in clusters (Aaronson *et al.* 1980). **(ii)** Using the distance to Fornax to tie into averages over previously published differential moduli for independently selected distant-field clusters, **(iii)** Recalibrating the Type Ia supernova luminosities at maximum light, and applying that calibration to events as distant as 30,000 km/sec.

38. BEYOND FORNAX: THE TULLY-FISHER RELATION

Quite independent of its association with the Fornax cluster as a whole, NGC 1365 provides an important calibration point for the Tully-Fisher relation which links the (distance-independent) peak

rotation rate of a galaxy to its intrinsic luminosity. In the left panel of Figure 35 we show NGC 1365 (in addition to NGC 925 (Silbermann *et al.* 1996), NGC 4536 (Saha *et al.* 1996) and NGC 4639 (Sandage *et al.* 1996) added to the ensemble of calibrators having published Cepheid distances (Freedman 1990), and I-band magnitudes (Pierce 1994 and references therein). As mentioned earlier, NGC 1365 does now provide the brightest data point in the relation; additional galaxies soon to be added include NGC 2090 (Phelps 1997), NGC 3351 (Graham 1997) and NGC 3621 (Rawson 1997).

Although we have only the Fornax cluster for comparison at the present time, it is interesting to note that there is no obvious discrepancy in the Tully-Fisher relation between galaxies in the (low-density) field and galaxies in this (high-density) cluster environment. The NGC 1365 data point is consistent with the data for other Cepheid calibrators. Adding in all of the other Fornax galaxies for which there are published I-band magnitudes and inclination-corrected HI line widths provides us with another comparison of field and cluster spirals. In the right panel of Figure 36 we see that the 21 Fornax galaxies (shifted by the true modulus of NGC 1365) agree extremely well with the 9 brightest Cepheid-based calibrators. The slope of the relation is virtually unchanged by this augmentation; with the scatter about the fitted line increasing somewhat to ± 0.35 mag. (Nevertheless, the small intrinsic scatter in the relation greatly diminishes the impact of Malmquist-bias.) In the following applications we adopt M_I = -8.80 log(V - 2.445) + 20.47 as the best-fitting least squares solution for the calibrating galaxies.

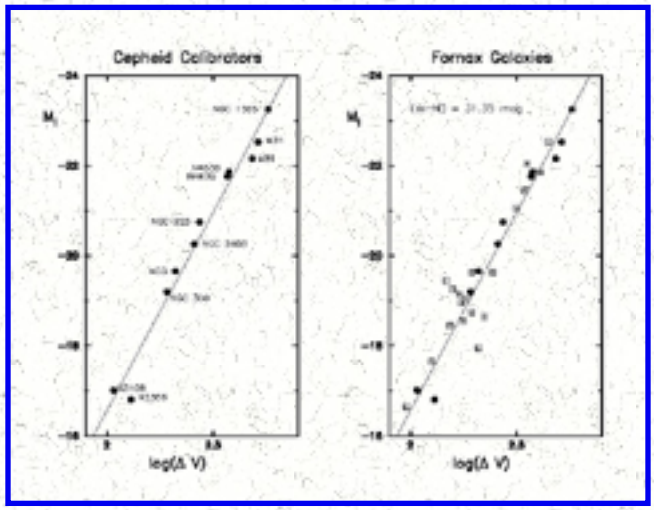

Figure 35. Tully-Fisher relations. The left panel shows the absolute I-band magnitude, M_I versus the inclination-corrected 21-cm line widths for galaxies having individually determined Cepheid distances. NGC 1365 is the brightest object in this sample; the position of this *cluster spiral* is fully consistent with an extrapolation of the relation defined by the lower luminosity *field galaxy sample*. The right panel shows the calibrating sample (filled circles) superimposed on the entire population of Fornax spiral galaxies for which I-band observations and line widths are available; the latter being shifted to absolute magnitudes by the Cepheid distance to NGC 1365.

Han (1992) has presented I-band photometry and neutral-hydrogen line widths for the determination of Tully-Fisher distances to individual galaxies in 16 clusters out to redshifts exceeding 10,000 km/sec. We have rederived distances and uncertainties to each of these clusters using the above-calibrated expression for the Tully-Fisher relation. The results are contained in Figure 36, where a linear fit to the data gives a Hubble constant of H_0 = 76 km/sec/Mpc with a total observed scatter giving a formal (random) uncertainty on the mean of only ± 2 km/sec/Mpc. It is significant that neither Fornax nor Virgo deviate to any significant degree from an inward extrapolation of this far-field solution. At face value, these results provide evidence for both of these clusters having only small motions with respect to their local

Hubble flow.

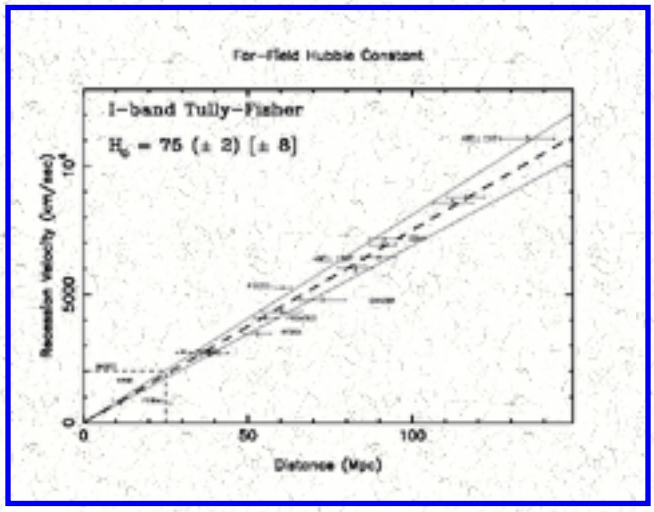

Figure 36. The velocity-distance relation for 16 clusters of galaxies out to 11,000 km/sec, having distance moduli determined from the I-band Tully-Fisher relation. A fit to the data gives a Hubble constant of H_0 = 76 ± 2 km/sec/Mpc. The solid lines mark one-sigma bounds on the observed internal scatter.

39. BEYOND FORNAX: OTHER RELATIVE DISTANCE DETERMINATIONS

In addition to the relative distances using the Tully-Fisher relation discussed above, a set of relative distance moduli based on a number of independent secondary distance indicators, including brightest cluster galaxies, Tully-Fisher and supernovae is also available (Jerjen & Tammann 1993). We adopt, without modification, their differential distance scale and tie into the Cepheid distance to the Fornax cluster, which was part of their cluster sample. The results are shown in Figure 37 which extends the velocity-distance relation out to more than 160 Mpc. No error bars are given in the published compilation but it is clear from the plot that the observed scatter is fully contained by 10% errors in distance or velocity. This sample is now sufficiently distant to average over the potentially biasing effects of large-scale flows, and yields a value of $H_0 = 72\ (\pm 1)_r$ km/sec (random), with a systematic error of 10% being associated with the distance (but not the velocity) of the Fornax cluster. Again the coincidence of H_0 at Fornax with that for the far field, argues for Fornax being relatively at rest with respect to the microwave background.

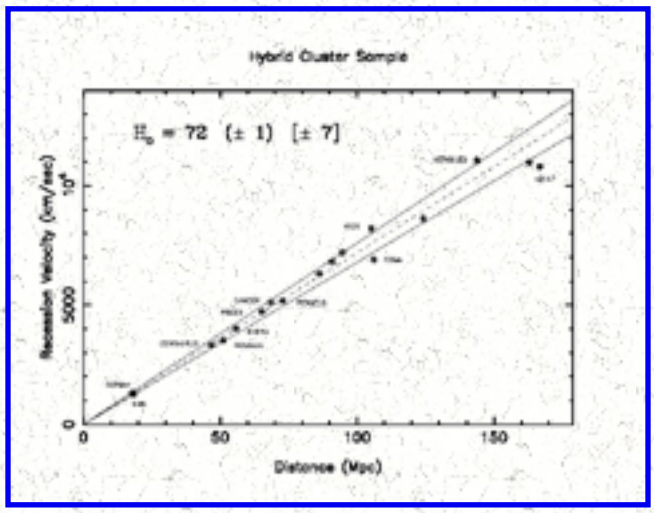

Figure 37. The velocity-distance relation for 17 clusters of galaxies with published differential distance moduli (Jerjen & Tammann 1993) scaled to the Fornax cluster. A fit to the data gives a Hubble constant of H_0 = 72 ± 1 km/sec/Mpc. As in Figure 36, the solid lines mark one-sigma bounds on the observed internal scatter.

40. BEYOND FORNAX: TYPE IA SUPERNOVAE

In a separate paper (Freedman *et al.* 1997) details are reported on the impact of a Cepheid distance to Fornax specifically on the calibration and application of Type Ia supernovae to the extragalactic distance scale. Various calibrations dealing with interstellar extinction and/or decline-rate correlations are presented. Application to the distant Type Ia supernovae (Hamuy *et al.* 1995) gives $H_0 = 68\ (\pm 8)_r$ km/sec/Mpc.

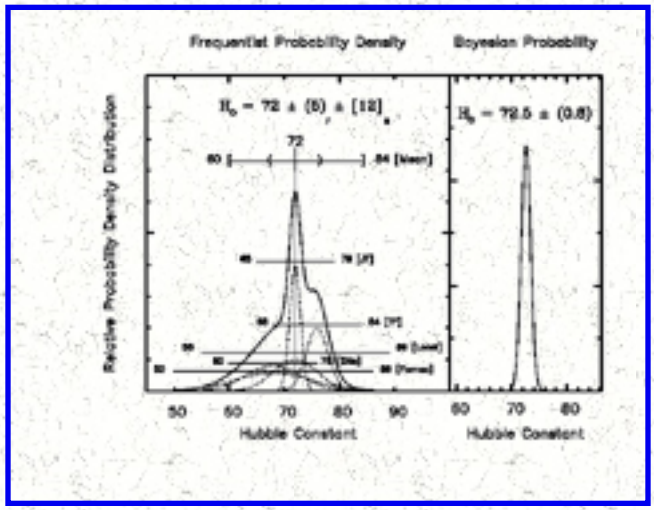

Figure 38. A graphical representation of Table 5 showing the various determinations of the Hubble constant, and the adopted mean. Each value of H_0 and its statistical uncertainty is represented by a Gaussian of unit area (linked dotted line) centred on its determined value and having a dispersion equal to the quoted *random* error. Superposed immediately above each Gaussian is a horizontal bar representing the one sigma limits of the calculated *systematic errors* derived for that determination. The adopted average value and its probability distribution function (continuous solid line) is the arithmetic sum of the individual Gaussians. (This simple representation treats each determination as independent, assuming no *a priori* reason to prefer one solution over another.)

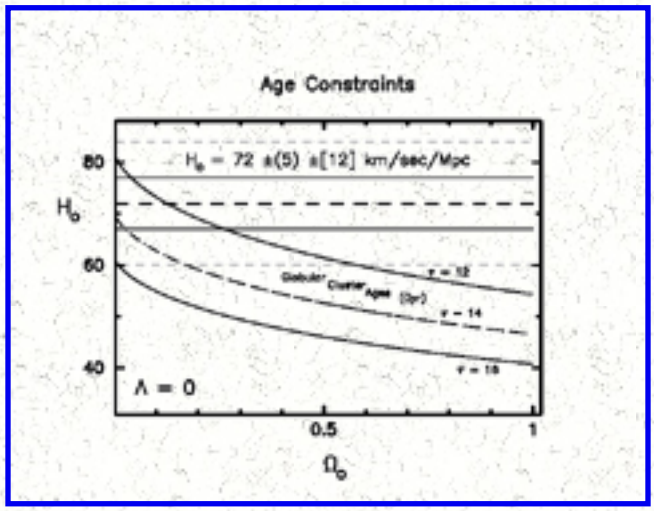

Figure 39. Lines of fixed time representing the theoretical ages of the oldest globular cluster stars are shown for 12, 14 and 16 Gyr, plotted as a function of the expansion rate H_0 and density parameter ω_0, for an Einstein-de Sitter universe with the cosmological constant $\lambda = 0$. The thick dashed horizontal line at $H = 72\ (\pm 2)_r\ [\pm 12]_s$ km/sec/Mpc is the average value of the Hubble constant given in Table 5. The parallel (solid) lines on either side of that solution represent the one-sigma random errors on that solution. Systematic errors on the solution for H_0 are represented by thin dashed lines at 61 and 83 km/sec/Mpc. The only region of (marginal) overlap between these two constraints is in the low density ($\omega < 0.2$) regime, unless $\lambda \neq 0$. If the globular cluster ages are assumed to place *a lower bound* on the age of the Universe, the region of plausible overlap between the two solutions is more severely restricted to even lower density models.

41. COSMOLOGICAL IMPLICATIONS

Given the consistency of Hubble constants derived, both locally and at large recessional velocities, then we can state that H_0 falls within the full-range extremes of 75 ± 1 and 68 ± 5 km/sec/Mpc, giving formally $H_0 = 72\ (\pm 2)_r\ [\pm 12]_s$ km/sec/Mpc out to a velocity-distance 0.1c (30,000 km/sec.) These results are summarized graphically in Figure 38 and numerically in Table 5.

Table 5. SUMMARY

Method	Hubble Constant	(Random)	[Systematic]
Fornax Cluster	68 km/sec/Mpc	± 7 (random)	± 18 [systematic]
Local Flow	72 km/sec/Mpc	± 4 (random)	± 17 [systematic]
Tully-Fisher	76 km/sec/Mpc	± 2 (random)	± 8 [systematic]
Hybrid Methods	72 km/sec/Mpc	± 1 (random)	± 7 [systematic]
Type Ia SNe	68 km/sec/Mpc	± 5 (random)	± 8 [systematic]
Modal Average:	72 km/sec/Mpc	± 5 (random)	± 12 [systematic]
Major Systematics:	± 11% [FLOWS]	± 5% [LMC]	± 4% [Fe/H]

A value of the Hubble constant, in combination with an independent estimate of the average density of the Universe, can be used to estimate a dynamical age for the Universe (*e.g.*, see Figure 39). For a value of of $H_0 = 72\ (\pm 2)_r$ km/sec/Mpc, the age ranges from a high of ~ 12 Gyr for a low-density ($\omega = 0.2$) Universe, to a young age of ~ 9 Gyr for a critical-density ($\omega = 1.0$) Universe. These ages change to 15 and 7.5 Gyr, respectively allowing for a systematic error of ± 10 km/sec/Mpc.

Other, independent constraints on the age of the Universe exist; most notably, the ages of the oldest stars, as typified by Galactic globular clusters. These ages traditionally are thought to fall in the range of 14 ± 2 Gyr (Chaboyer *et al.* 1996), however the subdwarf parallaxes obtained by the Hipparcos satellite (Reid 1997) may reduce these ages considerably. For τ = 14 Gyr and $\omega = 1.0$, H_0 would have to be ~45 km/sec/Mpc. If constrained by the stellar ages, and interpreted within the context of the standard Einstein-de Sitter model, our value of H_0 = 72 km/sec/Mpc, is incompatible with a high-density (ω =

1.0) model universe without a cosmological constant (at the 2.5-sigma level defined by the identified systematic errors).

42. CONCLUSIONS

In the past decade considerable progress has been made in understanding the systematics of the Cepheid distance scale. The amplitudes of individual Cepheids decrease at longer wavelengths. In addition, the width of the instability strip decreases as a function of increasing wavelength. By making use of these two observed properties, it has been possible **(1)** to reobserve known Cepheids efficiently and optimally, and **(2)** to optimize the methods by which new Cepheids are being discovered. Moreover, the ability to obtain multiwavelength data has made it possible to undertake corrections for reddening, and to begin to explore the residual effects of metallicity on the PL relation zero point.

Also in the past decade, a number of completely independent external checks of the Cepheid distance scale within the Local Group have been made using RR Lyrae stars, and also using the Pop II TRGB method. These nearby distances now agree to within ± 10% *rms*. Several programs are currently underway to increase the accuracy of the calibration of the Cepheid period-luminosity relation, as well as to test for potential remaining systematic effects in the zero point.

Cepheids have now been discovered out as far as the Virgo cluster and observations have just been completed for their discovery in the Fornax cluster galaxy NGC 1365; their implications are discussed below. As part of the H_0 Key Project, Cepheid distances to approximately 20 galaxies will be obtained which will allow the calibration of 5-6 independent secondary methods, several of which can be applied at velocity distances out to or beyond 10,000 km/sec where the effects of peculiar flows are minimized. Independent, direct Cepheid distances will be measured to three galaxies in each of the Virgo and Fornax clusters. At the end of this program, there will be a solid basis for the intercomparison of secondary distance indicators and therefore for an accurate application to the problem of determining the size scale of the Universe and its absolute expansion rate, the Hubble constant.

We thank the various time allocation committees and observatories that have over the years supported our observational program into the systematic calibration and subsequent application of Cepheids to the extragalactic distance scale; these include Las Campanas, Palomar, KPNO, CTIO and the CFHT, and most recently, the HST. WLF acknowledges support from the NSF in the form of grants AST 87-13889 and 91-16496. Support for this work was also provided by National Aeronuatics and Space Administration (NASA) through grant number GO-2227 from the Space Telescope Science Institute (STScI), which is operated by the Association of Universities for Research in Astronomy, Inc., under NASA contract NAS 5-26555. BFM thanks NASA for support through STScI, JPL, LTSA, and the NASA / IPAC Extragalactic Database (NED). We both also wish to thank our collaborators on the distance scale for their contributions over the past decade: R. Bernstein, J. Catanzarite, I. Horowitz, M.

G. Lee, D. Murphy, E. Persson, D. Welch, C. Wilson, and the members of the HST Key Project team: R. Kennicutt, J. Mould, F. Bresolin, L. Ferrarese, H. Ford, B. Gibson, J. Graham, M. Han, P. Harding, J. Hoessel, R. Hill, J. Huchra, S. Hughes, G. Illingworth, D. Kelson, L. Macri, R. Phelps, S. Sakai, A. Saha, N. Silbermann, P. Stetson, and A. Turner. We acknowledge having had illuminating correspondence with Drs. M. Feast, A. Gould, N. Reid and F. van Leeuwen in the course of preparing these lecture notes.

REFERENCES

1. Aaronson, M., Mould, J., Huchra, J., Sullivan, W.T., Schommer, R.A. & Bothun, G.D. 1980, *Astrophys. J.*, **239**, 12
2. Alves, B.R. & Cook, K.H. 1995, *Astron. J.*, **110**, 192
3. Baade, W. 1963 in *Evolution of Stars and Galaxies*, ed. C. Payne-Gaposchkin, (Harvard, MIT Press).
4. Baade, W. & Swope, H.H. 1963, *Astron. J.*, **68**, 435
5. Baade, W. & Swope, H.H. 1965, *Astron. J.*, **70**, 212
6. Baker, N.H. & Kippenhahn, R. 1965, *Astrophys. J.*, **142**, 868
7. Becker, S.A. & Cox, A.N. 1982, *Astrophys. J.*, **260**, 707
8. Bureau, M., Mould, J.R. & Staveley-Smith, L. 1996, *Astrophys.J.*, **463**, 60
9. Burstein, D. & Heiles, C. 1984, *Astrophys. J. Suppl.*, **54**, 33
10. Bica, E., Ortolani, S. & Barbuy, B. 1994, *Astron. Ap.*, **106**, 161
11. Bohm-Vitense, E. 1994, *Astron. J.*, **107**, 673
12. Bohm-Vitense, E. 1997, *Astron. J.*, **113**, 13
13. Brown, A.G.A., Arenou, F., van Leeuwen, F., Lindgren, L. & Luri, X. 1997, preprint
14. Caldwell, J. A.R. & Coulson, I.M. 1985, *Mon. Not. R. Astron. Soc.*, **212**, 879
15. Caldwell, J. A. 1991, in *The Magellanic Clouds and Their Dynamical Interactions with the Milky Way*, IAU No. 148, eds. R. F. Haynes & D. K. Milne, (Reidel: Dordrecht)
16. Caldwell, N., Schommer, R.A. & Graham, J. 1988, *PASP*, **100**, 1217
17. Caldwell, N. & Schommer, R.A. 1988, *ASP Conf. Series*, **4**, 77
18. Caldwell, J.A.R. & Laney, C.D. in IAU Symp. 148, *The Magellanic Clouds*, ed. R. Haynes & D. Milne (Dordrecht: Kluwer), 249
19. Caldwell, N., Schommer, R.A. & Graham, J.A. 1988, *Bull. Amer. Astron. Soc.*, **20**, 1084
20. Cardelli, J.A., Clayton, G.G. & Mathis, J.S. 1989, *Astrophys. J.*, **345**, 245
21. Carlson, G. & Sandage, A.R. 1990, *Astrophys. J.*, **352**, 587
22. Carney, B.W., Storm, J. & Jones, R.V. 1992, *Astrophys. J.*, **386**, 663
23. Chaboyer, B., Demarque, P., Kernan, P.J. & Krauss, L.M. 1996, *Science*, **271**, 957
24. Chiosi, C. 1990, ASP Conf. Ser. **11**, *Confrontation Between Stellar Pulsation and Evolution*, eds. C. Cacciari & G. Clementini (ASP: San Fransisco), p. 158
25. Chiosi, C., Wood, P. & Capitanio, N. 1993, *Astrophys. J. Suppl.*, **86**, 541
26. Ciardiulo, R., Jacoby, G.H., Ford, H.C. & Neill, J.D. 1989, *Astrophys. J.*, **339**, 53

27. Clube, S.V.M. & Dawe, J.A. 1980, *Mon. Not. R. Astron. Soc.*, **190**, 591
28. Code, A.D. 1947, *Astrophys. J.*, **106**, 309
29. Coles, P. & Lucchin, F. 1995, In *Cosmology*, Wiley, 399
30. Cook, K., Aaronson, M. & Illingworth, G. 1986, *Astrophys. J.*, **301**, L45
31. Cook, K. 1996 in *Astropysical Applications of Stellar Pulsation*, ed. R.S. Stobie, IAU Coll. 155, (Cambridge Univ. Press: Cambridge), in press
32. Coulson, I.M., Caldwell, J.A.R. & Gieren, W.P. 1986, *Astrophys. J.*, **303**, 273
33. Cousins, A.W.J. 1978a, *Observatory*, **98**, 54
34. Cousins, A.W.J. 1978b, *Mon. Not. Astron. Soc. So. Africa*, **37**, 62
35. Cox, A.N., Michaud, G. & Hodson, S.W. 1978, *Astrophys. J.*, **222**, 621
36. Cox, J.P. 1980, in *Theory of Stellar Pulsation*, (Princeton University Press, Princeton)
37. Crotts, A.P.S., Kunkel, W.E. & Heathcote, S.R. 1995, *Astrophys. J.*, **438**, 724
38. Da Costa, G.S. & Armandroff, T.E. 1990, *Astron. J.*, **100**, 162
39. Dean, J.F., Warren, P.R. & Cousins, A.W.J. 1978, *Mon. Not. R. Astron. Soc.*, **183**, 569
40. Demers, S., Kunkel, W.E. & Irwin, M.J. 1985, *Astron. J.*, **90**, 1967
41. Deupree, R.G. 1977, *Astrophys. J.*, **215**, 620
42. de Vaucouleurs, G., 1975, In *Stars and Stellar Systems*, **9**, (A.R. Sandage, M. Sandage, J. Kristian, eds.), Univ Chicago Press, 557
43. Dressler, A. 1987, *Astrophys. J.*, **317**, 1
44. Feast, M.W. & Catchpole, R.M. 1997, *Mon. Not R. Astron. Soc.*, **286**, 1
45. Feast, M.W. & Walker, A.R. 1987, *Ann. Rev. Astron. Ap.*, **25**, 345
46. Feldmeier, J.J., Ciardullo, R. & Jacoby, G.H. 1996, *Astrophys. J. (Lett.)*, **461**, 25
47. Fernie, J.D. 1969, *Publ. Astron. Soc. Pacific*, **81**, 707
48. Fernie, J.D. 1990, *Astrophys. J.*, **354**, 295
49. Fernie, J.D. & McGonegal, R. 1983, *Astrophys. J.*, **275**, 732
50. Fernie, J.D., Kamper, K.W. & Seager, S. 1993, *Astrophys. J.*, **416**, 820
51. Ferrarese, L. *et al.* 1996, *Astrophys. J.*, **464**, 568
52. Ferraro, F.R., Fusi Pecci, F., Tosi, M. & Buonnano, R. 1989, *Mon. Not. R. Astron. Soc.*, **241**, 433.
53. Ferguson, H.C. & Sandage, A.R. 1988, *Astron. J.*, **96**, 1520
54. Ferguson, H.C. 1989, *Astron. J.*, **98**, 367
55. Freedman, W.L. 1988a, *Astrophys. J.*, **326**, 691
56. Freedman, W.L. 1988b, in ASP Conference Series, **4**, ed. S. van den Bergh & C. Pritchet (Provo, Brigham Young University Press) p. 24
57. Freedman, W.L. 1988c, *Astron. J.*, **96**, 1248
58. Freedman, W.L. 1990, *Astrophys. J. (Lett.)*, **355**, L35
59. Freedman, W.L., Grieve, G.R. & Madore, B.F. 1985, *Astrophys. J. Suppl.*, **59**, 311
60. Freedman, W.L., Horowitz, I., Madore, B.F., Mould, J. & Graham, J. 1988a, in ASP Conference Series, **4**, ed. S. van den Bergh & C. Pritchet (Provo, Brigham Young University Press) p. 207
61. Freedman, W.L., Horowitz, I., Madore, B.F. & Mould, J. 1988b, PASP, **100**, 1219

62. Freedman, W.L. & Madore, B.F. 1988, *Astrophys. J.*, **332**, L63
63. Freedman, W.L. & Madore, B.F. 1990, *Astrophys. J.*, **365**, 186
64. Freedman, W.L. & Madore, B.F. 1996, in *Clusters, Lensing and the Future of the Universe*, ASP Conf. Series, eds. V. Trimble & A. Reisenegger, p. 9
65. Freedman, W.L., Madore, B.F. & Kennicutt, R.C. 1997, in *The Extragalactic Distance Scale*, eds. M. Livio, M. Donahue & N. Panagia, (Cambridge, Cambridge Univ. Press), p. 171
66. Freedman, W.L., Madore, B.F., Stetson, P.B., *et al.* 1994, *Astrophys. J.*, **435**, L31
67. Freedman, W.L. & Madore, B.F. 1990, *Astrophys. J.*, **365**, 186
68. Freedman, W.L. & Madore, B.F. 1993, in *New Perspectives on Stellar Pulsation and Pulsating Variable Stars*, eds. J.M. Nemec & J.M. Matthews, (Cambridge Univ. Press: Cambridge)
69. Freedman, W.L., Wilson, C.D. & Madore, B.F. 1991, *Astrophys. J.*, **372**, 455
70. Freedman, W.L. *et al.* 1992, *Astrophys. J.*, **396**, 80
71. Freedman, W.L. *et al.* 1994a, *Nature*, **371**, 757
72. Freedman, W.L. *et al.* 1994b, *Astrophys. J.*, **427**, 628
73. Freedman, W.L. *et al.* 1994c, *Astrophys. J.*, **435**, L31
74. Freedman, W.L. *et al.* 1997, in preparation
75. Gallart. C., Aparicio, A. & Vilchez, J.M. 1996, *Astron. J.*, **112**, 1928
76. Gaposchkin, S. 1962, *Astron. J.*, **67**, 334
77. Gould, A. 1994, *Astrophys. J.*, **426**, 542
78. Gould, A. & Uza, O. 1997, *Astrophys. J.*, submitted
79. Graham, J.A. 1984, *Astron. J.*, **89**, 1332
80. Graham, J.A. *et al.* 1997, *Astrophys. J.*, **477**, 535
81. Gratton, R.G., Fusi Pecci, F., Carretta, E., Clementini, G., Corsi, C.E. & Lattanzi, M. 1997, *Astrophys. J.*, **491**, 749
82. Hamuy, M. 1995, *et al. A. J.*, **109**, 1
83. Han, M.S. 1992, *Astrophys. J. Suppl.*, **81**, 35
84. Han, M. & Mould J.R. 1990, *Astrophys. J.*, **360**, 448
85. Hanes, D.A. 1982, *Mon. Not. R. Astron. Soc.*, **201**, 145
86. Hill, R. *et al.* 1997, *Astrophys. J. Suppl.*, in press
87. Hodge, P.W. 1977, *Astrophys. J. Suppl.*, **33**, 69
88. Hodge, P.W. 1981 *Ann. Rev. Astron. Ap.*, **19**, 357
89. Holtzmann, J. *et al.* 1995, *Publs Astron. Soc. Pacif.*, **107**, 156
90. Hoessel, J.G., Abbott, M.J., Saha, A., Mossman, A.E. & Danielson, G.E. 1990, *Astron. J.*, **100**, 1151
91. Hoessel, J.G., Schommer, R.A. & Danielson, G.E. 1983, *Astrophys. J.*, **274**, 577
92. Hoessel, J.G., Saha, A., Krist, J. & Danielson, G.E. 1994, *Astron. J.*, **108**, 645
93. Hubble, E.P. 1925, *Astrophys. J.*, **62**, 409
94. Hubble, E.P. 1926, *Astrophys. J.*, **63**, 236
95. Hubble, E.P. 1929, *Proc. Nat. Acad. Sci.*, **15**, 168

96. Iben, I. 1974, *Ann. Rev. Astron. Astrophys.*, **12**, 215
97. Iben, I. & Renzini, A. 1983, *Ann. Rev. Astron. Ap.*, **21**, 271
98. Jacoby, G. H. *et al.* 1992, *Publ. Astron. Soc. Pacific*, **104**, 599
99. Jerjen, H. & Tammann, G.A. 1993, *Astr. Ap.*, **276**, 1
100. Johnson, H. L. 1963, Stars & Stellar Systems, Vol. III, *Basic Astronomical Data*, ed. K.A. Strand, (Univ. Chicago Press, Chicago), p. 204
101. Kayser, S.E. 1967, *Astron. J.*, **72**, 134
102. Kennicutt, R.C., Freedman, W.L. & Mould, J.R. 1995, *Astron. J.*, **110**, 1476
103. Kelson, D. *et al.* 1996, *Astrophys. J.*, **463**, 26
104. Kinman, T., Mould, J. & Wood, P.R. 1987, *Astron. J.*, **93**, 833
105. Kraft, R.P. 1960 *Astrophys. J.*, **131**, 330
106. Kraan-Korteweg, R. 1986, *Astron. Astrophys. Suppl*, **66**, 255
107. Lafler, J. & Kinman, T.D. 1965, *Astrophys. J. Suppl.*, **11**, 216
108. Laney, C.D. & Stobie, R.S. 1986a, *So. African Astron. Obs. Circ.*, **10**, 51
109. Laney, C.D. & Stobie, R. S. 1986b, *Mon. Not. R. Astron. Soc.*, **222**, 449
110. Laney, C.D. & Stobie, R.S. 1992, *Astron. Astrophys. Suppl.*, **93**, 93
111. Laney, C.D. & Stobie, R.S. 1994, *Astron. Astrophys.*, **266**, 441
112. Lauterborn, D., Refsdal, S. & Weigert, A. 1971, *Astrophys. J.*, **10**, 97
113. Lauterborn, D. & Siquig, R.A. 1974, *Astrophys. J.*, **191**, 589
114. Leavitt, H. 1906, *Ann. Harvard Coll. Obs.*, **60**, 87
115. Lee, M.G. 1993, *Astrophys. J.*, **408**, 409
116. Lee, Y.-W., Demarque, P. & Zinn, R. 1990, *Astrophys. J.*, **350**, 155
117. Lee, M.G., Freedman, W.L. & Madore, B.F. 1993, *Astrophys. J.*, **417**, 553
118. Madore, B.F. 1976, *Mon. Not. R. Astron. Soc.*, **177**, 157
119. Madore, B.F. 1982, *Astrophys. J.*, **253**, 575
120. Madore, B.F. 1985, *Cepheids: Theory and Observations*, ed: B.F. Madore, Cambridge Univ. Press: Cambridge, p. 166
121. Madore, B.F. 1986 in *Galaxy Distances and Deviations from Universal Expansion*, ed. B. F. Madore & R. B. Tully (Dordrecht, Reidel), p. 29
122. Madore, B.F. *et al.* 1997, *Nature*, submitted
123. Madore, B.F. & Freedman, W.L. 1985, *Astron. J.*, **90**, 1104
124. Madore, B.F. & Freedman, W.L. 1991, *Publ. Astron. Soc. Pacific*, **103**, 933 (MF91)
125. Madore, B.F. & Freedman, W.L. 1995, *Astron. J.*, **109**, 1645
126. Madore, B.F. & Freedman, W.L. 1997, *Astrophys. J. (Lett.)*, in press.
127. Madore, B.F., Freedman, W.L. & Lee, M.G. 1993, *Astron. J.*, **106**, 2243
128. Madore, B.F., Freedman, W.L. & Pevunova, O. 1998, *Astron. J.*, (in preparation)
129. Madore, B.F., McAlary, C.W., McLaren, R.A., Welch, D.L., Neugebauer, G. & Matthews, K. 1985, *Astrophys. J.*, **294**, 560
130. Madore, B.F., Welch, D.L., McAlary, C.W. & McLaren, R.A. 1987, *Astrophys. J.*, **320**, 26

131. Martin, P.R., Warren, P.R. & Feast, M.W. 1979, *Mon. Not. R. Astron. Soc.*, **188**, 139
132. Mathewson, D.S., Ford, V.L. & Visvanathan, N. 1986, *Astrophys. J.*, **301**, 664
133. Mathewson, D.S., Ford, V.L. & Visvanathan, N., 1988, *Astrophys. J.*, **333**, 617
134. Mathewson, D.S., Ford, V.L. & Buchhorn, M. 1992, *Astrophys. J. Suppl.* **81**, 413
135. McAlary, C.W. & Madore, B.F. 1984, *Astrophys. J.*, **282**, 101
136. McAlary, C.W., Madore, B.F. & Davis, L.E. 1984, *Astrophys. J.*, **276**, 487
137. McAlary, C.W., Madore, B.F., McGonegal, R., McLaren, R.A. & Welch D.L. 1983, *Astrophys. J.*, **273**, 539
138. McCall, M.L., 1993, *Astrophys. J. (Lett.)*, **417**, L75
139. McGonegal, R., McLaren, R.A., McAlary, C.W. & Madore, B.F., 1982, *Astrophys. J. (Lett.)*, **257**, L33
140. Mould, J.R. & Kristian, J. 1990, *Astrophys. J.*, **354**, 438
141. Mould, J.R. & Kristian, J. 1986, *Astrophys. J.*, **305**, 591
142. Mould, J.R., Kristian, J. & Da Costa, G.S. 1983, *Astrophys. J.*, **270**, 471
143. Mould, J.R., Kristian, J. & Da Costa, G.S. 1984, *Astrophys. J.*, **278**, 575
144. Panagia, N. *et al.* 1996, unpublished poster papers from the STScI Symposium, *The Extragalactic Distance Scale*
145. Panagia, N., Gilmozzi, R., Macchetto, F., Adorf, H.-M. & Kirschner, R.P. 1991, *Astrophys. J.*, **380**, L23
146. Payne-Gaposchkin, C. 1971, *Smithsonian Contr. Ap.*, **13**, (Smithsonian Inst. Press, Washington D. C.)
147. Payne-Gaposchkin, C. & Gaposchkin, S. 1966, *Smithsonian Contr. Ap.*, **9**, (Smithsonian Inst. Press, Washington D.C.)
148. Pel, J.W. 1985, in IAU Colloq. 82, *Cepheids: Theory and Observations*, ed. B.F. Madore (Cambridge: Cambridge Univ. Press), 1
149. Phelps, R. *et al.* 1998, *Astrophys. J.*, in preparation
150. Pierce, M. 1994, *Astrophys. J.*, **430**, 53
151. Rawson, D.M. *et al.* 1998, *Astrophys. J.*, in preparation
152. Reid, I.N. & Freedman, W.L. 1994, *Mon. Not. R. Astron. Soc.*, **267**, 821
153. Reid, I.N. 1997, *Astron. J.*, **114**, 161
154. Rowan-Robinson, M. 1985, in *The Cosmological Distance Ladder*, (Freeman, San Fransisco)
155. Saha, A., Hoessel, J.G., Krist, J. & Danielson, G.E. 1996 *Astron. J.*, **111**, 197
156. Saha, A. *et al.* 1995, *Astrophys. J.*, **438**, 8
157. Saha, A., Freedman, W.F., Hoessel, J.G. & Mossman, A.E. 1992, *Astron. J.*, **104**, 1072
158. Saha, A., Sandage, A.R., Labhardt, L., Tammann, G.A., Macchetto, F.D. & Panagia, N. 1996, *Astrophys. J.*, **466**, 55
159. Saha, A. *et al.* 1994, *Astrophys. J.*, **425**, 14
160. Sakai, S., Madore, B.F. & Freedman, W.L. 1996a, *Astrophys. J.*, **461**, 713
161. Sakai, S., Madore, B. F. & Freedman, W. L. 1996b, *Astrophys. J.*, **480**, 589

162. Sakai, S., Madore B.F., Freedman, W.L., Lauer, T.R., Ajhar, E.A., & Baum, W.A. 1997, *Astrophys. J.*, **478**, 49
163. Sandage, A.R. 1958, *Astrophys. J.*, **127**, 513
164. Sandage, A.R. 1972, *Q.J.R.A.S*, **13**, 202
165. Sandage, A.R. 1983, *Astron. J.*, **88**, 1108
166. Sandage, A.R. 1984, *Astron. J.*, **89**, 621
167. Sandage, A.R. 1988a, *Astrophys. J.*, **331**, 605
168. Sandage, A.R. 1988b, *Publ. Astron. Soc. Pacific*, **100**, 935
169. Sandage, A.R. & Cacciari, C. 1990, *Astrophys. J.*, **350**, 645
170. Sandage, A.R. & Carlson, G. 1983b, *Astrophys. J.*, **258**, 439
171. Sandage, A.R. & Carlson, G. 1983a, *Astrophys. J.*, **267**, L25
172. Sandage, A.R. & Carlson, G. 1985a, *Astron. J.*, **90**, 1464
173. Sandage, A.R. & Carlson, G. 1985b, *Astron. J.*, **90**, 1019
174. Sandage, A.R. & Carlson, G. 1988, *Astron. J.*, **96**, 1599
175. Sandage, A.R. & Gratton, L. 1963, in *Star Evolution*, (New York: Academic Press), p. 11
176. Sandage, A.R., Saha, A., Tammann, G.A., Labhardt, L., Panagia, N. & Macchetto, F.D. 1996, *Astrophys. J. (Lett.)*, **460**, L15
177. Sandage, A.R. & Tammann, G.A. 1968, *Astrophys. J.*, **151**, 531
178. Sandage, A.R. & Tammann, G.A. 1969, *Astrophys. J.*, **157**, 683
179. Sandage, A.R. & Tammann, G.A. 1971, *Astrophys. J.*, **167**, 293
180. Sandage, A.R. & Tammann, G.A. 1974, *Astrophys. J.*, **194**, 223
181. Sandage, A.R, & Tammann, G.A. 1997, *Mon. Not. R. Astron. Soc.*, (submitted)
182. Sandage, A.R. *et al.* 1994, *Astrophys. J.*, **423**, L13
183. Schaltenbrand, R. & Tammann, G.A. 1970, *Astron. Astrophys.*, **7**, 289
184. Schechter, P. 1980, *Astron. J.*, **85**, 801
185. Schmidt, E. 1991, *Observatory*, **111**, 178
186. Schmidt, E. & Simon, N.R. 1987, in *Stellar Pulsation*, eds. A.N. Cox, W.M. Sparks, and S.G. Starrfield, (Springer-Verlag, Berlin), p. 180
187. Schmidt, E. & Spear, G.G. 1987, *Bull. Amer. Astron. Soc.*, **19**, 1036
188. Schmidt, E. & Spear, G.G. 1989, *Mon. Not. R. Astron. Soc.*, **236**, 567
189. Schmidt, E., Spear, G.G. & Simon, N.N. 1986, *Bull. Amer. Astron. Soc.*, **18**, 964
190. Schmidt-Kaler, Th. 1992, *ASP Conf. Ser.*, **30**, 195
191. Schroder, A. 1995, Doctoral Thesis, University of Basel
192. Schroder, A. & Richter, O.-G., 1997, in preparation
193. Silbermann, N.A. *et al.* 1996, *Astrophys. J.*, **470**, 1
194. Silbermann, N.A. *et al.* 1998, *Astrophys. J.*, in preparation
195. Simon, N., 1990, ASP Conf. Ser., **11**, *Confrontation Between Stellar Pulsation and Evolution*, ed. C. Cacciari (ASP: San Fransisco), p. 193
196. Soria, R. *et al.* 1996, *Astrophys. J.*, **465**, 79

197. Stellingwerf, R.F. 1986, *Astrophys. J.*, **303**, 119
198. Stetson, P.B. 1994, *Publs Astron. Soc. Pacif.*, **106**, 250
199. Stift, M.J. 1982, *Astron. Astrophys.*, **112**, 149
200. Stift, M.J. 1990, *Astron. Astrophys.*, **229**, 143
201. Stothers, R. 1982, *Astrophys. J.*, **255**, 227
202. Stothers, R. 1983, *Astrophys. J.*, **274**, 20
203. Stothers, R. 1988, *Astrophys. J.*, **329**, 712
204. Tammann, G.A. & Sandage, A.R. 1968, *Astrophys. J.*, **151**, 825
205. Tanvir, N.R. *et al.* 1995, *Nature*, **377**, 27
206. Tanvir, N.R. 1997, in *The Extragalactic Distance Scale*, eds. M. Livio, M. Donahue & N. Panagia, (Cambridge, Cambridge Univ. Press), p. 91
207. Thomas, H.-C. 1967 *Zeit. Ap.*, **67**, 420
208. Tolstoy, E., Saha, A., Hoessel, J.G., & Danielson, G.E. 1995, *Astron. J.*, **109**, 579
209. Tolstoy, E., Saha, A., Hoessel, J.G. & Mcquade, K. 1995, *Astron. J.*, **110**, 1640
210. Turner, D. G. 1990, *Publ. Astron. Soc. Pacific*, **102**, 1331
211. van den Bergh, S. 1995, *Astrophys. J.*, **446**, 39
212. van den Bergh, S. 1975, Stars & Stellar Systems, Vol. IX, *Galaxies and the Universe*, ed. A.R. Sandage, M. Sandage & J. Kristian, (Univ. Chicago Press, Chicago), p. 509
213. van den Bergh, S. 1979, *Astron. J.*, **84**, 604
214. van Leeuwen, F. 1983, Ph.D. thesis, Leiden Univ., Netherlands
215. Visvanathan, N. 1988, *Publ. Astron. Soc. Pacific*, **100**, 949
216. Visvanathan, N. 1989, *Astrophys. J.*, **346**, 629
217. Walker, A.R. 1987, SAAO Circ. **11**, 125
218. Walker, A.R. 1988, in ASP Conference Series Vol. 4, ed. S. van den Bergh & C. Pritchet (Provo, Brigham Young University Press) p. 89
219. Walker, A.R. 1992 CCD Photometry of Magellanic Cloud RR Lyrae Variables in *The Extragalactic Distance Scale*, ed. S. van den Bergh & C. Pritchet, (Provo: Brigham Young Univ. Press) **Vol. 4**, 69
220. Welch, D.L., McAlary, C.W., McLaren, R. & Madore, B.F. 1986, *Astrophys. J.*, **305**, 583
221. Welch, D.L., McLaren, R., Madore, B.F. & McAlary, C.W. 1987, *Astrophys. J.*, **321**, 162
222. Welch, D.L., Wieland, F., McAlary, C.W., McGonegal, R., Madore, B.F., McLaren, R.A. & Neugebauer, G. 1984, *Astrophys. J. Suppl.*, **54**, 547
223. Westerlund, B.E. 1990, *Astron. Astrophys. Reviews*, **2**, 29
224. Westerlund, B.E. 1997, *The Magellanic Clouds* Cambridge Astrophysics Series: 29, (Cambridge: Cambridge University Press)
225. Wilson, C.D., Welch, D.L., Reid, I.N., Saha, A. & Hoessel, J. 1996, *Astron. J.*, **111**, 1106
226. Wisniewski, W.Z. & Johnson, H.L. 1968, *Comm. Lunar Planet. Lab.*, **7**, 57